1972

A Search For Weak Longitudinal Magnetic Fields In Bright Stars

Ermanno Franco Borra

CANADA

ATIONAL LIBRARY OF CANADA

CANADIAN THESES ON MICROFILM

BIBLIOTHÈ NATIONA DU CANA

THÈSES CANADII SUR MICROFI

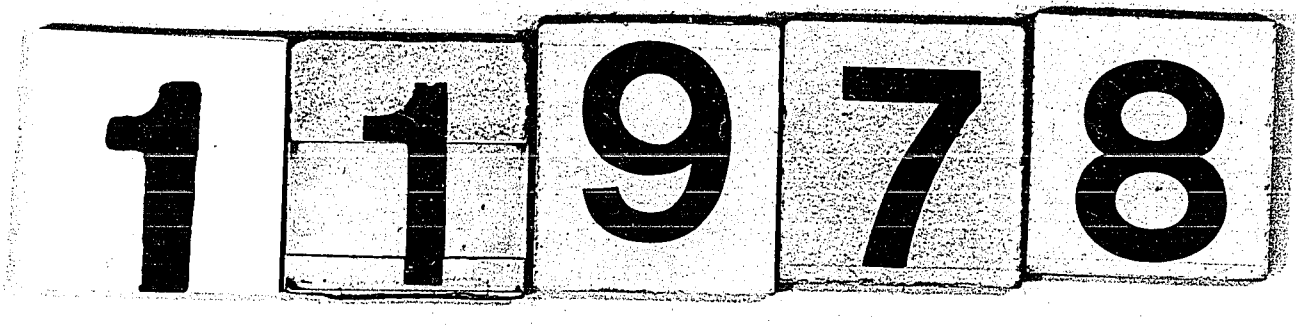

A SEARCH FOR WEAK LONGITUDINAL MAGNETIC FIELDS IN BRIGHT STARS

by

Ermanno Franco Borra

Department of Astronomy

Submitted in partial fulfillment
of the requirements for the degree of
Doctor of Philosophy

Faculty of Graduate Studies
The University of Western Ontario
London Canada

July 1972

ABSTRACT

The results of a search for weak longitudinal magnetic fields in bright stars using a photoelectric polarimeter and coudé line profile scanner are reported. γ Cygni appears to have a longitudinal magnetic field of the order of a few hundred gauss. There is some evidence for a longitudinal field of the same order of magnitude in α Arietis and α Aurigae. High-resolution (0.038 A) polarization observations have been obtained with a Fabry-Perot interferometer for α^2 Librae, Sirius, ι Coronae Borealis and β Coronae Borealis. Upper limits ranging from 5 to 200 gauss are reported for 16 other stars.

The problems of spurious instrumental polarization and phase shifts and of the efficiency of the instrument have been examined. Techniques of observation and reduction are developed and tested using numerical models under the main assumptions of dipole geometry and Milne-Eddington approximation. Oblique rotator models for the magnetic stars β Coronae Borealis and 53 Camelopardalis are briefly discussed and compared to existing observations.

ACKNOWLEDGMENT

I wish to thank Dr. J. D. Landstreet, my thesis advisor, for his advice and assistance throughout this investigation. I have benefitted from discussions with Dr. W. H. Wehlau, Dr. J. M. Marlborough and Mr. J. R. Roy. This investigation was made possible by the use of the coudé line profile scanner built by Drs. D. F. Gray and W. H. Wehlau. I am grateful for the hospitality given to me during nine nights at Mt. Wilson Observatory (Hale Observatories, Carnegie Institution of Washington, California Institute of Technology). In particular I wish to thank Dr. G. W. Preston and Dr. A. H. Vaughan, Jr. for their help in familiarizing with the telescope and coudé scanner. Throughout my studies I have received financial assistance from Province of Ontario Graduate Fellowships. Financial assistance for this research was provided by the National Research Council of Canada. Finally, I wish particularly to thank Ms. Gail E. M. Stewart for typing several drafts of my thesis, including the final one.

TABLE OF CONTENTS

LIST OF TABLES

LIST OF FIGURES

I. INTRODUCTION

Measurement of stellar magnetic fields is generally made through the Zeeman effect (Babcock 1960, Preston 1971). The phenomenology and theory of the Zeeman effect is treated in many elementary textbooks. It will therefore not be discussed in detail.

In the simple case of the normal Zeeman effect, for emission from an optically thin gas, a magnetic field splits an atomic line into three components. These are an undisplaced π component and two σ components displaced $\pm \delta\lambda$ from the π component, with

$$\delta\lambda = 4.67 \times 10^{-13} g H \lambda^2 \qquad (1)$$

where g is the Landé g factor, H the magnetic field strength in gauss and λ the wavelength in Ångstroms. If the magnetic field vector is parallel to the line of sight, only the two σ components are visible. In emission lines the component at longer wavelength is right circularly polarized (R.C.P.), the other is left circularly polarized (L.C.P.) when H points towards the observer. Reversing the direction of the magnetic field vector will reverse the signs of polarization. When the magnetic field vector is inclined at an angle γ with the line of sight, the π and σ components are present simultaneously.

For emission lines the relative intensities of the components are given by (Babcock 1949a)

$$I_{\sigma v} : I_{\pi} : I_{\sigma R} = \frac{1}{4}(1+\cos^2\gamma) : \frac{1}{2}\sin^2\gamma : \frac{1}{4}(1+\cos^2\gamma) \qquad (2)$$

The π component is linearly polarized and the σ components polarized elliptically. When the field is purely transverse, the σ components are linearly polarized perpendicular to the field lines and their intensity is ½ the intensity of the π component, which is linearly polarized along the field lines.

The Zeeman effect in absorption lines is called inverse Zeeman effect. Let us consider a simple reversing layer model of an atmosphere in which a longitudinal magnetic field directed towards the observer is present. The unpolarized continuum can be represented (Jenkins and White, 1937, p. 314) as a mixture of left and right circularly polarized photons in equal number. An atom which was absorbing at a wavelength λ_0 will, in the presence of a magnetic field, absorb at two wavelengths $\lambda_0 - \delta\lambda$ and $\lambda_0 + \delta\lambda$. If the field points towards the observer, the left circularly polarized photons from the continuum will be absorbed at $\lambda_0 - \delta\lambda$; thus a net right circular polarization will be detected. Similarly, we will detect a net left circular polarization at $\lambda_0 + \delta\lambda$. Thus the signs of polarization are reversed with respect to the emission case. A similar situation holds for the case where the field lines are inclined at an angle γ to the line of sight.

The relative intensities of the Zeeman components in the absorption case are given by equation (2) only for very weak lines (Bray and Loughhead 1964, p. 174). The

correct treatment of the inverse Zeeman effect involves the solution of the radiation transfer problem of the formation of a spectral line in the presence of a magnetic field. This problem has been treated by Unno (1956) and Stepanov (1958).

Although in the case of very strong fields and sharp lines, the separation of the σ components can be large enough to be seen in high dispersion spectrograms of A_p stars such as HD215441 and 53 Cam (Babcock 1960, Preston 1969), usually it is small compared with the width of spectral lines in stars. Thus it cannot be measured directly.

By making use of a quarter wave plate and calcite to produce two parallel spectra of a star simultaneously, one in left circularly polarized light and the other in right circularly polarized light, the separation of the two σ components of a spectral line in a magnetic star can still be measured spectroscopically for strengths of the longitudinal component of the magnetic field of the order of a few hundred gauss (Babcock 1958). However, this method is limited to sharp-lined stars, and even in the best case, the standard errors of the measurements are at least 100 to 200 gauss due to various systematic errors (Preston 1969_b). The very existence of some of the fields reported is sometimes questioned. Such is the case for example for RR Lyrae (Preston 1967) and for the weak fields reported in some A_m stars (Preston 1971). The use

of the photographic techniques has been successful only in the one class of stars fulfilling both the requirements of strong fields and sharp lines: the A_p stars.

A photoelectric method capable of detecting much weaker magnetic fields was devised by Hale (1933) and Kiepenheuer (1953) and perfected by Babcock (1953), for the observation of sunspots. Basically, one wing of a spectral line is observed photoelectrically with a narrow bandpass. In the presence of a longitudinal field, the line is split in two components displaced $\pm \delta\lambda$ from the zero-field wavelength, one L.C.P., the other R.C.P.. A reversible quarter wave plate and polarizer ahead of the spectrograph (chapter II) transmits alternately L.C.P. and R.C.P. light, enabling one to measure the difference in intensity between the lines seen in the two polarization signs (shaded area in figure 1). The difference in intensity is proportional to the displacement $\delta\lambda$, which in turn is proportional to the longitudinal component of the magnetic field when one observes emission lines or weak absorption lines in a weak field. By adding an additional quarter-wave plate, the instrument can measure all of the Stokes parameters across a spectral line. The data can then be interpreted in terms of a theoretical model.

Kiepenheuer used a rotating quarter-wave plate and a fixed polaroid through which the L.C.P. and R.C.P. components pass alternately, modulated by the rotation of

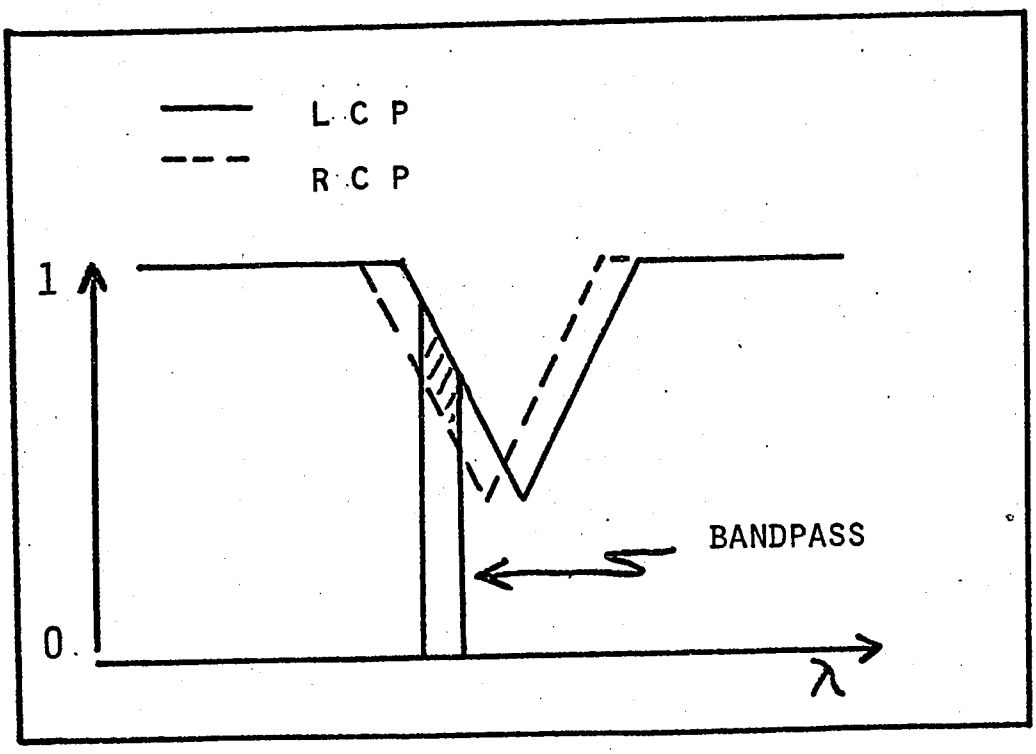

FIGURE 1

The line in left circularly polarized light (L.C.P.) is drawn in dashed lines. The line in right circularly polarized light (R.C.P.) is drawn in solid lines. The instrument measures the difference of intensidy represented by the shaded area. The continuum is at intensity 1 .

the quarter-wave plate.

Babcock replaced the rotating analyzer by an electro-optic crystal of ammonium dihydrogen phosphate (ADP). Alternating the direction of the electric field across the crystal produces the necessary alternation between positive and negative quarter-wave retardation. This improves the accuracy of the technique as it avoids spurious mechanical modulations of the light at the same frequency of the modulation of the signal. Any speck of dust or imperfection in a rotating wave plate introduces such a modulation, giving rise to a spurious signal.

In stellar astronomy, the principle of this magnetograph has been applied to the detection of magnetic fields by Babcock (1955), Angel and Landstreet (1970) and Severny (1970).

The photoelectric measurement of magnetic fields presents several advantages over photographic techniques. It is not limited to sharp-lined stars. It can measure much weaker fields as it does not suffer from saturation, in other words, longer integration times yield a higher signal to noise ratio. It has the advantage of high quantum efficiency and linearity, so that it is possible to do much more precise measurements. The main advantage that the photographic technique has is the much larger spectral region observed in a single exposure; however, television and image dissector techniques may soon eliminate this advantage.

II. THE COUDE POLARIMETER

1) Principle of operation

Figure 2 illustrates the principle of operation of the polarizing optics.

The first element is a Babinet-Soleil compensator (BSC), a variable retardation plate. Adjusting its thickness with a micrometer screw varies the retardation it introduces on the light entering its faces. The compensator is used to cancel the phase shifts introduced by the telescope through oblique reflections from metallic mirrors in the coudé optical train (chapter IV). Thus, the compensator restores the polarization entering the telescope. The second element is an electro-optic crystal (EOM) which exhibits the Pockel effect. When an electric field is applied to the faces of the crystal, it acts as a retardation plate. The retardation is proportional to the voltage applied and reverses sign when reversing the sign of the field. The third element is a linear polarizer (P) which transmits light linearly polarized along its transmission axis and extinguishes light linearly polarized perpendicular to it.

Let us examine the operation of the optics when used to measure circular polarization. When the compensator is adjusted correctly, the light entering the face of the electro-optic crystal has the same polarization as it did entering the telescope; the voltage applied to the crystal is such as to give a quarter-wave retardation. Thus L.C.P.

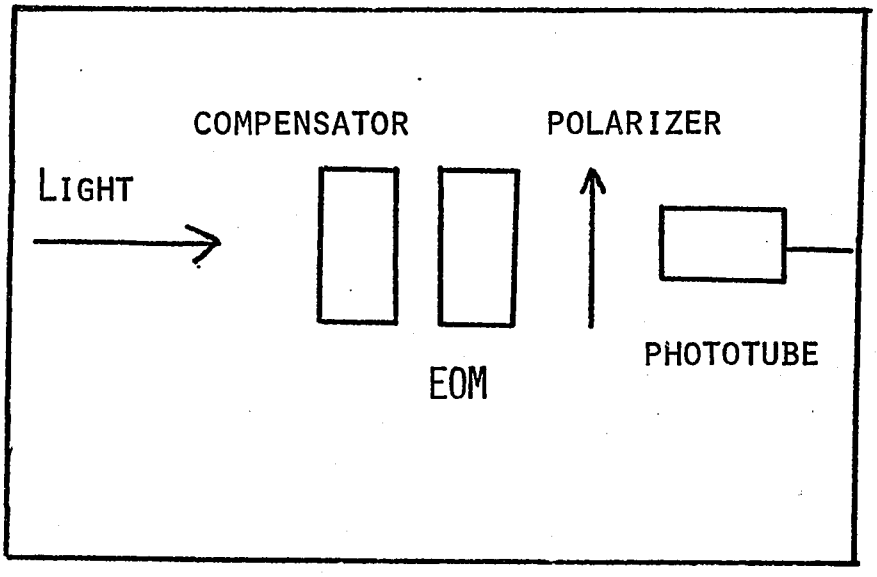

FIGURE 2

The polarizing optics of the polarimeter are shown schematically.

light entering the crystal is transformed into light linearly polarized with the electric vector at 45° with one of the axes of the crystal. The R.C.P. light is transformed into linear at -45° to the same axis. The unpolarized component of the light is unaffected by the quarter-wave plate. The linear polarizer is oriented with its transmission axis at 45° to the same axis of the crystal, thus it will transmit the linearly polarized light which entered the crystal as L.C.P. The R.C.P. component is extinguished by the linear polarizer as it is now linearly polarized perpendicular to the transmission axis. Reversing the sign of the field we now admit the R.C.P. component and extinguish the L.C.P. Thus, by detecting the difference in intensity between measurements of intensity with opposite polarities of the field, we can measure the net circular polarization. When the correct voltage for a $\lambda/4$ retardation is applied to the faces of the crystal, the instrument is insensitive to linear polarization entering the crystal.

The great advantage of this technique devised by Babcock (1953) is that the polarization is detected as a difference in intensity, measured with only one tube, when the crystal polarity is reversed, rather than a difference in intensity between two tubes. If the polarity is switched rapidly enough, the polarimeter is insensitive to drifts in tube sensitivity or changes in intensity due to variable atmospheric extinction, atmospheric

scintillation or guiding errors. In practice we reverse the polarity 1000 times per second.

2) The instrument

Figure 3 gives the lay-out of the polarimeter.

The light beam from the telescope converges at f/30.9. Although the Babinet-Soleil compensator and electro-optic crystal require collimated light, the errors resulting from using an f/30.9 beam are small since light only goes 1° off axis. The electro-optic crystal used is potassium dideuterium phosphate (KD*P), which has the advantage of requiring a voltage per retardation lower than any other electro-optic material. The theory and experimental properties of electro-optic crystals can be found in the literature (Billings $1949_{a,b}$). Two different crystal units were used. One, an Isomet crystal, had gold grid electrodes. The other, a Lasermetrics 402A, uses conductive film electrodes. The second crystal has a MgF antireflection coating and higher transmission (90% against 40%). The linear polarizer is a Lambrecht UV Glan-Thompson prism with anti-reflection coating which is oriented, with respect to the grating grooves, to give the highest efficiency.

The polarizing optics are placed before the entrance slit to the spectrograph in order to reduce spurious polarization and phase shifts due to reflections to a minimum. The dispersive element is a coudé spectrograph used with a line profile scanner at a dispersion of

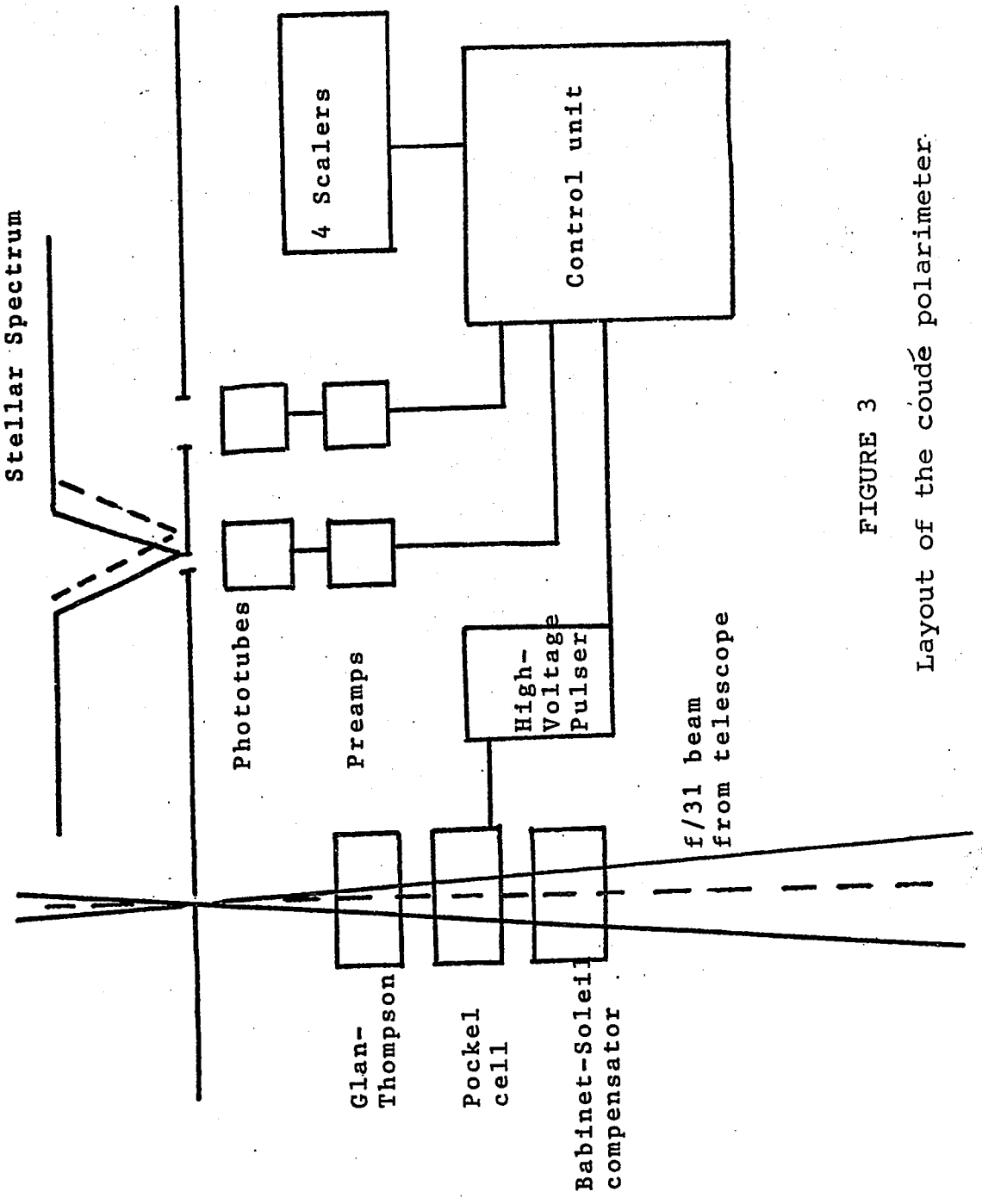

FIGURE 3

Layout of the coudé polarimeter

.9 Å/mm. The line profile scanner used at the University of Western Ontario has been described by Gray and Wehlau (1972). A fixed photomultiplier monitors a large band in the continuum while the second photomultiplier is moveable on a precision table and can scan the line profile. The photomultipliers are ITT FW 130 tubes with S-20 cathodes. Their output is amplified and shaped by SSR pulse-counting preamplifiers and discriminators.

A control unit does the necessary gating, switching and timing. The amplified pulses from each photomultiplier pass through gates which are open only after a time delay to ensure that the voltage applied to the crystal has risen to the correct steady value. Thus, transients during the switching are not detected. A gate is open only when one polarity is applied to the crystal, channeling the pulses to the appropriate scaler recording one sign of polarization. When the polarity of the voltage is reversed, the gate is closed and another gate is opened, the pulses are channeled to another scaler counting the opposite sign of polarization. A crystal clock sets the switching period and ensures that each gate is open for exactly the same period of time. The net polarization is detected as a difference of counts in the two scalers. A set of two scalers monitors the profile, another set of two monitors the continuum. A high voltage pulser driven by the control unit provides square pulses of adjustable amplitude to the electro-

optic crystal.

The efficiency may be improved by eliminating the Glan-Thompson prism and replacing it by a block of calcite. One then obtains two slightly separated parallel spectra at the focal plane of the spectrograph. Two adjacent photomultipliers can view the spectral line, each one viewing the opposite polarization sense of the other, during one cycle of the switching.

3) Detecting linear polarization

The polarimeter can measure both linear and circular polarization. Linear polarization can be measured either by introducing a quarter-wave plate in the beam and modulating the crystal $\pm \lambda/4$, or by modulating $0 \rightarrow \lambda/2$ the crystal with the voltage appropriate for a half wave retardation. To be able to determine the total linear polarization and the orientation of the electric vector, one must be able to rotate the quarter-wave plate, or the EOM and polaroid assembly when it is used with a $\lambda/2$ retardation.

CHAPTER III

INSTRUMENTAL POLARIZATION AND PHASE SHIFTS

1) Introduction

In order to interpret the raw data obtained at the telescope, it is vital to have a thorough understanding of the effects introduced on the starlight by the experimental apparatus. As the present work is done at the coudé focus, one has to consider the effects introduced by oblique reflections from metallic mirrors. There are two effects: spurious linear polarization of the unpolarized component and phase shifts of the polarized component.

2) Oblique reflections from metallic mirrors.

It is well known (e.g., Jenkins and White 1957) that oblique reflection of light from a metallic surface will have two effects.

1. The electric vector of the incoming light is resolved into two components, one in the plane of incidence and the other perpendicular to it. The two components are then reflected with a phase difference depending on the angle of incidence.
2. The reflectivity in the plane of incidence is different from the reflectivity in the plane perpendicular to the plane of incidence.

Let us call Δ the phase shift and r_s and r_p the reflection coefficients, respectively, for the parallel (P) and perpendicular (S) components of the electric vector.

The optical properties of a metal can be expressed in terms of η , the index of refraction, and k, the absorption coefficient. We have (Drude 1959)

$$\tan \Delta = \sin Q \tan 2P$$

$$\cos 2\gamma = \cos Q \sin 2P$$

where $\tan Q = k$

$$\tan P = \frac{\eta \sqrt{1+k^2}}{\sin\phi \tan\phi}$$

where ϕ is the angle of incidence

$$\tan \gamma = r_p / r_s$$

and $\Delta = \delta_p - \delta_s$ is the phase difference between the p and s components. These formulae are approximations in that terms with $\sin^2\phi$ have been omitted. However, they are accurate enough for our purposes, as $\sin^2\phi \ll \eta^2+\eta^2k^2 \approx 30$. The optical constants of aluminum have been determined experimentally by several authors (O'Bryan 1936, Schulz 1954, Schulz and Tangherlini 1954, Hass and Waylonis 1961). These coefficients are wave-length dependent (figure 4), so we can expect a wavelength dependence of phase shifts and instrumental polarization.

One sees statements in the astronomical literature (Babcock 1962, Gollnow 1965) that the phase shifts depend on thickness, structure, age and state of cleanliness of

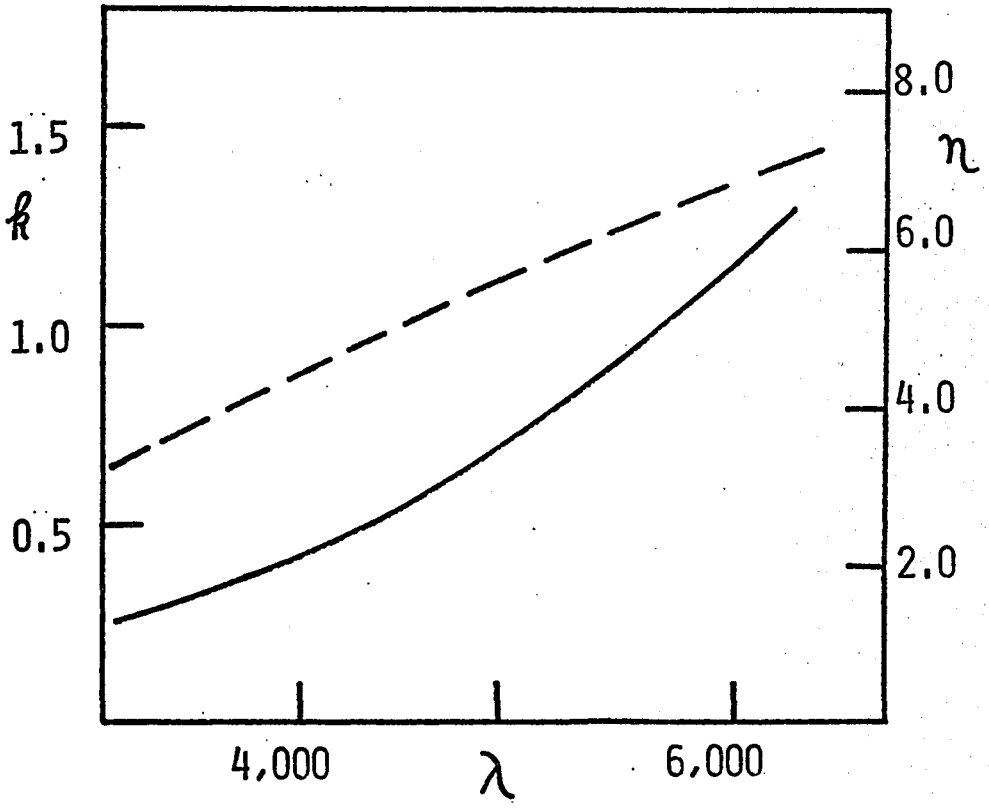

FIGURE 4

Wavelength dependence of the index of refraction (dashed line) and the absorption coefficient k (full line) for solid oxide-free aluminum (Hass and Waylonis 1961).

the aluminum coating. Indeed, Schulz and Tangherlini (1954) find changes with ageing and annealing for n (but not for k; Schulz 1954). However, among the metals they consider, aluminum is the one presenting the smallest changes with age. Moreover, Schulz found that ageing and annealing made all of the samples equal as they removed strains and crystal defects responsible for the differences. Hass and Waylonis (1961) found that the optical constants of aluminum films evaporated at high speed remain unchanged down to a film thickness of about 100 Å. This is considerably smaller than the thickness of an opaque layer. Therefore, we do not expect changes with thickness for the typical opaque mirrors used in telescopes.

3) Phase shifts determined experimentally.

To determine what parameters of a mirror strongly affect phase shifts, I have measured the phase shifts of several aluminized mirrors accessible inside the coudé room and along the coudé path. The phase shifts were determined by illuminating the mirror at a known angle of incidence, with light of a known wavelength. A suitably oriented polaroid was placed in front of the light source. The reflected beam was viewed through a Babinet-Soleil compensator and a second polaroid crossing the first one. The thickness of the Babinet-Soleil compensator was adjusted to obtain minimum light, thus compensating the phase

shifts introduced by the mirror. The minima were determined visually. The wavelength selection at 5100 Å, 4850 Å and 3870 Å was obtained with an incandescent bulb and interference filters. The measurements at 6300 Å were obtained using a laser.

a) Uniformity of phase shifts on different parts of a mirror

The camera mirror of the line profile scanner was chosen because its aluminum coating had a highly non-uniform appearance. Using the laser as a light source, I sampled several spots on the mirror. Figures 5a and 5b show the phase shifts registered for different spots on the mirror for angles of incidence of 60 and 70 degrees. The laser was used as it gives a narrow collimated and monochromatic beam. We can see that there are no noticeable differences within the experimental accuracy of $\pm$ .007 λ .

b) Wavelength dependence.

Figures 6a, 6b, 6c, 6d show the phase shifts as a function of angle of incidence for the wavelengths of 6300, 5100, 4850, 3870 Å. The mirror illustrated is the flat mirror of the line profile scanner. The phase shifts become lower for shorter wavelengths. The crosses in the figure are the phase shifts computed through equation (3). The agreement between theoretical and experimental values is satisfactory around 5000 Å but poor at longer and shorter wavelengths. This is probably

FIGURES 5a, 5b

Phase shifts as a function of position on the surface of a mirror with a highly non-uniform appearance. The position in cm. (arbitrary zero point) locates the point of incidence of the beam on the mirror surface. The wavelength is 6300 A. Angles of incidence of 60° and 70° are illustrated. The crosses and points indicate two consecutive measurements.

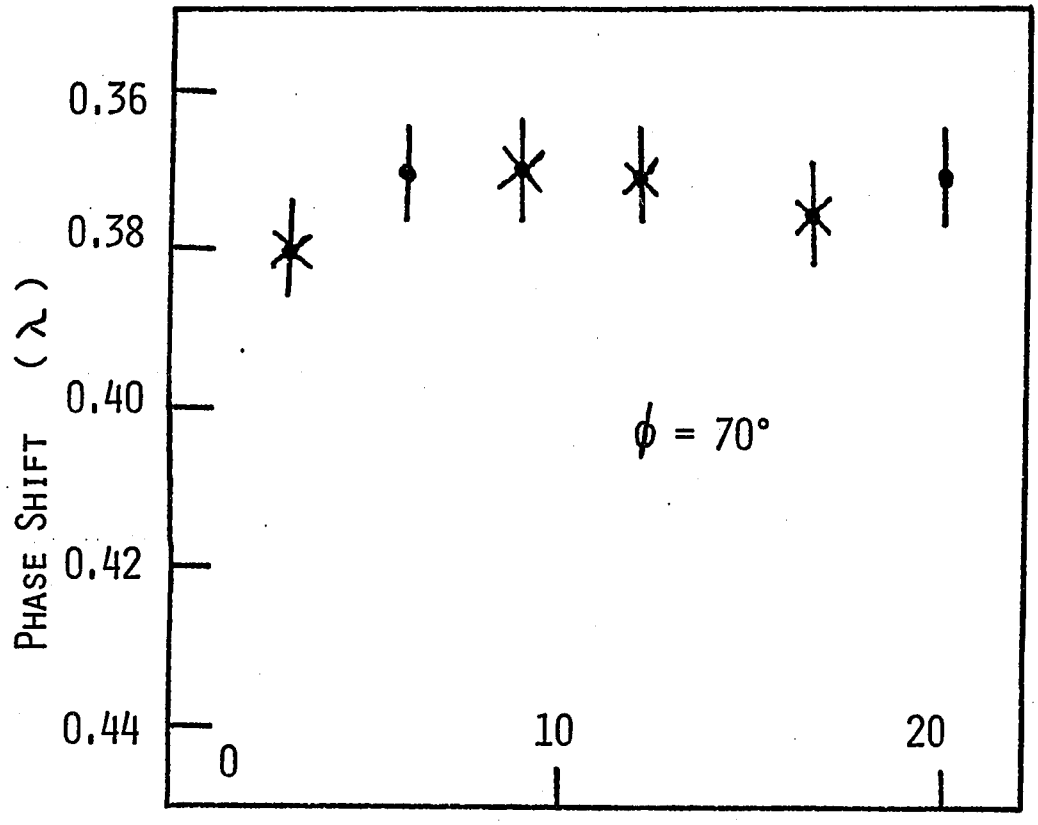
0.36
0.38
0.40
0.42
0.44
PHASE SHIFT (λ)
φ = 70°
0
10
20

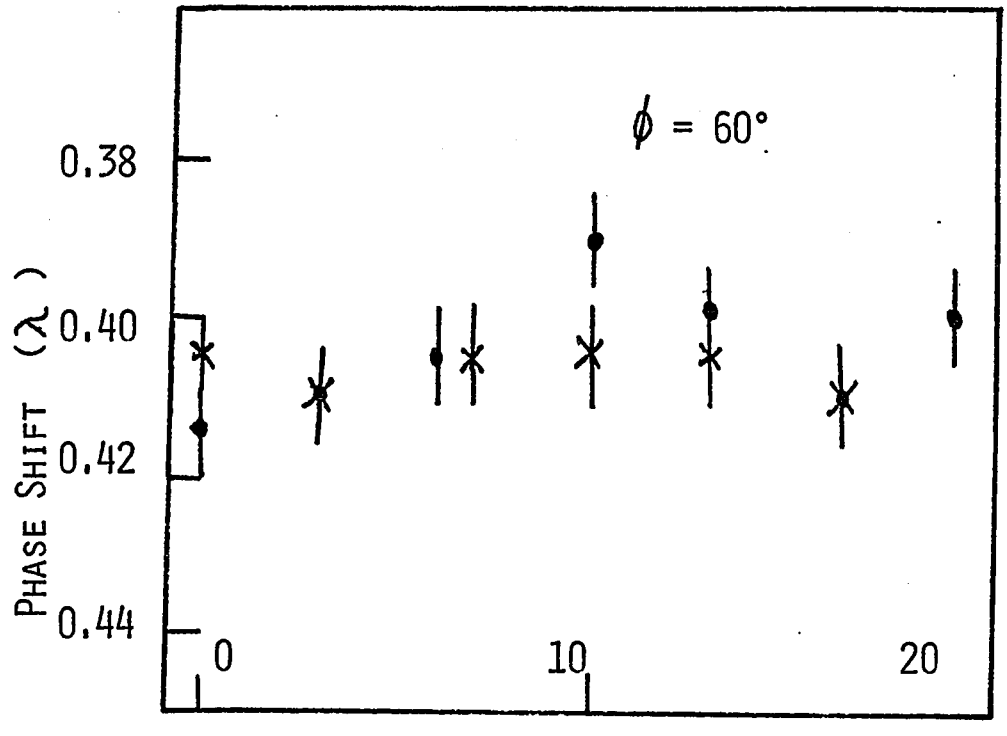
φ = 60°
0.38
0.40
0.42
0.44
PHASE SHIFT (λ)
0
10
20

FIGURES 6a, 6b, 6c, 6d

Phase shifts as a function of the angle of incidence for four wavelengths. The points indicate experimental values, the crosses theoretical ones.

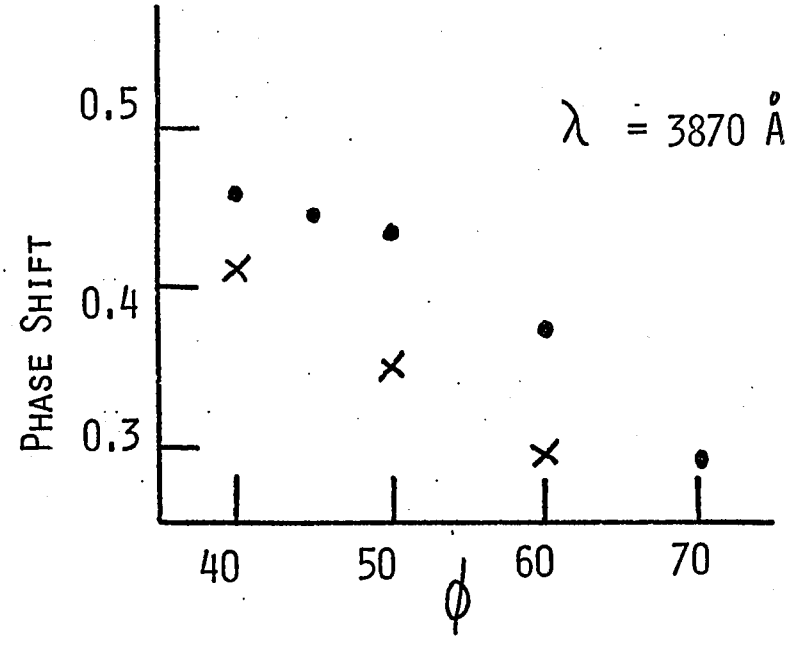
0.5
0.4
0.3
PHASE SHIFT
λ = 3870 Å
40
50
60
70
φ

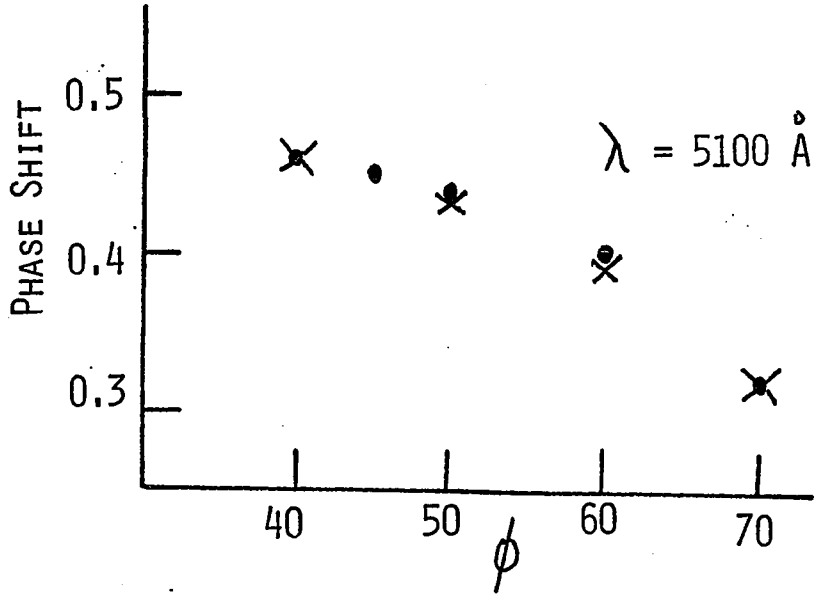
0.5
0.4
0.3
PHASE SHIFT
λ = 5100 Å
40
50
60
70
φ

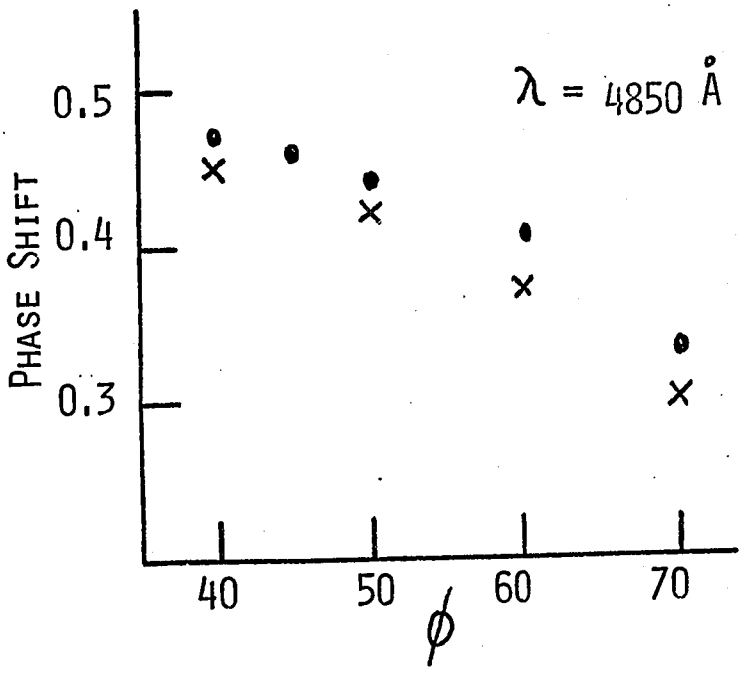
λ = 4850 Å
PHASE SHIFT
0.5
0.4
0.3
40
50
60
70
φ

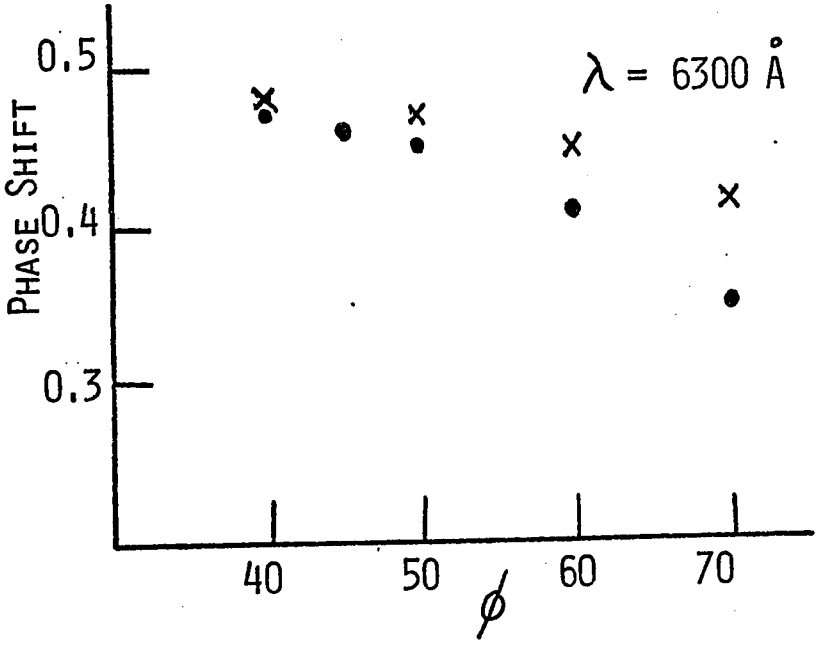
λ = 6300 Å
PHASE SHIFT
0.5
0.4
0.3
40
50
60
70
φ

due to the fact that the optical coefficients used are for oxide-free metals.

Table I lists the experimental phase shifts in units of one wavelength for angles of incidence of 60° and 70° and for the four wavelengths. The variation of phase shift with wavelength is noticeable at 70° but decreases with the angle of incidence. At 45° there is not a significant difference ($.01 \pm .007 \lambda$) going from a wavelength of 3900 Å to 6300 Å.

c) Differences between mirrors

I have measured the phase shifts as a function of angle of incidence and wavelength for four mirrors accessible along the coudé system of the 48-inch telescope at the University of Western Ontario. Similarly, I have measured the phase shifts for the flat mirror of the 100-inch telescope at Mt. Wilson. The mirrors examined are in various states of age, oxidation and cleanliness. The mirrors at the University of Western Ontario measured before aluminizing have the original coating from various manufacturers. The mirror of the 100-inch has been aluminized at Mt. Wilson.

Within the experimental accuracy, the phase shifts for a given wavelength and angle of incidence are the same for all mirrors. As all the curves are the same as the ones in figures 6a, 6b, 6c, 6d they are not reproduced here. Preston (private communication) finds no

TABLE 1

PHASE SHIFTS DETERMINED EXPERIMENTALLY

Angles of incidence		Wavelengths
60°	70°	
0.37	0.29	3870 Å
0.39	0.325	4850 Å
0.395	0.325	5100 Å
0.41	0.345	6300 Å

difference between the phase shifts of the Mt. Wilson 100-inch, the Mt. Palomar 200-inch and the Lick 120-inch, confirming our conclusion.

d) Ageing effect

The mirrors of the 48-inch telescope were aluminized in the week beginning April 10, 1972. Two weeks later I checked the phase shifts of number five mirror. Table 2 lists the phase shifts in units of one wavelength. The wavelength is 6300 Å.

Comparing table 2 to table 1 we can see that the phase shifts after aluminizing are larger and closer to the phase shifts determined using equation 3 and oxide-free values for the optical constants of aluminum (see figure 6d).

Two months after aluminizing I measured again the phase shifts for all four mirrors using a wavelength of 6300 Å. The phase shifts measured are the same as in table 2. We must conclude that indeed there are ageing effects. From the conclusions reached in the previous section, it is probable that ageing will slowly modify the phase shifts to the values of figures 6a, 6b, 6c, 6d.

4) Spurious linear polarization

Because of the different reflectances in the p and s planes, an oblique reflection will introduce a spurious linear polarization. From equation 3 we see that the

TABLE 2

PHASE SHIFTS DETERMINED EXPERIMENTALLY

SHORTLY AFTER ALUMINIZING (WAVELENGTH 6300 Å)

Angles of incidence	Phase shifts
40°	0.47
45°	0.465
50°	0.46
60°	0.43
70°	0.385

polarization will depend on the angle of incidence, and through the optical constants, on the wavelength. Figure 7 shows the ratio of the reflection coefficients as a function of the angle of incidence and for a wavelength of 4850 Å .

I did not investigate the spurious linear polarization in the same manner as the phase shifts for two reasons. First, it requires more precise and elaborate equipment. Secondly, it is easy to subtract the spurious polarization from the signal by observing the stellar continuum. This last procedure has the additional advantage of removing as well the interstellar polarization from the signal.

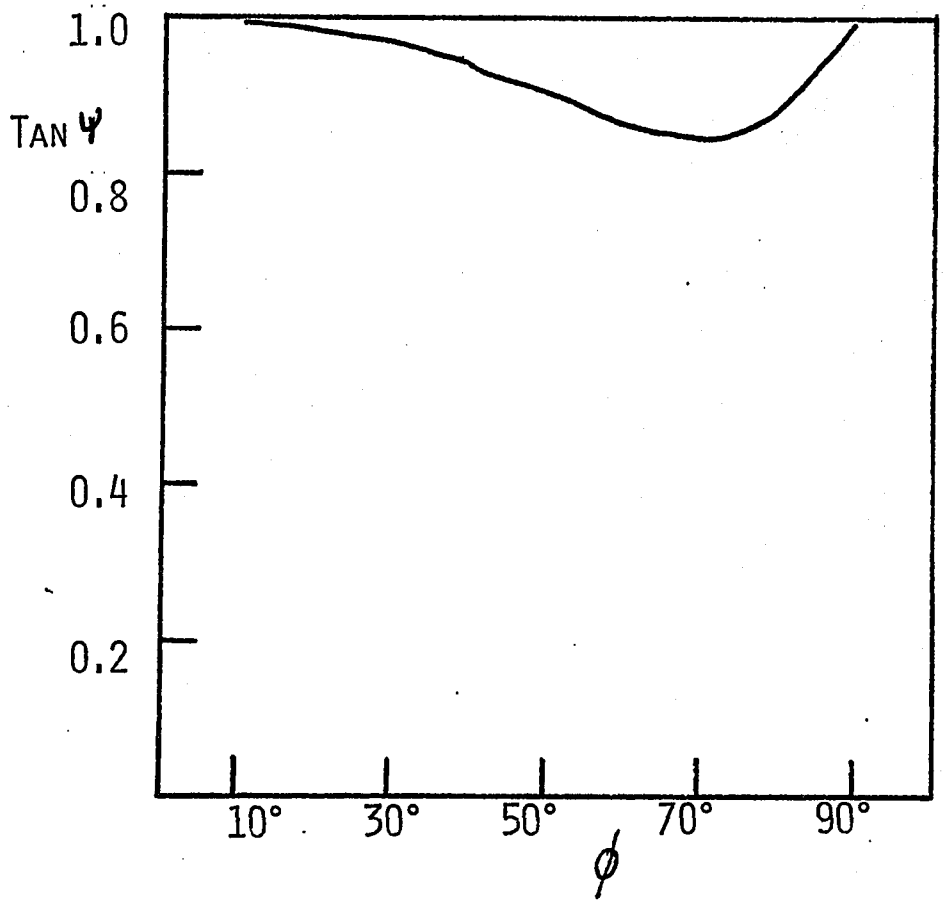

FIGURE 7

The ratio $\tan\Psi = r_1/r_3$ is plotted as a function of angle of incidence. The wavelength is 4850 Å.

CHAPTER IV

PHASE SHIFTS AND INSTRUMENTAL POLARIZATION FOR THE 48-INCH TELESCOPE OF THE UNIVERSITY OF WESTERN ONTARIO

1) Introduction

The coudé system of the 48-inch telescope is a five mirror system. It involves two normal reflections and three oblique reflections at 45° (Wehlau 1970). The first two reflections from the primary and the secondary are essentially normal to the aluminum surfaces. Each reflection introduces a 180° phase shift and the two reflections cancel each other.

Three flat mirrors are used to bring the starlight from the secondary down to the coudé spectrograph. The reflections are at 45° and the angles of incidence do not change as the telescope swings in hour angle and declination. Therefore, the phase shifts Δ and the reflection coefficients r_s and r_p do not change for each individual mirror. What will change with hour angle and declination are the relative orientations of the fast axis and transmission axis of the mirrors considered as retarders and polarizers. Essentially the problem is the problem of having three retardation plates and polarizers rotating with respect to each other. The problem can be tackled in two different ways. One can make use of Mueller calculus solving the matrix algebra problem or one can follow

analytically the electromagnetic wave from mirror to mirror, keeping track of thephase shifts and amplitudes of the electric vectors. The first method is easier for computations and is more powerful. The second one is intuitively easier to understand. As the apparatus has been used only to measure circular polarization, I have used the analytical approach for the case of circularly polarized light in appendix I.

2) Mueller matrices for the 48-inch telescope

Mirrors 3, 4, and 5 can be represented each by the product of two Mueller matrices. [M] will be appropriate for the mirror as a retardation plate, [P] for the mirror as a polarizer.

Let [I] be the Stokes vector for the incoming beam,

$$[I] = \{I, Q, U, V\}$$

Let [M3] , [M4] , [M5] and [P3] , [P4] , [P5] be the Mueller matrices for mirrors 3, 4, and 5 respectively. The Stokes vector off mirror 5 can be represented by [I'] with

$$[P5] \times [M5] \times [P4] \times [M4] \times [P3] \times [M3] \times [I] = [I'] \qquad (5)$$

We have that $[P_i] \times [M_i] = [M_i] \times [P_i]$, as the transmission axes of the mirror as a polarizer are also the fast and slow axes of the mirror as a retardation plate. Note that the whole telescope could be represented by a single Mueller matrix, product of the six matrices in equation 5. The Mueller matrices [P] and [M] are

derived in appendix II.

The retardance Δ and the reflection coefficients r_s and r_p are constant for each mirror. The problem is therefore reduced to finding the angles ρ and θ for each mirror, where ρ and θ are respectively, the angle of the fast axis and the angle of the highest transmission axis of a mirror, with respect to the principal direction (appendix II).

The principal direction chosen will be contained in the plane of incidence of the light on mirror # 5. The Stokes parameters are measured with respect to this direction.

For mirror 3 $\rho = H.A. - 90° + DEC.$

For mirror 4 $\rho = H.A.$

For mirror 5 $\rho = 0°$

$\theta = \rho + 90°$

I have used the Mueller matrices to examine the effects introduced by the telescope on different types of polarization. The results are discussed in the next sections.

3) Modifications to circularly polarized light.

Figure 8 shows the V Stokes parameter resulting from a R.C.P. beam $\{1,0,0,1\}$ entering the telescope for a few declinations. The phase shift Δ and reflection coefficients r_s and r_p for each mirror are the theoretical ones from equation 3 and for a wavelength of 5200 Å. We can see that there usually is a significant

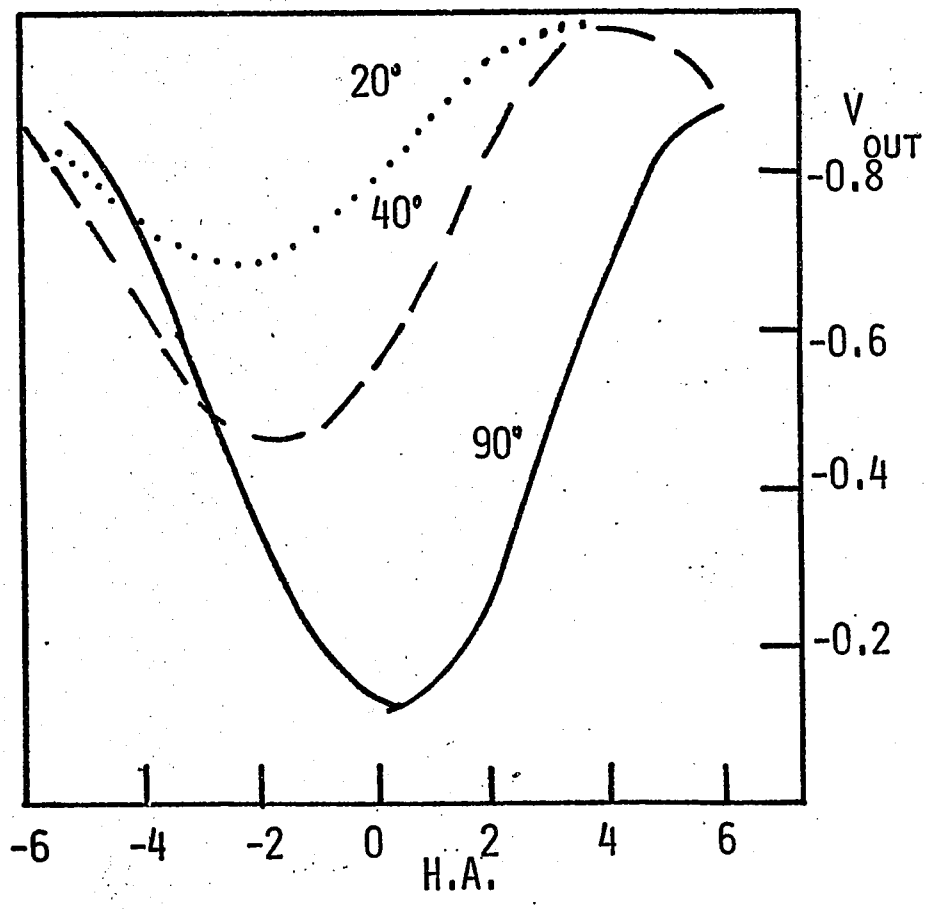

FIGURE 8

Circular polarization for light leaving mirror number five (V_{out}) for a pure right circularly polarized beam entering the telescope $\{1,0,0,1\}$. V_{out} is a function of hour angle and declination.

loss of V signal, the loss being a function of hour angle and declination. The loss decreases with decreasing declination. For a declination of 0.0 degrees V does not vary with H.A. and is constant at -0.88 .

It is possible to apply numerical corrections to the raw data; however, in practice it is preferable to compensate optically for the phase shifts. The reason for doing this is that, when observing stellar fields, the signal to noise ratio is low. A loss of, say 50% of the signal, might mean going from a signal to noise ratio of 3 to 1.5 . Therefore, at all effects we have a complete loss of the signal which is now buried in the noise.

To correct optically for the phase shifts we make use of a Babinet-Soleil compensator. Figure 9 shows some compensation curves determined experimentally. A laser was placed on the spider holding the secondary mirror. A circular polarizer (polaroid and $\lambda/4$ plate) was placed in front of the laser. The laser light was then viewed at the slit area with the compensator, a $\lambda/4$ plate and a polaroid. When the compensator gives the correct compensation it restores circular polarization, which the $\lambda/4$ plate subsequently turns into linear, which is then extinguished by the polaroid. Thus, correct compensation gives zero light intensity. This visual method is cheap, easy to set up, and when using a bright, collimated light source such as a laser, very accurate, well within the accuracy of the compensator itself. Figure 10 shows the

FIGURE 9

Experimental compensation curves as a function of hour angle for four representative declinations.

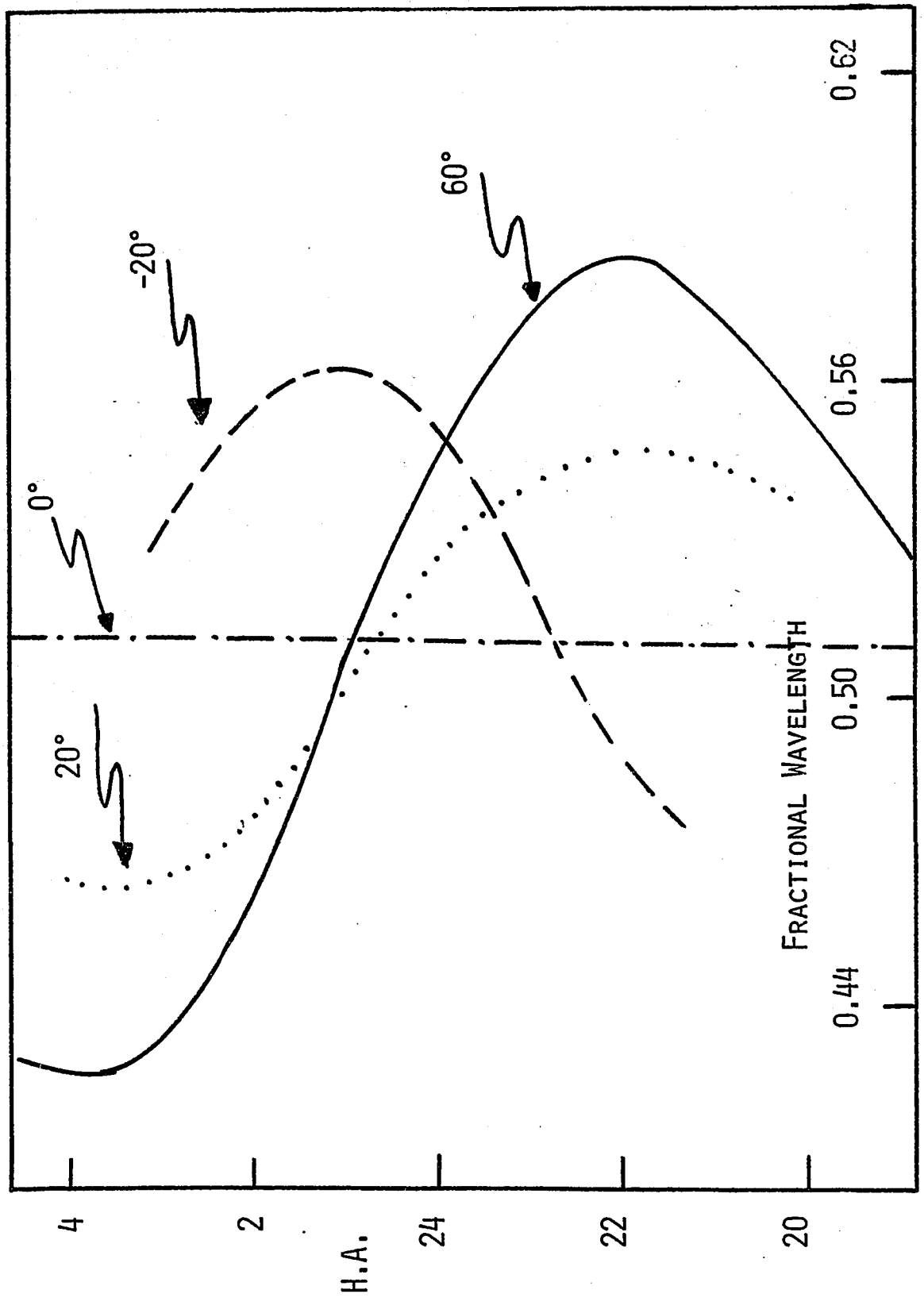
0°
20°
-20°
60°
0.62
0.56
0.50
0.44
FRACTIONAL WAVELENGTH
4
2
24
22
20
H.A.

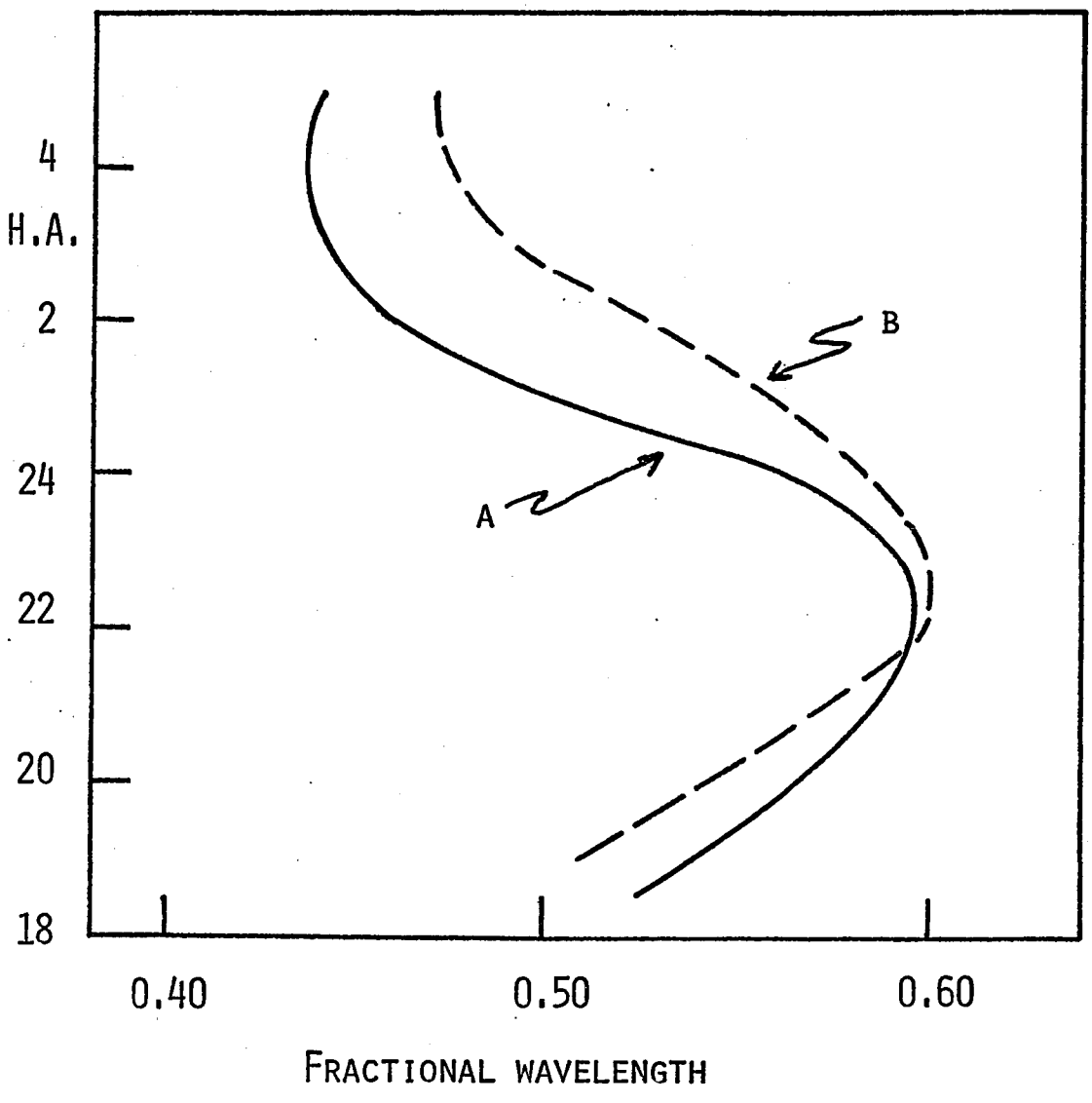

FIGURE 10

Theoretical (curve b) and experimental compensation curves as a function of hour angle for a declination of 60° .

compensation curves determined theoretically (curve b) and experimentally (curve a) for a declination of 60°. The agreement is satisfactory, the differences can be explained by the fact that the circular polarizer is not perfect and the fact that η_s and η_p in the theoretical curve b are computed through equation 3. (the retardation Δ is experimental).

4) Instrumental polarization

Figure 11 shows the V signal resulting from an unpolarized $\{1,0,0,0\}$ input beam. We can see a sizeable spurious circular polarization varying with H.A. and declination. In practice we have an additional phase shifter in the compensator. Figure 12, curve (a) shows the theoretical instrumental circular polarization at a declination of 40 degrees when the compensation is applied. Curve b in figure 12 shows the instrumental polarization measured in Vega (declination +39°) for a wavelength of 4300 Å. The qualitative agreement with the theoretical curve b is good. The residual differences are mostly due to the fact that η_s and η_p are the theoretical ones for curve a .

5) Linear to circular conversion

Figure 13 shows the spurious V parameter resulting from an input linearly polarized $\{1,0,1,0\}$ beam. The curves for $\{1,1,0,0\}$ input are very similar in appearance. We can see a sizeable conversion from linear to

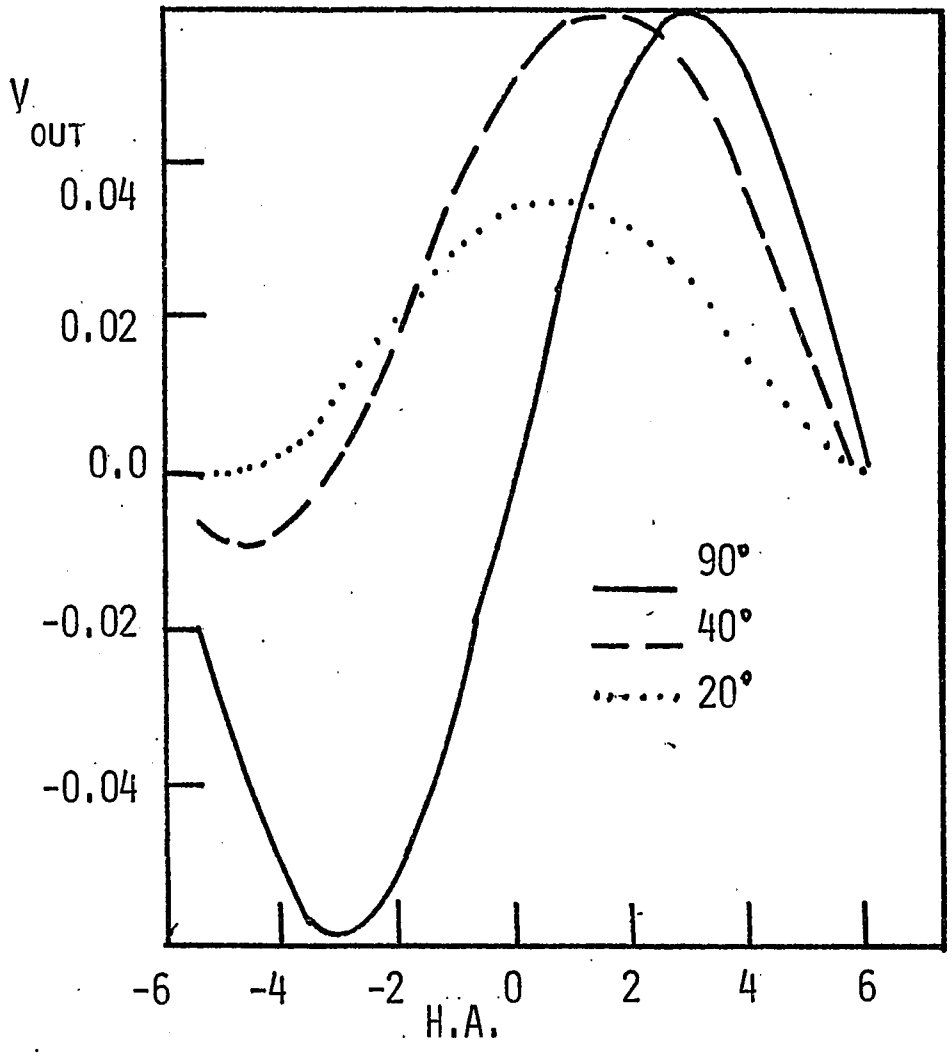

FIGURE 11

Spurious circular polarization resulting from an unpolarized input beam $\{1,0,0,0\}$ as a function of H.A.

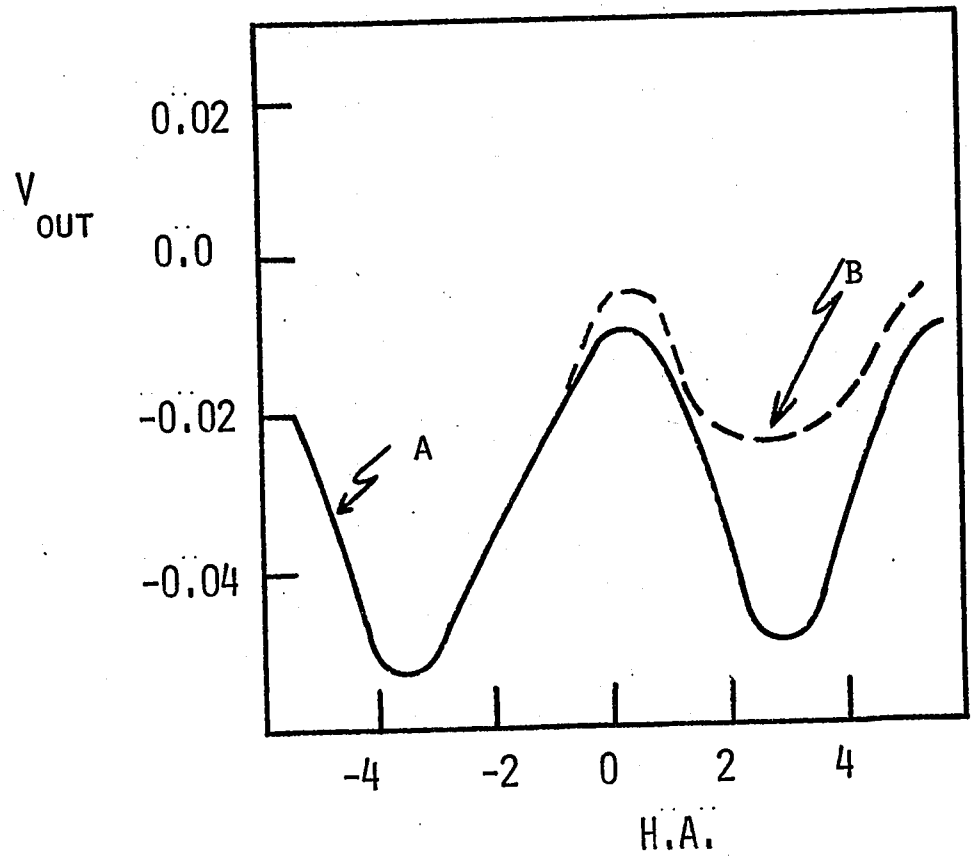

FIGURE 12

Spurious circular polarization resulting from an unpolarized input beam when the compensation is applied. Curve a is obtained theoretically for a declination of 40° , curve b is determined experimentally by observing the continuum in Vega (+39°) .

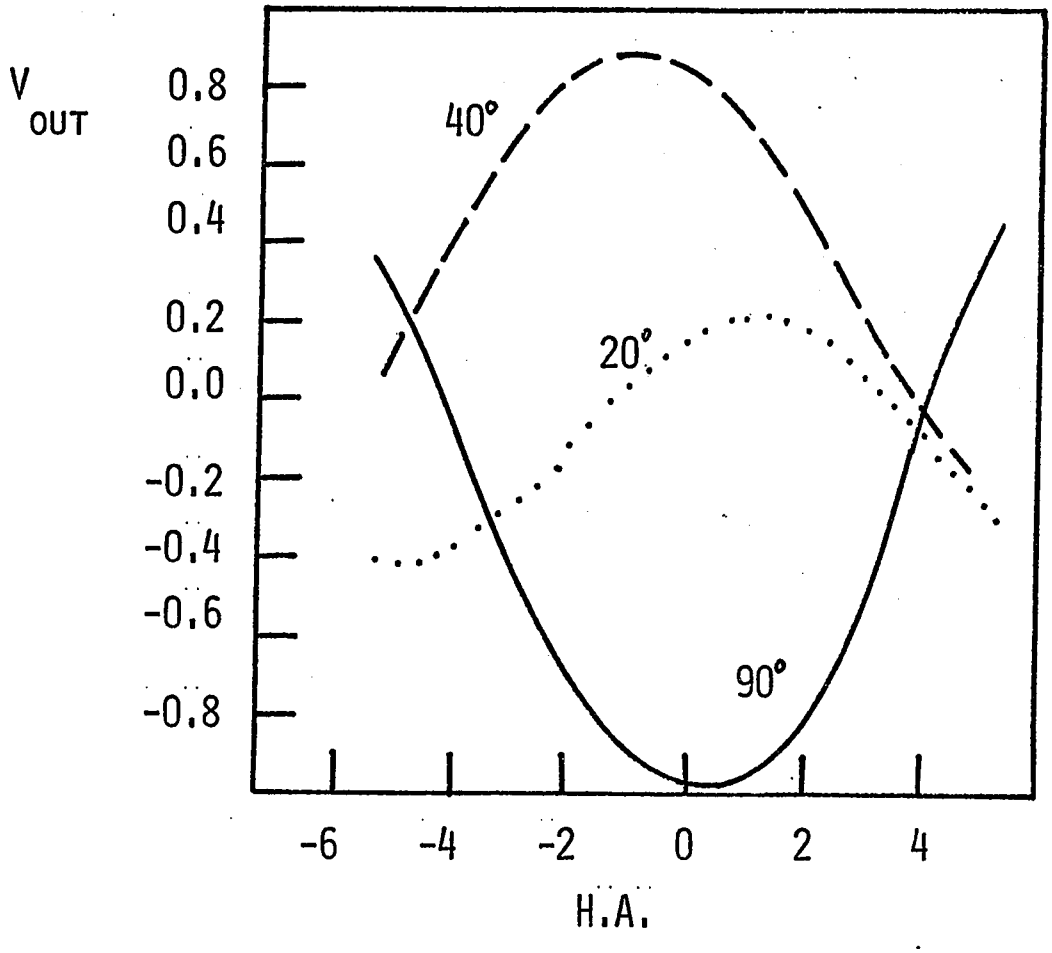

FIGURE 13

Spurious circular polarization for a linearly polarized input beam $\{1,0,1,0\}$.

circular, varying with H.A. and decreasing with declination. We can therefore expect a V signal coming from converted interstellar polarization, superimposed on the instrumental polarization. Figure 14 shows the V signal from $\{1,0,1,0\}$ input for a declination of 40° when the compensation is applied.

6) Impossibility of complete compensation

It is possible to obtain circular polarization from a compensator with eigen axes parallel to the s and p planes of mirror 5 only if the electric vectors in the s and p planes of mirror 5 are equal. If the vectors are not equal, restoring a phase difference of 90° will not give circular but rather elliptical polarization. Figure 15 shows the electric vectors in the s and p planes of mirror 5 as a function of H.A. for L.C.P. input light and a declination of 40 degrees. We can see that they are generally not equal. This arises partly because the reflection coefficients in the s and p planes are not equal and partly because mirrors 4 and 5 usually see elliptically polarized light and not circular.

It would appear possible to cure the problem by rotating the compensator by an appropriate angle. However, there is no unique thickness and orientation of the compensator that will restore completely both the L.C.P. and R.C.P. light. This may be shown analytically. However, the demonstration involves exceedingly long and cumber-

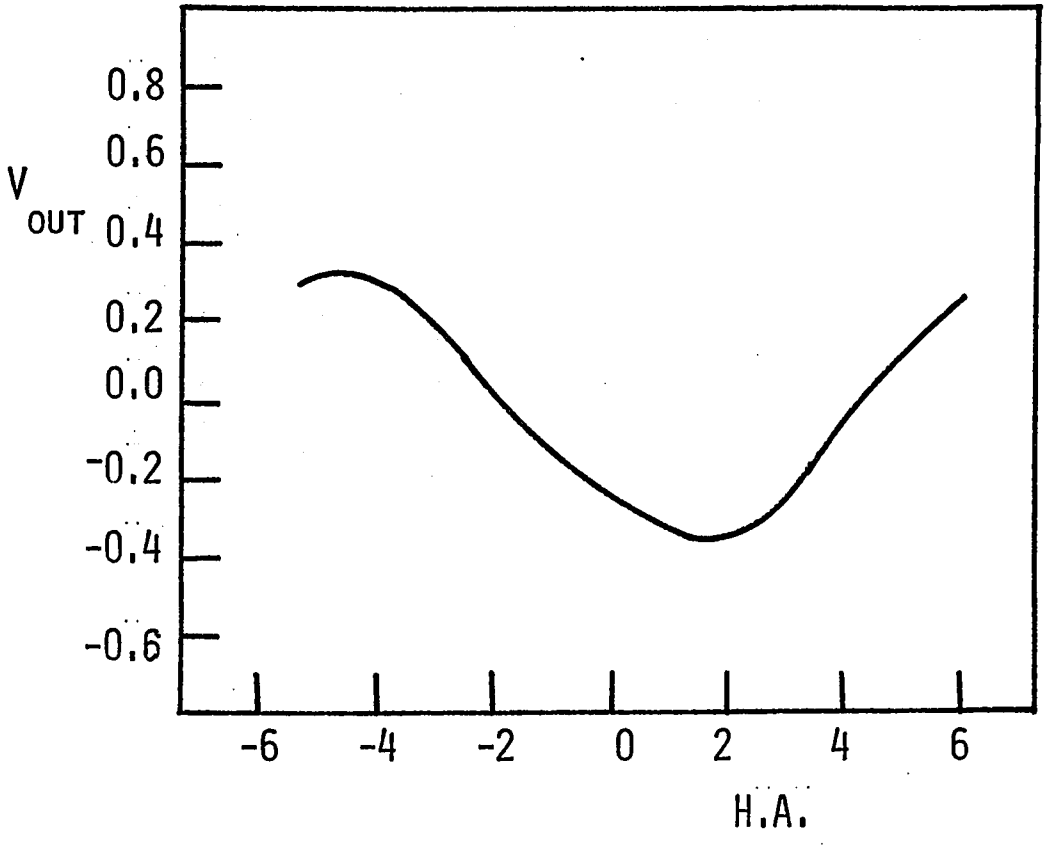

FIGURE 14

Spurious circular polarization for a linearly polarized input beam $\{1,0,1,0\}$ when the compensation is applied. The declination is + 40° .

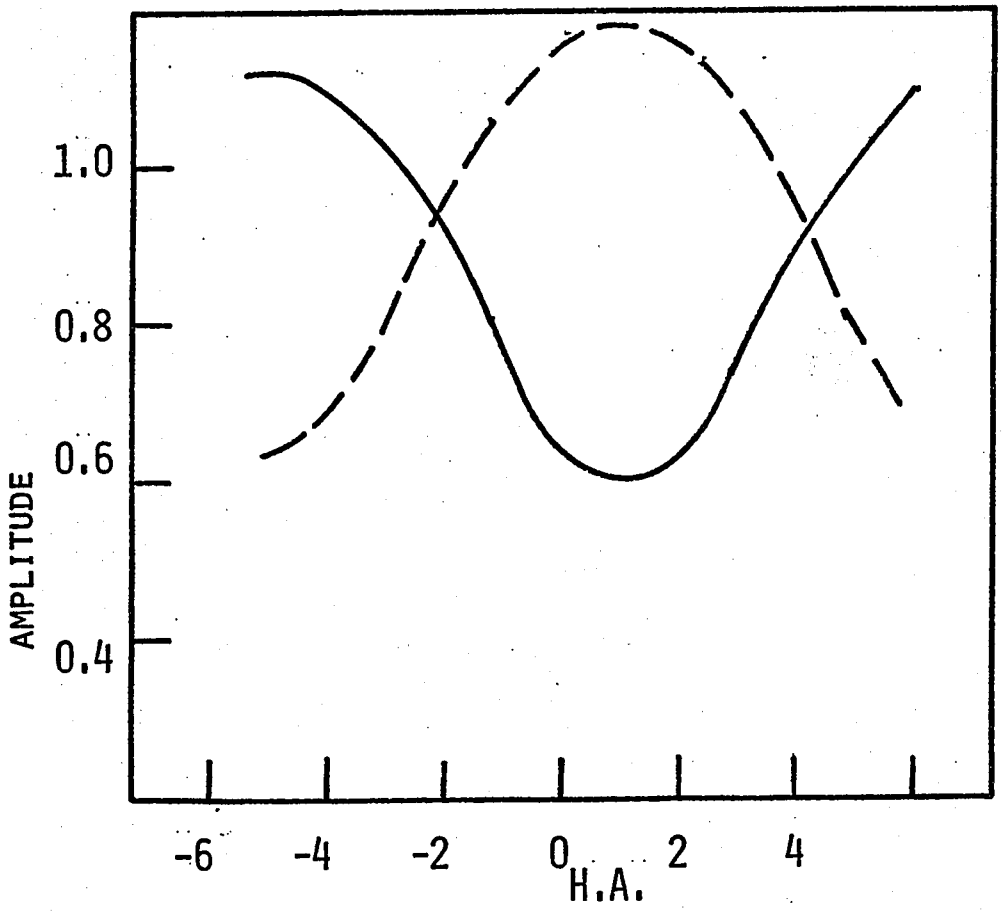

FIGURE 15

Amplitudes of the electric vectors (arbitrary units) in the p and s planes of mirror number 5 for a pure left circularly polarized input beam. The declination is + 40° .

some algebra and I will not reproduce it here. It is easy to understand the problem intuitivelly. Consider two beams, one L.C.P. and the other R.C.P., entering the telescope, andlet us view them after mirror 5. The amplitudes of the electric vectors in the p and s planes will be the same for the two beams. But, because the handedness are of opposite sign, the major axes of the polarization ellipses will be inclined in opposite directions. Therefore, if the compensator, with a retardation d , is rotated at an angle θ to the plane of incidence of number 5 mirror, to compensate one sign of polarization, it should be rotated to an angle $-\theta$ to compensate the opposite sign of polarization. It is therefore not possible to compensate completely both handedness at the same time. The same problem has been discussed by Preston and Pyper (1965).

In practice, the azimuth of the compensator is therefore held fixed, its axis parallel to the axis of mirror 5. We have thus a loss of V signal even in our compensated beam. Figure 16 shows the V parameter for input $\{1,0,0,-1\}$, the compensator set to restore 90° phase difference and for a declination of 40° . We can see that the loss of signal is usually very small and the correction can be applied numerically. The loss of signal increases with the absolute value of the declination and is negligible for declination zero degrees

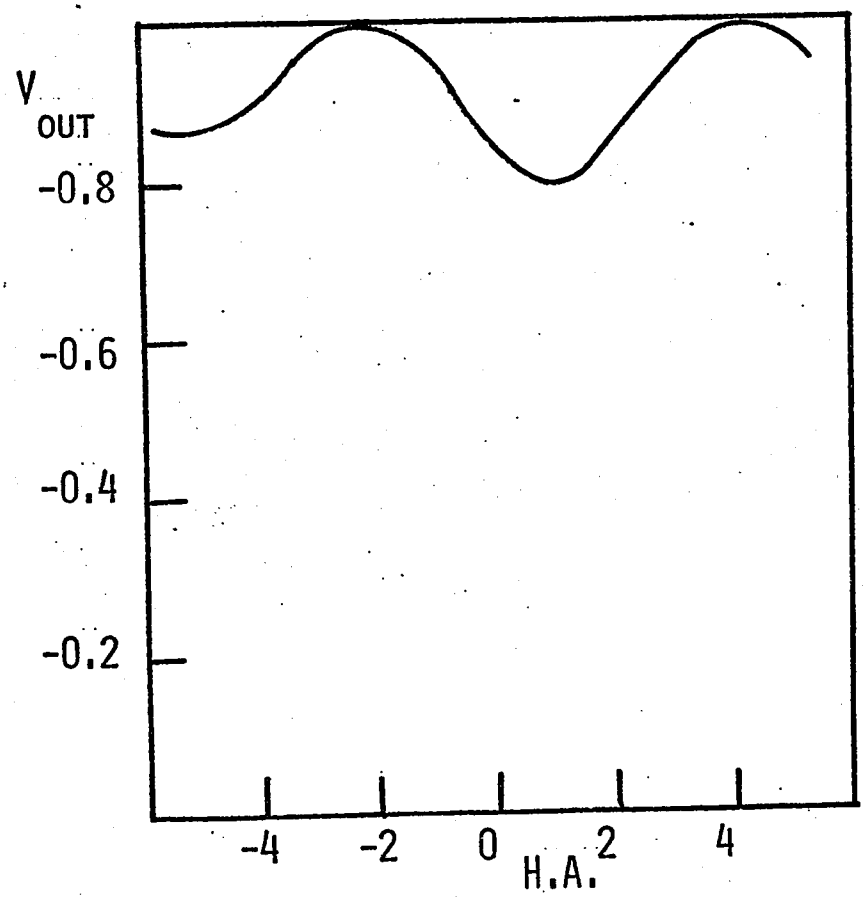

FIGURE 16

Restored circular polarization when the compensation is applied. Notice that usually one does not obtain 100% circular polarization.

7) Conclusion

From the previous discussions it appears that a complicated mirror system is not the ideal for polarization measurements. However, a careful consideration of the problem permits one to overcome many of the difficulties. Very accurate absolute polarimetry is still probably impossible to achieve with such a coudé system, but measurements of variation of polarization with wavelength over limited spectral regions can have high accuracy. Solar physicists do measure magnetic fields with solar towers which have usually a complicated mirror system.

CHAPTER V

EFFICIENCY OF THE POLARIMETER AS A ZEEMAN ANALYZER

1) Longitudinal fields

It is instructive to examine analytically the behavior of the signal to noise ratio in the case in which the polarimeter is used to measure the longitudinal component of the magnetic field.

Let us assume, in a simple case, that we have a purely longitudinal field in the star observed, and that the line is split into the two undistorted σ components of a normal Zeeman triplet. The L.C.P. component is obtained by displacing the line profile $+\delta\lambda$ and the R.C.P. component by displacing it $-\delta\lambda$. Note that if the field lines are inclined to the line of sight, this simplified picture does not apply, unless the line and the magnetic field are weak (Bray and Loughhead 1965, chapter V).

The number of left circularly polarized photons at a wavelength λ and seen through a bandpass $\Delta\lambda$ with an integration time t and an efficiency of the detector Q is given by

$$N_L(\lambda) = \frac{1}{2} N I(\lambda-\delta\lambda) \Delta\lambda Q t \quad (6)$$

N is the number of photons on the continuum per $\mathring{A}$ per unit time falling on the detector, I(λ) is the normal-

ized intensity distribution in the line profile.

$\delta\lambda = 4.67\times10^{-13} g H \lambda^2$ is the displacement of each σ component due to the magnetic field.

Similarly; $$N_R(\lambda) = \frac{1}{2} N I(\lambda - \delta\lambda)\, \Delta\lambda\, Qt \qquad (7)$$

The factor ½ takes into account that only ½ the light in the continuum goes into each polarization form.

The signal is given by

$$S = N_R(\lambda) - N_L(\lambda) \qquad (8)$$

and the noise $$\sigma^2 = N_R(\lambda) + N_L(\lambda) \qquad (9)$$

so that $$\frac{S}{\sigma} = \frac{N_R(\lambda) - N_L(\lambda)}{(N_R(\lambda) + N_L(\lambda))^{1/2}} \qquad (10)$$

In a first order approximation (small $\delta\lambda$) we can write

$$N_R(\lambda) = \frac{1}{2} N \Delta\lambda\, Qt \left(I(\lambda) - \delta\lambda \frac{dI}{d\lambda}\right) \qquad (11)$$

$$N_L(\lambda) = \frac{1}{2} N \Delta\lambda\, Qt \left(I(\lambda) + \delta\lambda \frac{dI}{d\lambda}\right) \qquad (12)$$

$$\frac{S}{\sigma} = \frac{\delta\lambda\, dI/d\lambda\, N Qt \Delta\lambda}{\sqrt{N Qt\, \Delta\lambda\, I}} \qquad (13)$$

$$= \delta\lambda \frac{dI}{d\lambda} \sqrt{\frac{N \Delta\lambda Qt}{I}} \qquad (14)$$

For a given field H and signal to noise ratio n, the integration time is given by

$$t_L = \frac{n^2 I}{\delta\lambda^2 \left(\frac{dI}{d\lambda}\right)^2 N \Delta\lambda Q} \qquad (15)$$

From the equation 15 we see that the most important factors to have short integration times are the splitting

of the line and the slope of the wing.

As $$t_L \propto \frac{n^2}{g^2 \lambda^4 \left(\frac{dI}{d\lambda}\right)^2 \Delta\lambda \, N H^2}$$

we have g, λ and $\frac{dI}{d\lambda}$ as important factors in the selection of a spectral line. The integration time is less dependent on the brightness of the star and the efficiency of the detector. Within limits imposed by the light available, it appears that one should rather use a narrow slit than a larger one. A larger slit gives more photons, but introduces a large instrumental profile, thus decreasing $dI/d\lambda$. Solar physicists (Livingston 1968) use a slit width ~ 0.6 times the half width of the line.

The only source of noise considered here is noise from statistical fluctuations in the photon counts.

2) Transverse fields

In the case of a transverse field we have two linearly polarized σ components. In the case of the inverse Zeeman effect, the number of photons polarized parallel to the field lines is given by

$$N_\sigma(\lambda) = \tfrac{1}{4} N Q t \Delta\lambda \left(I(\lambda+\delta\lambda) + I(\lambda-\delta\lambda)\right) \quad (16)$$

Now: $$I(\lambda+\delta\lambda) = I(\lambda) + \delta\lambda \frac{dI}{d\lambda} + \tfrac{1}{2} \delta\lambda^2 \frac{d^2I}{d\lambda^2} + \dots \quad (17)$$

$$I(\lambda-\delta\lambda) = I(\lambda) - \delta\lambda \frac{dI}{d\lambda} + \tfrac{1}{2} \delta\lambda^2 \frac{d^2I}{d\lambda^2} + \dots \quad (18)$$

therefore $$I_\sigma(\lambda) = \tfrac{1}{2} I(\lambda) + \tfrac{1}{4} \delta\lambda^2 \frac{d^2I}{d\lambda^2} \quad (19)$$

and $$N_\sigma(\lambda) = N Q t \Delta\lambda \, I_\sigma(\lambda)$$

There is also an undisplaced π component linearly polarized perpendicular to the field lines. It gives a

number of photons $$N_\pi(\lambda) = \tfrac{1}{2} NQt\,\Delta\lambda\, I(\lambda) \qquad (20)$$

One half the light in the continuum goes into each polarization form and each of the σ components has the same strength.

The analyzer measures $$S = N_\sigma - N_\pi = \tfrac{1}{4} NQt\,\Delta\lambda\,\delta\lambda^2 \frac{d^2I}{d\lambda^2} \qquad (21)$$

and the noise is given by $$\sigma^2 = N_\sigma + N_\pi = NQt\, I\,\Delta\lambda \qquad (22)$$

$$\eta = \frac{S}{\sigma} = \frac{1}{4}\,\delta\lambda^2 \frac{d^2I}{d\lambda^2}\sqrt{\frac{NQt\,\Delta\lambda}{I}} \qquad (23)$$

$$t_T = \frac{16\,\eta^2 I}{NQ\,\Delta\lambda\,\delta\lambda^4 (d^2I/d\lambda^2)^2} \qquad (24)$$

Again we see the importance of having a large splitting and sharp lines.

Let us also compare the integration times necessary to measure longitudinal and transverse fields.

From equations 15 and 24 we have

$$\frac{t_T}{t_L} = \frac{16\,(dI/d\lambda)^2}{\delta\lambda^2\,(d^2I/d\lambda^2)^2} \qquad (25)$$

Consider a line with a gaussian profile

$$I(x) = 1 - (1 - I_o)\, e^{-x^2}$$

where I_o is the central intensity in units of the continuum, and $$x^2 = (\lambda - \lambda_o)^2 \Big/ (\Delta\lambda_{Doppler})^2 \qquad (26)$$

$$\frac{dI}{dx} = 2x\,(1 - I_o)\, e^{-x^2} \qquad (27)$$

$$\frac{d^2I}{dx^2} = 2\,(1 - 2x^2)\,(1 - I_o)\, e^{-x^2} \qquad (28)$$

and $$\left(\frac{dI}{dx}\right)^2 \Big/ \left(\frac{d^2I}{dx^2}\right)^2 = \frac{x^2}{1 + 4x^4 - 4x^2} \qquad (29)$$

$$\frac{t_T}{t_L} = \frac{16}{\delta\lambda^2}\,\frac{x^2}{1 + 4x^4 - 4x^2} \qquad (30)$$

where $\delta\lambda'$ is now in units of $\Delta\lambda$ Doppler. Notice that in equation 30 t_T/t_L is independent of all line parameters except $\delta\lambda'$. Let us measure the signal at x = 1, for a line 50% deep. Let us take the λ = 5250 FeI line, g = 3 and $\Delta\lambda_{Doppler}$ = 0.05 Å.

$$\frac{t_T}{t_L} \simeq 3\frac{10^7}{H^2}$$

We can thus expect, for weak fields, longer integration times for transverse fields than for longitudinal ones. Note that the ratio $\frac{t_T}{t_L} \propto H^{-2}$, thus decreases for strong fields. For a field of $\sim 3\times10^3$ gauss we would have

$$\frac{t_T}{t_L} = 1$$

The theory used in deriving equations 15 and 24 is crude. The formulae are valid only for small $\delta\lambda$ because of the neglect of higher order terms in the series expansion. Moreover, we assume that the line profiles seen in circularly and linearly polarized light are nearly the same as for the unperturbed line. This is true only for weak fields or purely longitudinal (or transverse) fields. For example, in the longitudinal case and lines of force inclined to the line of sight, there will be some contribution to the line profile from the linearly polarized π component and from the linearly polarized light from the other σ component. Thus, the line profile see through the circular analyzer will appear asymmetrical (Moe 1968). Finally, equation 24 is valid only for weak, unsaturated lines as each of the σ is taken to have ½ the depth of the π component.

Therefore, the equations derived are valid only for weak lines and fields less than $\sim$ 1000 gauss, this limit depending on the inclination of the lines of force on the line of sight, the landé g factor, the wavelength and doppler width of the line. However, they are still very useful for estimating the importance of various factors in choosing lines to observe.

3) Choice of lines

To be usable a spectral line should satisfy the following requirements:

a) be present and be recognizable with certainty,

b) be as sharp as possible, for a high efficiency,

c) be free from blends with close neighbors,

d) have as large as possible a Landé g factor,

e) be at a favorable wavelength for high efficiency,

f) for simplicity in the interpretation of the data, exhibit a simple triplet splitting.

Let us examine some of these criteria more in detail.

a) Many of the lines present in the solar spectrum are present from spectral type F5 to essentially M5, some are present in stars as early as AO . Therefore, one can make use of many of the lines used by solar physicists. One should try to use these lines as often as possible. They are well studied and this can present advantages. For example, see Harvey and Livingston (1969). For earlier spectral types one has either to take photographic spectra or search the literature for lists of lines iden-

tified.

c) The absence of blends can be insured only by inspection of the stellar spectrum. One must remember that the red region of the spectrum is usually less crowded with lines.

d) Table 3 gives a list containing some of the lines that have been used in the present study. It is desirable, however, to search for other lines with possible larger landé g factors. Kiess and Meggers (1928) and, more recently, Beckers (1969) have published a list of landé g factors computed under the assumption of L-S coupling. Some of the transitions have landé g factors as high as 4.3 . A search for magnetic sensitive lines could be carried by making use of the spectrum of a sunspot taken through a Hale-Nicholson grid. The lines exhibiting strong splitting can be identified by visual inspection. For earlier spectral types than the sun, one should take Zeeman-analyzed spectra of known magnetic stars in the yellow and red region of the spectrum.

e) Several conflicting criteria have to be used. We see that from equation 15 a long wavelength is desirable. However, at long wavelengths the doppler broadening decreases $dI/d\lambda$ reducing the efficiency. One still has a gain by going to long wavelength, if he considers that $t_L \propto \frac{\Delta\lambda^2_{Doppler}}{\lambda^4}$ as $\Delta\lambda_{Doppler} \propto \lambda$ and therefore $t_L \propto \frac{1}{\lambda^2}$. On the other hand, $dI/d\lambda$ is not determined only by Doppler broadening. For most lines and for a bandpass of 0.2 Å the instrumental pro-

TABLE 3

LIST OF MAGNETIC SENSITIVE LINES

λ	ion	g	$g\lambda^2$ ($10^6 Å^2$)
4210.35	FeI	3.0	54
4233	FeII	1.2	41
4254.36	CrI	1.8	32
4365.56	FeIII	2.5	48
4574.78	SiIII	2.0	42
5131.48	FeI	2.5	66
5247.58	CrI	2.5	69
5250.2	FeI	3.0	83
6173.35	FeI	2.50	95
6258.58	VI	3.40	132
6302.51	FeI	2.5	100
6733.16	FeI	2.5	114
8468.4	FeI	2.5	180

file dominates the line shape and the decrease in efficiency towards long wavelength is not as severe as for pure Doppler broadening.

A drawback of working at long wavelengths is the poor efficiency of most photoelectric detectors. Figure 17 shows the quantum efficiency of the line profile scanner as a function of wavelength. It has been determined by scanning the AOV star α CrB and correcting for the energy distribution of the star. The atmospheric extinction has purposely not been removed. The phototubes have S 20 photosurfaces and the grating efficiency peaks at 5600 Å. The red efficiency could be improved by making use of a prism or half-silvered hemisphere on the photocathode. A substantial improvement could also be made by making use of photomultipliers with the new, highly red-sensitive GaAs photosurfaces.

Another criterion in selecting a line is the energy distribution of the star itself.

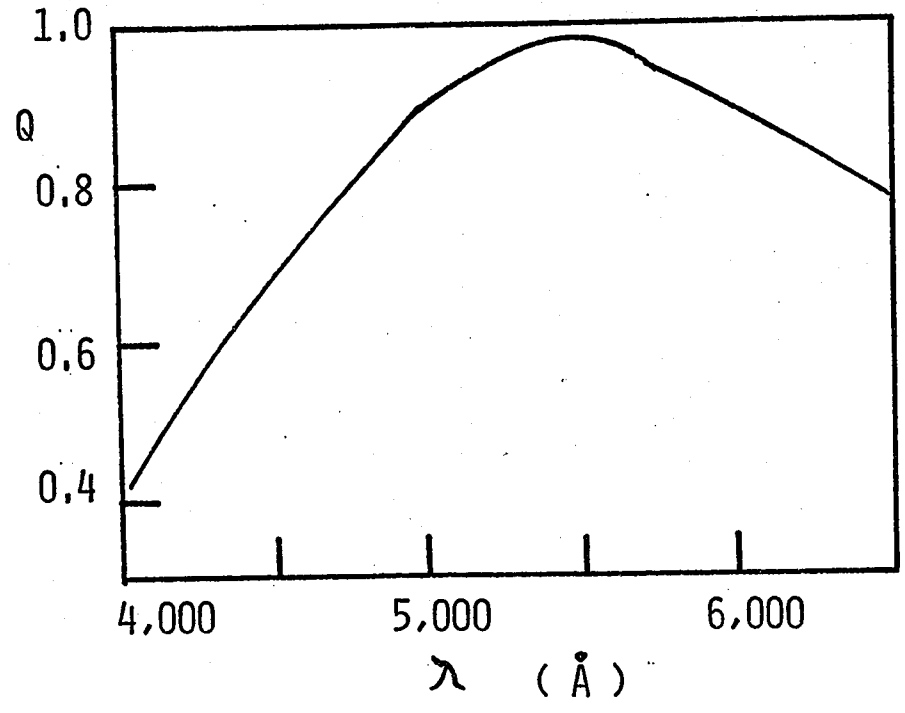

FIGURE 17

Efficiency of the line profile scanner as a function of wavelength. The atmospheric absorption is included.

CHAPTER VI

SOURCES OF ERROR

1) Random error

The random error is mostly caused by photon noise and the standard deviation is given by $\sigma^2 = N$, where N is the total number of photoevents counted. The rapid switching eliminates essentially completely other sources of noise, such as scintillation noise, changes in light distribution on the nonuniformly sensitive photocathode, drifts in the tube sensitivity, etc.... I have checked the validity of the above assertion in two fashions: by observing an unmodulated light source, and by computing the deviation from the instrumental polarization for all the stellar observations. These two tests revealed errors consistent with the above formula. At low light levels, the dark counts from the photomultipliers do contribute to the error. The standard deviation is then given by $\sigma^2 = N+N_D$ where N_D is the total number of dark counts. In the observations reported here, the dark counts never contribute more than 30% of the total counts. Note that the beams of left and right circularly polarized light enter the spectrograph through exactly the same optical path and with the same polarization form; thus we are comparing the intensities of two beams which differ only

in intensity after leaving the polarizing optics.

2) Systematic errors in the polarimetry

These can be divided in three categories: errors in the electronics; errors in the alignment of the polarizing optics; and errors in the phase shifts introduced by the polarizing optics.

The gating of the pulses is controlled by a crystal clock which is orders of magnitude more accurate than needed. The only serious source of error could come from incorrect discriminator setting in one of the scalers used, resulting in a spurious polarization signal. The scalers are checked periodically for drifts in the discrimination (chapter VII). The polarimetry should therefore be free from errors introduced by the electronics.

The polarizing optics must be aligned axially with the telescope beam. They are mounted on three point mounts that allow accurate alignment. The Glan-Thompson prism has a wide field (15°) and the Babinet-Soleil compensator is insensitive to small tilts. These two elements are aligned with their faces perpendicular to the beam by tracing the axis of the beam with a laser. The laser itself is aligned on the optical axis by placing it in such a manner that its beam hits the centre of the spectrograph slit and the centre of the collimator in the coudé room. If the faces of the compensator and the Glan-Thompson prism are perpendicular to the beam, the

laser light is reflected on itself. This alignment procedure is accurate to better than a degree.

The z axis of the KD*P must be adjusted parallel to the beam. To do this, the crystal is placed between crossed polaroids on the optical bench in front of the slit. The telescope is pointed on the bright daytime sky with no electric field applied to the crystal faces. If no field is applied to the crystal, it acts as an uniaxial crystal with the optical axis along the z axis. Therefore, if the light from the first polaroid travels along the z axis, it is unaffected and is extinguished by the second polaroid. If the beam is inclined to the optical axis, it will be retarded and partially transmitted by the second polaroid. Therefore, to establish the correct inclination, one must search for minimum light. This is done visually. The accuracy achieved in the alignment is better than one degree. It is difficult to estimate the error introduced by this uncertainty in the alignment. Billings (1952) gives formulae for the retardation as a function of the angle of incidence and azimuth. An indication of the error introduced is given by tests on the contrast ratio when the crystal is placed between crossed polaroids and is switched from zero to half-wave retardation. The manufacturer gives a contrast of 1200:1 for a 1° divergence. Baur (1971), for the same model of EOM we use, finds the ratio to be 200:1 for an f/20 beam (1½° divergence). He also finds that the voltage for

$\lambda/4$ retardation is 2.15 $\pm$ .1 kV for collimated light and 2.13 $\pm$ .1 kV for an f/20 beam.

An estimate of the error introduced by working with an f/30.9 beam instead of collimated light is given by the previous discussion on contrast ratio and retardation for an f/20 beam.

For very accurate work, the calibration voltage for a $\lambda/4$ retardation should be checked every time the crystal is moved in its mounting (Baur 1971). Fortunately, as we will see below, the polarimetry is fairly insensitive to errors in the retardation.

The fast and slow axis of the KD*P must be aligned at 45° with the transmission axis of the Glan-Thompson. This is done by crossing the prism with a polaroid, the KD*P in between. One then applied a DC voltage to the KD*P which now acts as a retardation plate. Rotation of the KD*P about the optical axis until minimum light occurs insures that the transmission axis of the Glan-Thompson prism and one of the axes of the KD*P are parallel. A subsequent rotation of the KD*P by 45° then gives it the correct orientation. The axes are oriented to better than one degree. As we will see later, the error introduced on the measurements is negligible for small errors in the orientation of the polarizer.

Next, the voltage to the EOM must be set to give a quarter wave retardation.

Theoretically the retardation is given by

$$\Delta = \frac{n_o^3 V r}{\lambda}$$

where Δ = number of wavelengths retarded

n_o = ordinary index of refraction of KD*P

r = electro-optic constant, microns/volt

V = longitudinal applied voltage, volts

λ = wavelength of light, microns

One could calculate the voltage to give the necessary retardation. The voltage calibration given by the manufacturer is not very reliable. For the Lasermetrics 402A EOM we found 1.4 kv for $\lambda/4$ retardation compared to the 1.9 kv given by the supplier at 5000 Å. The correct voltage is found by placing in the beam a circular polarizer; the voltage is set to obtain 100% circular polarization. It is found that the retardation is strongly dependent on frequency and weakly temperature dependent. Figure 18 shows the voltage for a $\lambda/4$ retardation as a function of wavelength for the 402A EOM.

We will now consider the errors introduced in the polarimetry by incorrect modulation and misalignment of the azimuth of the EOM. Let us examine a beam of polarized light, described by the Stokes vector $\{I,Q,U,V\}$, with a retardation plate (retardation = δ) and polarizing prism (figure 19). The x axis gives the principal direction with respect to which the Stokes parameters are measured. The fast and slow axis of the plate are

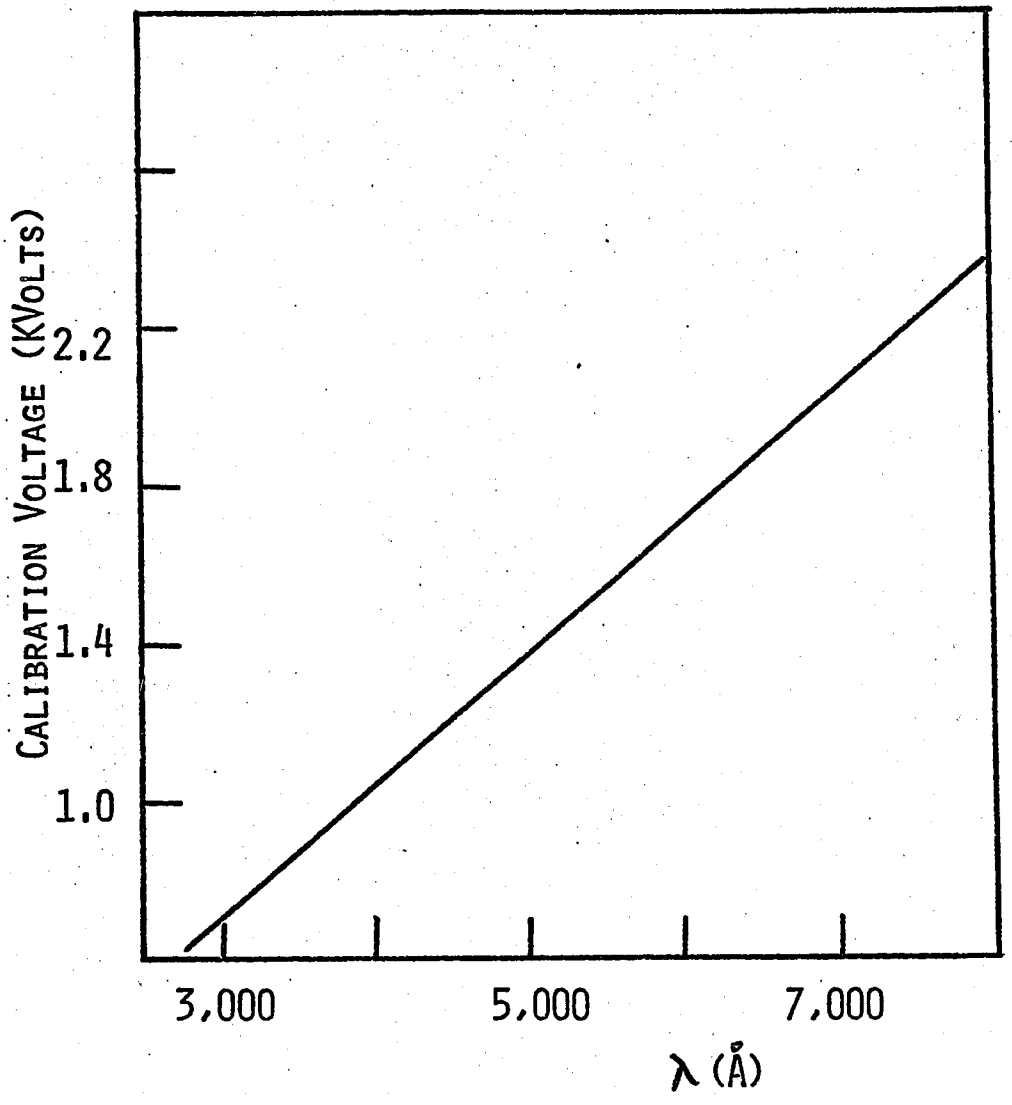

FIGURE 18

Voltage calibration line (kilovolts) for the Lasermetrics EOM . The relation is linear.

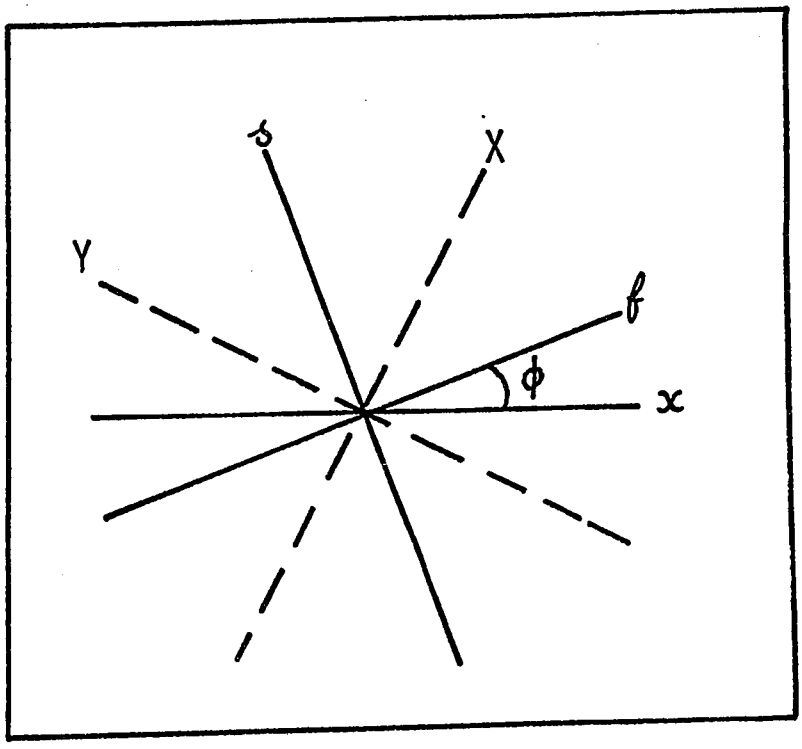

FIGURE 19

Eigenaxis of the retardation plate and linear polarizer.

indicated by f and s. The X and Y axis indicate the direction of vibration of the electric vector of the ordinary and the extraordinary rays in the calcite. The X axis is at 45° with the fast axis of the plate. ϕ is the angle between the fast axis and the horizontal direction.

We have for the intensity of the radiation after passing through the retarder and polarizing prism:

$$I_\delta = \frac{1}{2}\left[I - Q \sin 2\phi \cos\delta + U \cos\delta \cos 2\phi + V \sin\delta\right]$$

When the sign of the electric field is reversed we have that $-\delta_2 = \delta_1 = \delta$ where the indices 1 and 2 indicate the two halves of the cycle and where we have assumed that the retardation reverses symmetrically. We have then that

$$I_{\delta_1} = \frac{1}{2}\left[I - Q \sin 2\phi \cos\delta + U \cos\delta \cos 2\phi + V \sin\delta\right]$$

$$I_{\delta_2} = \frac{1}{2}\left[I - Q \sin 2\phi \cos\delta + U \cos\delta \cos 2\phi - V \sin\delta\right]$$

The polarization is detected as a difference of intensity

$$\Delta I = I_{\delta_1} - I_{\delta_2} = V \sin\delta \qquad (31)$$

We can see that the apparatus is insensitive to linear polarization if modulated $\pm\ \delta$ and the polarizer and waveplate have the correct relative orientation. From equation 31 we also see that the apparatus is fairly insensitive to errors in the retardation δ as the

signal is $\propto \sin\delta$ with $\delta \sim 90°$. For example, an error of 30% in the retardation introduces an error of only 6% in the signal.

The assumption made here is that the crystal is aligned correctly and that the retardation reverses symmetrically. In practice this is not quite the case and there is a small amount of cross-talk between the Stokes parameters, of the order of a few percent. Let us suppose that the voltage does not reverse quite symmetrically and that the polarizer is not oriented quite at 45° to the axis of the EOM. We have then that $\delta_i = 90° + \varepsilon_i$ and $\psi = 45° + \alpha$, where the δ_i are the retardations during the two halves of the cycle, ψ is the azimuth of the polarizer relative to the waveplate, ε_i and α the errors in retardation and azimuth, and i = 1,2 stand for the two halves of the cycle. We assume ε_i and α are small. After expanding to first order in α and ε_i the Mueller matrix describing the EOM and polaroid assembly, we obtain that we detect the difference of intensity

$$\Delta I = \frac{1}{2} Q (\varepsilon_1 - \varepsilon_2) + V$$

The horizontal direction is here taken to be parallel to the fast axis. From this equation we can see that for small ε_i and α the signal ΔI is independent from errors in the azimuth of the polarizer. We can also see that if $\varepsilon_1 \neq \varepsilon_2$, so that the retardation does not reverse exactly, we have a cross-talk between Q and V.

As seen earlier, the error α is of the order of 1° . From monitoring of the pulses in the high-voltage pulser we have found that the voltage reverses within about one percent. Thus the cross-talk is of the order of a few percent. The cross-talk from the linear instrumental polarization does not create any problem, as it is subtracted as a spurious signal from the continuum. However, if there is a strong transverse field in the star, there will be a cross-talk only in the line, thus creating an error in the longitudinal field estimate. For weak fields the linear polarization is orders of magnitude lower than the circular and the cross-talk does not contribute significantly to the error.

Similarly, there will be some cross-talk when measuring transverse fields. The problem will then be more serious as V is usually much stronger than Q or U.

Let us now consider the errors introduced by the Babinet-Soleil compensator. In terms of the electric vector amplitudes from mirror number five E_s and E_p , we have for the Stokes parameters of the polarized component

$$I = \langle E_s^2 + E_p^2 \rangle$$

$$Q = \langle E_s^2 - E_p^2 \rangle$$

$$U = \langle 2 E_s E_p \cos\delta \rangle$$

$$V = \langle 2 E_s E_p \sin\delta \rangle$$

where δ is the phase difference between the electric vectors. We can see that for predominantly longitudinal fields where the linear component is small $\delta \sim 90°$.

Therefore, any error due to the compensation will be small. An error of 30° in the compensation introduces 6% error in the V signal.

It can be shown that the error introduced on the polarimetry by a small error in the azimuth of the compensator (it is less than 1°) is small.

In the case of strong transverse fields where Q and U can be comparable to or larger than V, errors in the compensation will introduce a serious cross-talk.

The systematic errors in the polarimetry are always small. A circular polarizer is observed several times throughout the night (chapter VII) to ensure that there is no sizeable error ($> 5\%$) in the detection of circular polarization. The total systematic errors in the polarimetry, including errors in the compensation are smaller than 10%. I did not correct for this small effect. If one considers that the few signals detected are of the order of three standard deviations, it is clear that the principal source of error is due to random noise.

3) Miscellaneous systematic errors

There is always an implicit assumption that, throughout the measurements, the spectrograph does not experience wavelength shifts. Coudé spectrographs are quite stable; however, there seem to be small shifts in wavelength affecting the line profile scanner. They can be as high as 0.2 $\mathring{A}$ in the span of a night. This does not affect

greatly the measurements, as a stellar observation usually lasts no more than two hours. In any event, drifts can be detected by observing periodically a hollow cathode emission lamp. Note that any drift can also be detected with the polarization data. We monitor simultaneously a wide band in the continuum and a narrow band in the line profile (chapter VII). If the counts in the two scalers on the profile are added and if we add to each other the counts in the two scalers in the continuum, taking the ratio of the two numbers obtained will give us the line profile. Drifts of the order of less than 0.10 Å can be detected when using a bandpass of 0.20 Å .

For the determination of the magnetic field strength from the observed polarization, one needs to know the slope of the wing of the line $\frac{dI}{d\lambda}$ (chapter VIII). This is typically known to 10% accuracy. It is time-consuming to obtain an accurate line profile. Besides scanning the line, one must scan a larger part of the spectrum to locate the continuum accurately. The time that would be spent in obtaining a very accurate $\frac{dI}{d\lambda}$ is not justifiable, because of the approximations in the reduction procedure itself.

CHAPTER VII

TECHNIQUES OF OBSERVATION

1) Choice of the bandpass

There are two modes of observation: observations of known magnetic stars and search for new ones.

The observation of known magnetic stars should be carried out with as small as possible a bandpass in order to obtain all of the information contained in the shape of the polarization signal across the line. However, there is a limit on the bandpass, imposed by the loss of light and increasing time to obtain the scan.

The search for new magnetic stars should be carried with as large as possible a bandpass. One gains because of the larger entrance and exit slit and because of the fewer points to observe in the line. For a given line in a particular star used, the time of observation increases as the cube of the resolving power. For example, increasing the resolving power by a factor of two, we have to decrease both entrance and exit slit widths by a factor of two, therefore increasing the integration times by a factor of four to obtain the same total photon count. At the same time, because the bandpass is smaller by a factor of two, we have to integrate on twice as many points to cover the line profile completely. However, a large bandpass introduces a large instrumental pro-

file, decreases the slope of the line $dI/d\lambda$ and therefore brings a decrease in the signal (equation 14). In more physical terms, a bandpass larger than the width of the signal will introduce unpolarized photons, thus increasing the background noise. Moreover, during cross-over, the polarization signal across the line is complicated and averaging over a large bandpass might give zero polarization if negative and positive polarization alternates in the bandpass. The term "cross-over effect" (Babcock 1960) is applied to the observation that line profiles are sharper in one circular polarization sense than in the other during part of the magnetic cycle of A_p stars. This can be interpreted in terms of two regions with opposite polarity of the magnetic field being Doppler shifted in opposite directions.

As a general guide, one can base the choice of the bandpass on the photographic Zeeman work on A_p stars. Babcock (1960) used dispersions ranging from 2 Å/mm to 10 Å/mm (most plates are at 4.9). Taking the resolution of the photographic plate as 20 microns, we have a resolution from 0.04 to 0.20 Å.

To search for new magnetic stars we usually make use of a bandpass of 0.2 Å. This bandpass seems to give a reasonable compromise, although it is somewhat large for sharp line stars. Severny (1970) made use of the same bandpass.

2) Procedures of observation

First, the grating has to be oriented to send the desired spectral region to the photomultipliers. The daytime sky, or a hollow cathode is then scanned, and the position of the desired laboratory wavelength is found. The location of the stellar line is then found by applying a correction for the radial velocity of the star and the earth's motion. A narrow spectral region of the stellar spectrum is then scanned to recognize the line with certainty and to obtain the line profile. After the line is located, the polarizing optics are placed on an optical bench in front of the slit. The polarimeter electronics are attached to the line scanner. The moveable photomultiplier is attached to one channel of the electronics, the fixed photomultiplier monitoring the continuum to a second channel. The correct voltage for a $\lambda/4$ retardation is applied to the faces of the crystal. A circular polarizer is then introduced in the beam and observed to insure that the apparatus is working properly and to calibrate the sign of polarization. The circular polarizer is always observed before and after each stellar observation. The circular polarizer is then removed, the Babinet-Soleil compensator is put in place, its thickness adjusted to the correct setting, the movable photomultiplier is placed in the desired location and observations begin. When necessary, (usually every ten minutes), the thickness of the compensator is changed.

Usually the movable photomultiplier observes at least five points, two in the wings, one in the core and two in the continuum.

The electronics are checked periodically. After each reading in the line, the wide band in the continuum is observed through the same electronics used previously for the line profile, to insure that it will give the same instrumental polarization as the electronics of the reference channel. As an additional check, periodically, the stellar light is blocked and an unmodulated artificial light source is observed.

CHAPTER VIII

OBSERVATIONS AT MT. WILSON OBSERVATORY

The 100-inch telescope at Mt. Wilson was used during nine nights in January and March 1972 to search for magnetic fields in stars.

The same electronics and polarizing optics used with the 48-inch telescope at the University of Western Ontario were used in conjunction with the Mt. Wilson line profile scanner. The instrument has been described by Wilson (1968). The techniques of observation are the same as for the observation at the University of Western Ontario.

The coudé system of the 100-inch telescope is a three-mirror one. A flat mirror brings the light from the secondary to the coude room. The angle of incidence made by the light falling on the flat is given by $\phi = \frac{1}{2}(90^\circ + \delta)$ where δ is the declination. The angle of incidence ϕ and therefore the phase shifts and instrumental polarization varies with declination, but only the direction of these effects vary with H.A. . The instrumental phase shifts are compensated with a Babinet-Soleil compensator mounted before the EOM . The compensator is not used for declinations less than 0 degrees, the phase shifts being very small for low declinations. Figure 20 shows the compensation as a function of declination for a wavelength of 4200 $\mathring{A}$. As the plane of incidence of

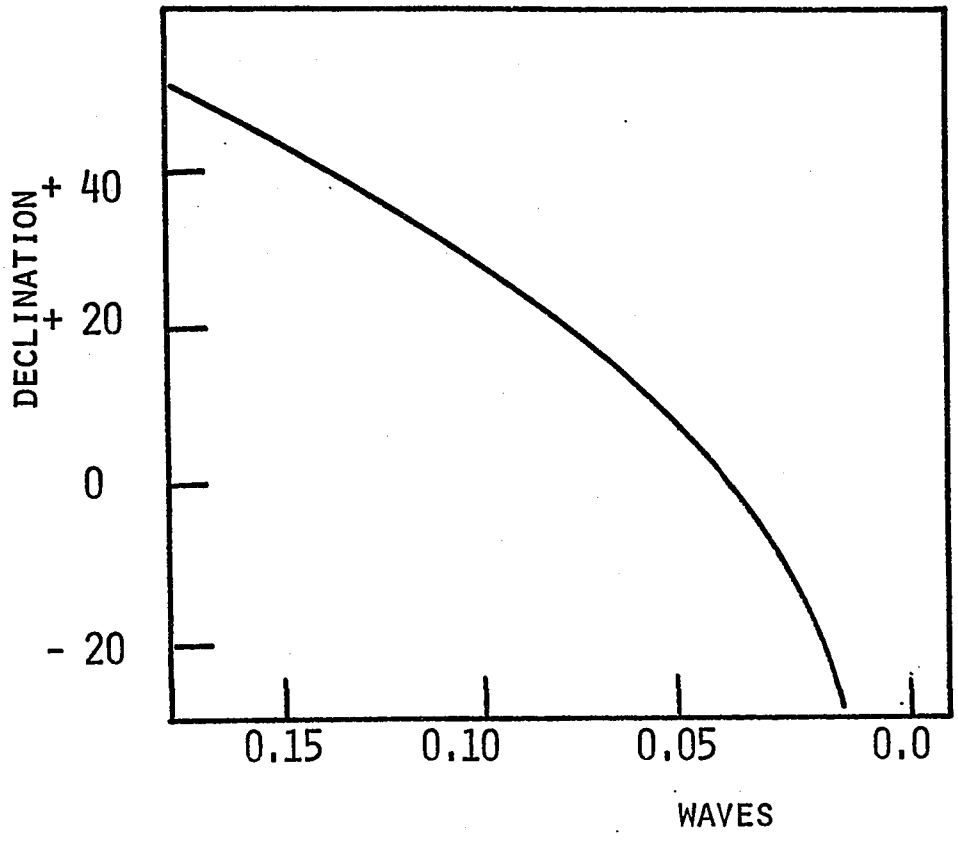

FIGURE 20

Compensation curve for the 100-inch telescope at Mt. Wilson. The wavelength is 4200 Å. The compensation in wavelength units is plotted as a function of declination. Note that the phase shifts are not cancelled, but advanced to ½ wave, thus the signs of polarization are changed.

the light on the flat mirror as seen from the slit rotates with H.A., the compensator is rotated by a motor to keep its axis aligned with the axis of the flat mirmor. Although there is no spurious circular polarization produced by the flat mirror but only linear, in practice there is a certain amount of circular polarization detected. This is caused mostly by errors in the alignment of the compensator converting the linear polarization from the flat mirror into elliptical and errors in the alignment of the crystal. Usually, if the compensator is aligned with care, the spurious signal is less than one percent. The spurious circular polarization appears to vary slowly and monotonically with H.A. . The scanner channel in the continuum is used to monitor the instrumental polarization, in the same fashion as with the University of Western Ontario observations. As the spurious polarization depends on alignment problems, it is preferable to monitor it during each observation rather than relying on previous measurements.

CHAPTER IX

RESULTS OF OBSERVATIONS

1) Introduction

The polarimeter has been used to search for longitudinal fields in twenty-three bright stars. Table 4 lists the stars observed with the number of nights of observations for each star. Given the exploratory nature of this investigation no particular criterion of selection for stars to observe was applied. As broad as possible a range in spectral types was deemed desirable. Only later investigations should concentrate on particular spectral types. The only condition the stars to observe had to fulfil was to be bright enough to be able to detect weak fields in them.

The reader must keep in mind four important facts. First, the polarimeter was used only to detect circular polarization; therefore, what is measured is related only to the net longitudinal component of the magnetic field averaged over the surface of the star. The stars observed could have surface fields much stronger than the upper limits reported if the field is mostly transverse. Secondly, the weak magnetic fields are probably variable. All the known stellar magnetic fields are variable (Preston 1971). One does not, therefore, necessarily expect the measurements to repeat from night to night, and a

TABLE 4

LIST OF THE STARS OBSERVED

	STAR	SPECTRAL TYPE	NUMBER OF NIGHTS OF OBSERVATIONS	OBSERVATORY
1	β Per	B8 V	1	UW
2	β Ori	B8 Ia	1	UW
3	α And	B9p	1	UW
4	α Lyr	AO V	2	UW
5	ι CrB	AOm	1	MW
6	ε UMa	AOp V	2	UW
7	α CMa	A1 V	4	UW, MW
8	α Cyg	A2 Ia	1	UW
9	α^2 Lib	A3m	1	MW
10	β CrB	A9p	8	UW, MW
11	α Per	F5 Ib	2	UW, MW
12	α CMi	F5 IV-V	1	UW
13	HD75332	dF7	1	MW
14	γ Cyg	F8 Ib	9	UW, MW
15	η Boo	GO IV	1	MW
16	ε Leo	GO II	1	MW
17	α Aur	G8 III	6	UW, MW
18	β Gem	KO III	3	UW, MW
19	α Boo	K2 IIIp	3	UW, MW
20	α Ari	K2 III	8	UW
21	ε Peg	K2 Ib	2	UW
22	α Tau	K5 III	1	UW
23	α Sco	M1 I	1	UW

UW: University of Western Ontario
MW: Mount Wilson Observatory

given star should be observed several times before drawing definitive conclusions on the upper limit of the longitudinal magnetic field. Thirdly, one does not necessarily expect an S-shaped signal across the line. The observed polarization is averaged over the surface of the star and the Doppler effect can give it a complicated wavelength dependence (cross-over effect). By analogy to the A_p stars we can expect the cross-over effect to be present during most of the cycle (Preston and Sturch 1967). Fourthly, the magnetic fields derived from the circular polarization are only indicative; much theoretical work has to be done before an accurate interpretation of the data can be carried out.

2) Obtaining the magnetic field strength from the circular polarization.

The polarimeter measures circular polarization which has to be translated into a magnetic field measurement. In this respect, throughout this investigation, we will make the implicit assumption that the circular polarization we measure is caused by the Zeeman effect. The procedure of reduction used here is the same as the one used by Severny (1970). Severny calibrated the signal of his instrument through the observation of a sunspot, and then obtains the field (in gauss) by comparing the calibration signal to the stellar one, correcting for the differences in the slope of the line. In one

paper, Nikulin, Kuvshinov and Severny (1971) give a calibration of 88 gauss per one percent polarization for the 4254.4 CrI line (ς = 1.8) in β CrB.

The signal of a magnetograph is (for weak fields) proportional to $g\lambda^2 \frac{dI}{d\lambda} H\cos\gamma$ (Bray and Loughhead 1965) where $H\cos\gamma$ is the longitudinal component of the magnetic field. We therefore correct Severny's calibration for the Landē g factor, the wavelength and slope of the line used. In Chapter X we will consider more in detail the difficulties and limitations of this reduction procedure. The signs of the magnetic fields are assigned using the usual Babcock convention (Babcock 1958), a field is positive when the blue wing gives right-handed polarization and the red wing left-handed polarization. We use the convention that we have right-handedness when the E vector rotates clockwise in a stationary plane for an observer looking at the star.

3) Observations of β Coronae Borealis

The known magnetic variable β CrB has been observed on several nights as a check on the polarimeter. β CrB was selected because it is bright, is a periodic magnetic variable and has a reasonably strong magnetic field. Figure 21 shows a scan taken August 2.2 U.T. 1971 at the University of Western Ontario. An S-shaped signal is visible across the line, and the field estimate is -600 gauss $\pm$ 140 gauss. This is in excellent agreement with

FIGURE 21

Observation of β CrB on J.D. 2441165.6, phase = 0.83 $\pm$ 0.1 (ephemeris from Preston and Sturch 1967). O is the observed field, C_p is the field computed from the magnetic field curve in Preston and Sturch (1967), C_w is from Wolff and Wolff (1970). The dashed line indicates the instrumental polarization. The line used is CrI 4254.4. Positive polarization indicates right circularly polarized light, negative polarization left circularly polarized light.

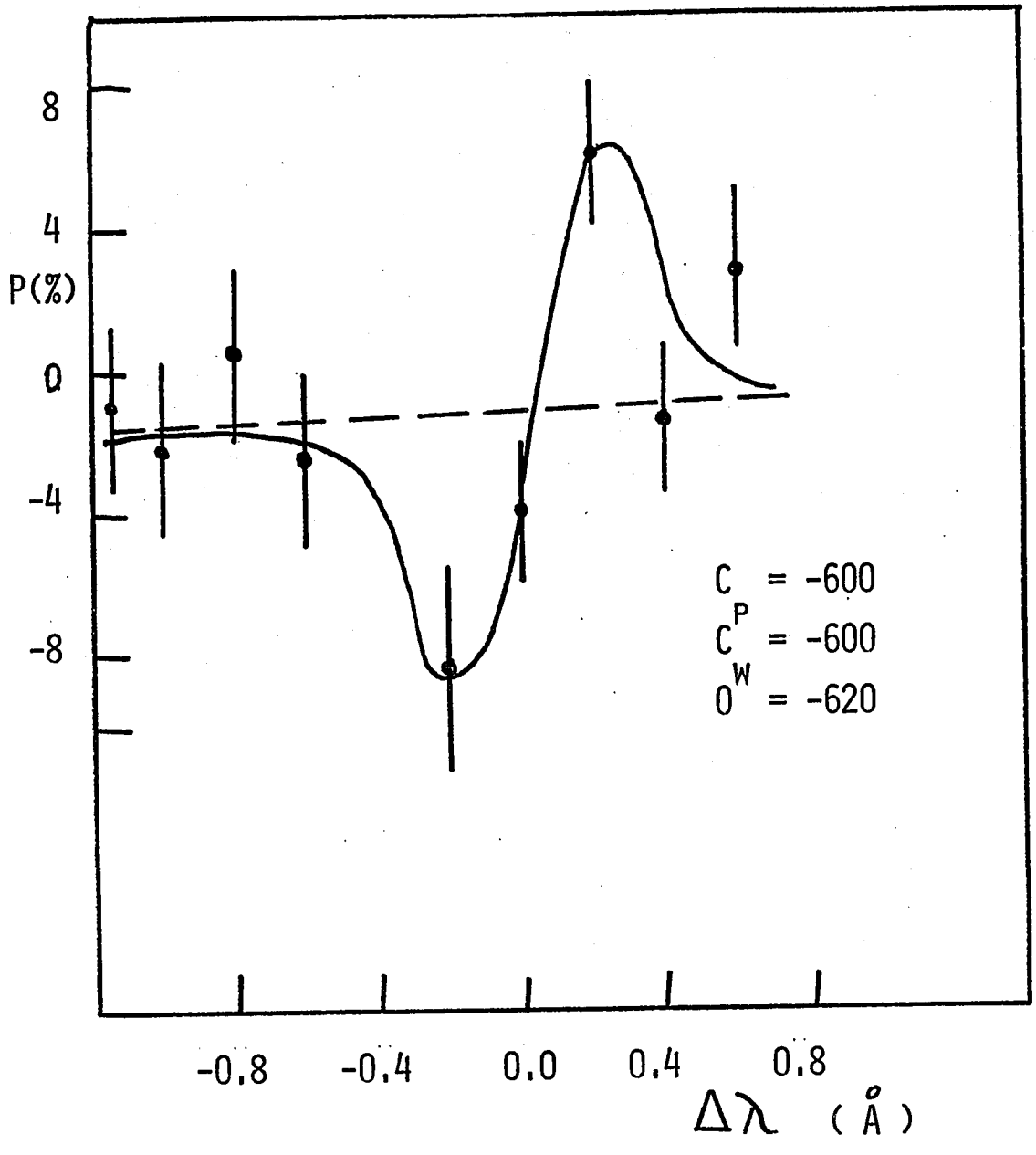

FIGURE 21

Observation of β CrB obtained at the University of Western Ontario.

the value of -600 gauss calculated with the ephemeris given by Preston and Sturch (1967). Figures 22 and 23 show two scans obtained with a Fabry-Perot interferometer on two consecutive nights. The observations were obtained at Mt. Wilson, in collaboration with Dr. A. H. Vaughan, Jr. Again the field estimates are in reasonable agreement with the ephemeris fitted to the curves given by Preston and Sturch (1967) and the model of β CrB given by Wolff and Wolff (1970). Figure 24 shows a scan of β CrB taken at the same phase with a bandpass of 0.2 Å. Much of the information has been lost with the larger bandpass. However, the sign and field estimate are consistent with the observations taken with the Fabry-Perot interferometer and with the ephemeris.

The agreement between our observations and the predicted fields is quite satisfactory even if it is not perfect. Relatively little is known about the exact behavior of the longitudinal field in β CrB. For example, when all of the available field measurements of β CrB are plotted together (Preston 1967) the scatter is larger than expected. Part of the explanation may be in the 10.5 year period for the negative extremum of the magnetic curve of the star (Preston and Sturch 1967) which seems to vary between 0.0 to -800 gauss. In any event, the measurement, reduction and interpretation of the fields are different for the two techniques. Especially during cross-over, when the lines in left and right circular

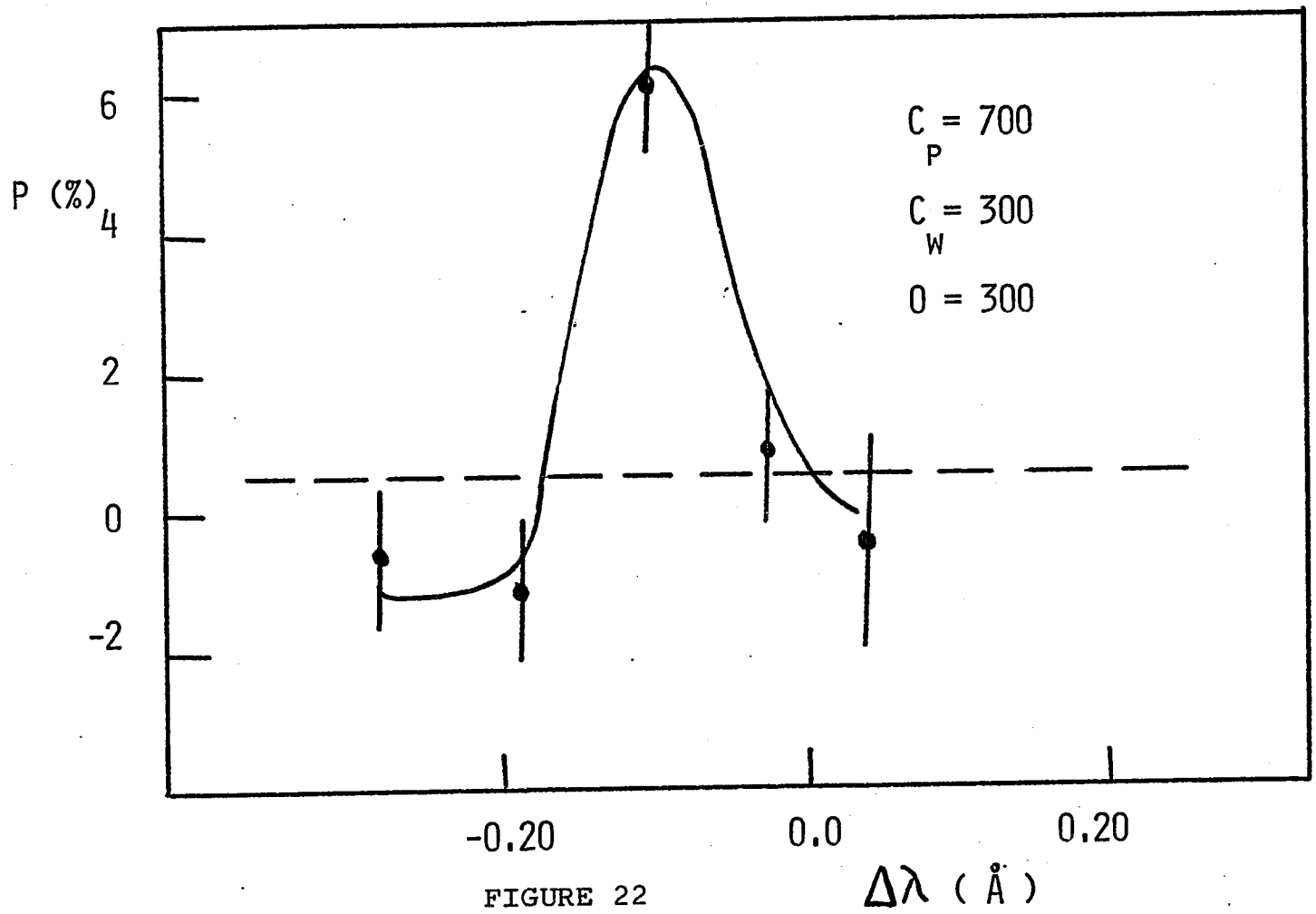

FIGURE 22

High resolution observation of β CrB on J.D. 2441381.0

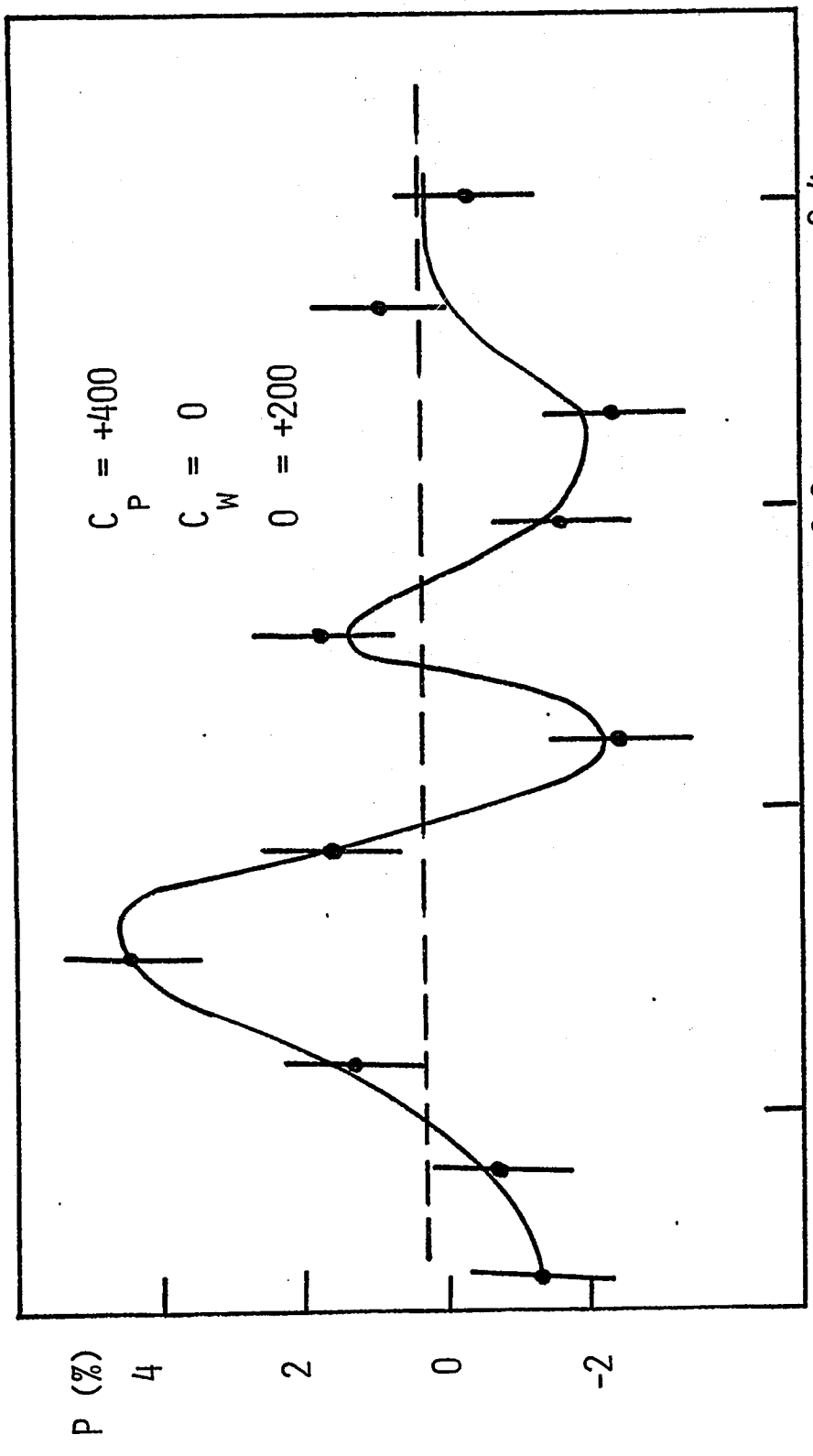

FIGURE 23

High resolution observation of β CrB on J.D. 2441382.0

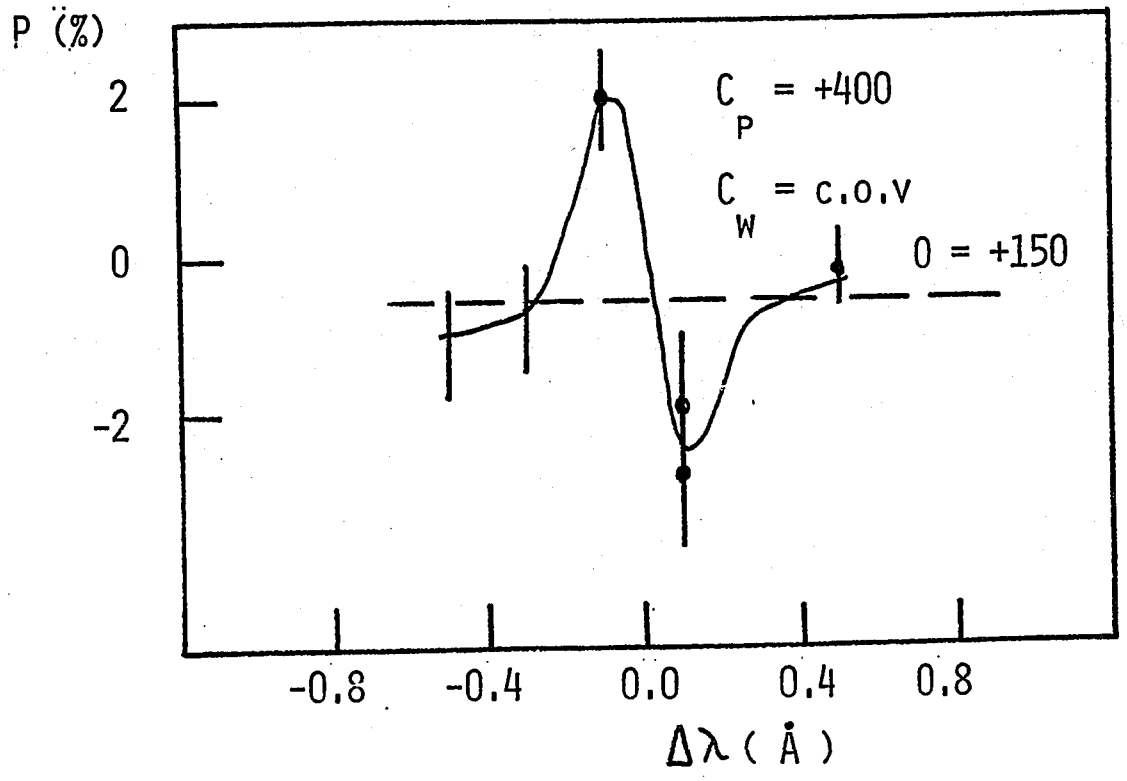

FIGURE 24

Observation of β CrB at Mt. Wilson on J.D. 2441344.0

polarization have different width and shapes, it is not clear what exactly is measured by the photographic technique. Severny (1970) encountered some problems in the agreement between predicted and observed fields. More work should be done on β CrB, possibly over several years to understand its behavior.

4) Observations of γ Cygni

γ Cygni has been reported by Severny (1970) to have a weak ($\sim$ 200 gauss) rapidly varying magnetic field. The star has been observed on several nights at the University of Western Ontario and on two nights at Mt. Wilson. Figure 25 shows some of the polarization scans at the University of Western Ontario. We can see the close agreement between the polarization measured in the continuum with the profile channel and the instrumental polarization (dashed lines). We see a significant deviation from the instrumental polarization only when the measurements are taken in the line itself. The polarization across the line shows the S-shaped profile to be expected for a pure longitudinal field.

Figure 26 shows polarization measurements taken at two points, one in each wing of the line. The polarization is plotted as a function of H.A. . We see that on the red wing (dots) the polarization is systematically higher than the instrumental polarization. In the violet wing (crosses) the polarization is systematically lower

TABLE 5

OBSERVATIONS OF γ CYGNI

OBSERVATORY	λ	POLARIZATION (%)	FIELD (GAUSS)	J.D. 2441+
UW	4254.4	+5.8 ± 1.8	+420 ± 130	154.85
UW	4254.4	-4.9 ± 1.6	-350 ± 115	155.80
UW	4254.4	+7.2 ± 1.7	+520 ± 125	164.83
UW	4254.4	4.3 ± 2.2	Cross-over?	165.75
UW	5247.6	2.0 ± 2.4	No line	171.70
UW	5250.2	2.1 ± 1.8	No line	171.75
UW	4210.4	-3.3 ± 0.9	-140 ± 39	229.60
UW	4210.4	+2.1 ± 1.8	+ 90 ± 43	232.60
MW	4210.4	0.6 ± 0.3	Cross-over?	382.94
MW	4210.4	0 ± 0.30	0 ± 10	383.94

FIGURE 25

Polarization observations of γ Cygni taken on three nights at the University of Western Ontario. A representative observed line profile is shown at the bottom.

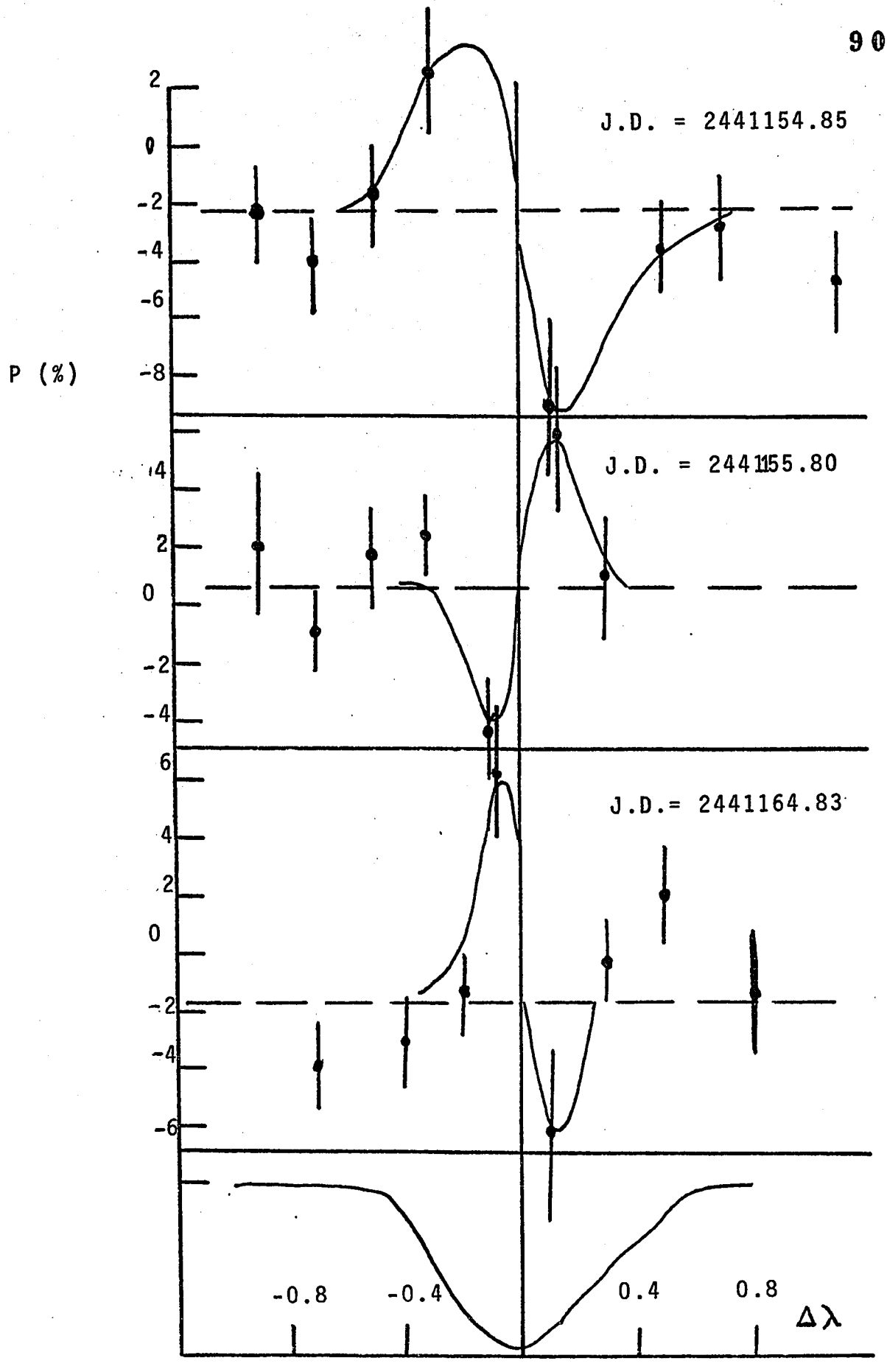
P (%)
J.D. = 2441154.85
J.D. = 2441155.80
J.D.= 2441164.83
2
0
-2
-4
-6
-8
4
2
0
-2
-4
6
4
2
0
-2
-4
-6
-0.8
-0.4
0.4
0.8
Δλ

FIGURE 26

Polarization plotted as a function of HA for γ Cyg and the FeI 4210.4 line. The crosses are readings in the blue wing, the dots in the red wing. The dashed line indicates the instrumental polarization.

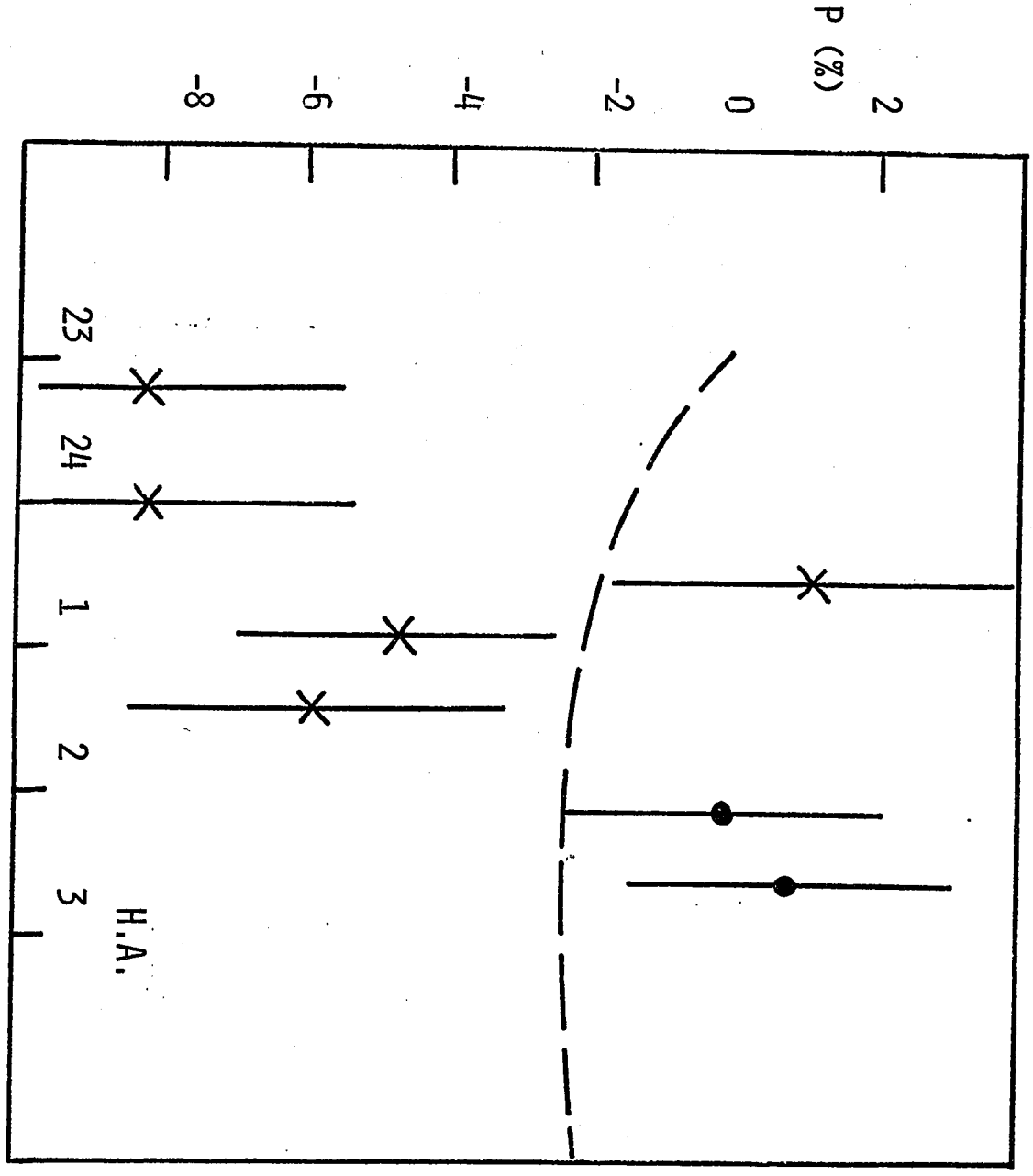
P (%)
2
0
-2
-4
-6
-8
23
24
1
2
3
H.A.

FIGURE 27

Null results for γ Cyg and the CrI 5247.6 and FeI 5250.2 lines. The polarization data are plotted as a function of HA. For the meaning of the symbols REF1, REF and Profile see text.

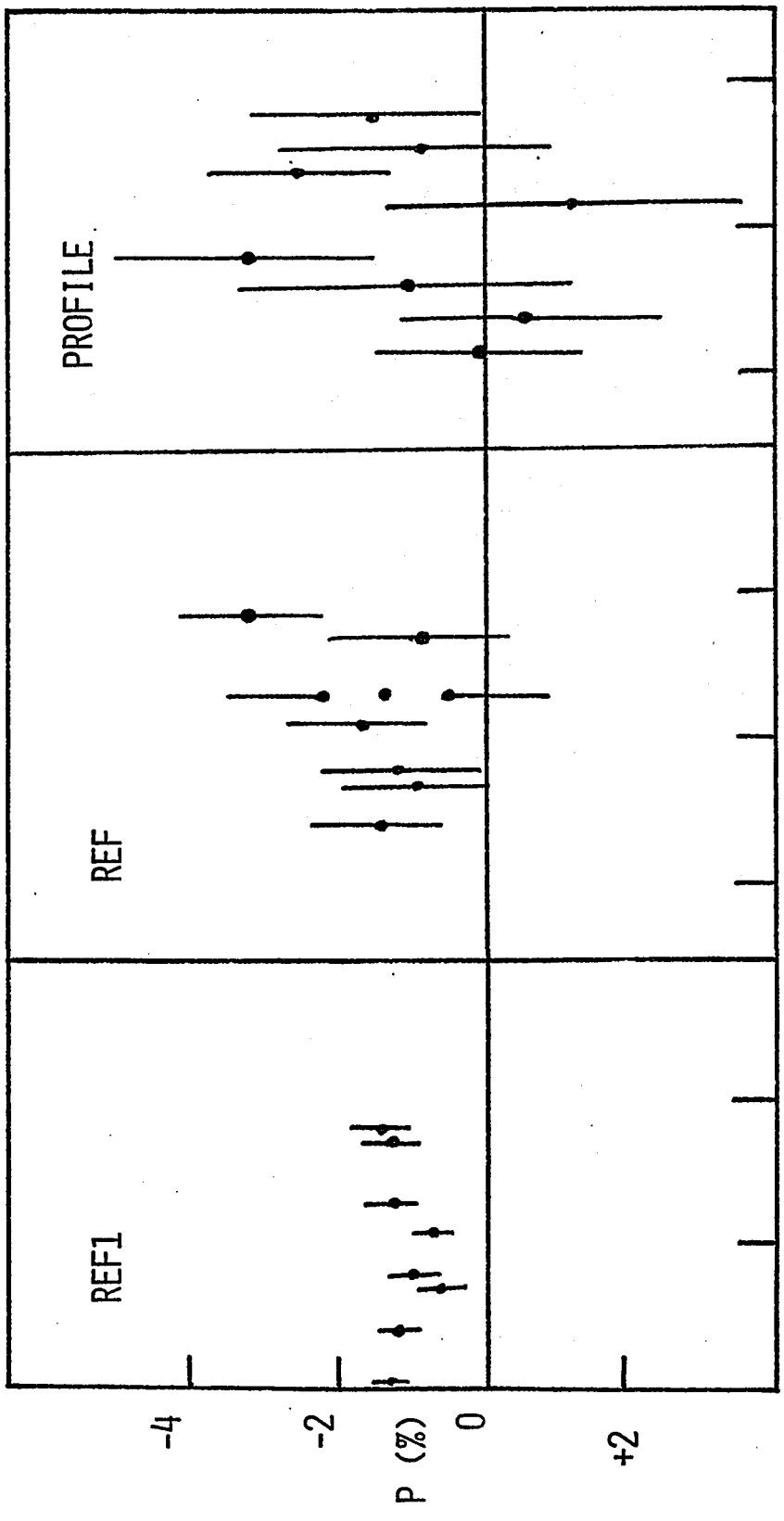
PROFILE
REF
REF1
H.A.
1
24
23
1
24
23
1
24
23
-4
-2
0
+2
P (%)

than the instrumental polarization. Table 5 lists all the measurements of γ Cyg. We can see that almost every time the star is observed, it gives a significant signal. On the night of J.D.2441171.7 the wavelengths scanned are at the location of the 5254.6 CrI line and the 5250.2 FeI line. These lines are not present in this star, or too weak to be observable. Figure 27 shows the polarization measurements plotted as a function of H.A. in the profile channel (prof), the reference channel (refl) during the integration and the measurements in the wide band continuum taken through the same electronics used for the previous profile polarization measurements. (Ref) . We can see the close agreement between these three different measurements. These null measurements give us an additional check, for this star, on the reliability of the techniques used.

The magnetic fields reported in table 5 are in reasonably good agreement with Severny's measurements. It seems quite probable that γ Cyg is a magnetic star.

5) Observations of α Ari and α Aur

Tables 6 and 7 list the observations of these two stars.

α Ari gave mostly no appreciable signal. However, on the night of J.D. 2441171.8 two successive polarization scans gave the same signal on the same point of the red wing of the 5250.2 FeI line. More data are needed to confirm the presence of a magnetic field in α Ari.

TABLE 6

OBSERVATIONS OF α ARI

OBSERVATORY	λ	POLARIZATION (%)	FIELD (GAUSS)	J.D. 2441+
UW	5250.2	0 ± 1.6	0 ± 45	170.8
UW	5250.2	5.6 ± 1.7	160 ± 48	171.8
UW	5250.2	5.6 ± 2.1	160 ± 60	171.85
UW	5250.2	0 ± 1.5	0 ± 42	184.90
UW	5250.2	0 ± 1.5	0 ± 42	185.90
UW	5250.2	0 ± 1.13	0 ± 31	257.80
UW	5250.2	0 ± 1.8	0 ± 51	258.75
UW	5250.2	0 ± 1.0	0 ± 28	204.85

TABLE 7

OBSERVATIONS OF α AUR

OBSERVATORY	λ	POLARIZATION (%)	FIELD (GAUSS)	J.D. 2441+
UW	5250.2	1.3 $\pm$ .60	100 $\pm$ 49	170.9
UW	5250.2	1.5 $\pm$ .50	cross-ov.?	171.9
UW	5250.2	2.2 $\pm$ .45	cross-ov.?	257.95
UW	5250.2	0 $\pm$ .5	0 $\pm$ 35	260.95
MW	6258.4	-0.23 $\pm$ .14	0 $\pm$ 7	379.67
MW	5250.2	0 $\pm$ .23	0 $\pm$ 8	382.75

αAur often seems to give a significant signal. On the night of J.D. 2441257.95 the signal is of the order of 4 standard deviations. On the night of 2441170.9 the signal is S-shaped. On the other nights the signal is more complicated, possibly indicating a cross-over. The presence of a weak magnetic field in αAur is likely, but more observations are desirable.

6) Upper limits

Table 8 lists the stars which do not appear to give significant signals. Usually, several points are measured in the line profile. Any one of them could carry a signal. A variety of shapes of the polarization signal can be obtained with combinations of field geometries and Doppler velocities. For example, suppose that the star has a magnetic "starspot" on the limb approaching us, the signal would then appear as S-shaped but positioned on the blue wing. Things are even more complicated by the fact that the period of variation for the magnetic field does not necessarily have to match the period of rotation of the star (Steinitz and Pyper 1971) and by the fact that if the polarization changes sign inside the bandpass, two successive scans displaced by an amount smaller than the bandpass will give different results.

We have thus no grounds to expect an S-shaped signal or a symmetrical cross-over in all cases. It appears meaningless trying to fit either of these curves to the

TABLE 8

LIST OF UPPER LIMITS

STAR	λ	σ(%)	σ(GAUSS)	J.D. 2441+	OBSERVATORY
β Per	4273.3	1.2	190	308.7	UW
β Ori	4273.3	0.5	80	308.8	UW
α And	4254.4	1.2	200	165.85	UW
α Lyr	4254.4	0.55	90	166.70	UW
α Lyr	4210.4	1.4	100	228.6	UW
ε Uma	4273.3	0.8	130	319.80	UW
α CMa	4273.3	0.4	60	308.9	UW
α Cyg	4254.4	1.9	300	166.70	UW
α Per	4210.4	0.8	35	232.85	UW
α CMi	4210.4	0.8	35	232.80	UW
β Gem	5250.2	0.9	27	260.95	UW
α Boo	5250.2	1.0	20	204.55	UW
ε Peg	5250.2	2.7	75	185.75	UW
ξ Peg	5250.2	1.1	30	204.65	UW
α Tau	5250.2	1.5	42	170.95	UW
α Sco	5247.6	2.2	100	170.65	UW
α Sco	5250.2	1.6	70	171.60	UW
α Per	4210.4	0.5	34	341.79	MW
HD75332	4210.4	1.2	85	383.87	MW
η Boo	4210.4	0.3	18	383.96	MW
ξ Leo	4210.4	0.5	20	341.87	MW
β Gem	5250.2	0.3	11	379.79	MW
β Gem	5250.2	0.14	5	382.71	MW
α Boo	5250.2	0.22	4	378.90	MW

data. Therefore, only the standard deviations for a typical point in the scan is listed in table 8. Typically, the "null scans" have no point more than 1.5 standard deviations from the instrumental polarization. Figures 28 and 29 show some typical scans. We can see the close agreement between the polarization in the spectral line and in the continuum (dashed line). The large amount of null results gives us confidence in the few positive measurements reported.

Among the upper limits reported in table 8 some are worth additional comments.

Radio bursts have been observed in the B8V eclipsing binary β Per (Hughes and Woodworth 1972, Hjellming, Wade and Webster 1972), probably indicating a solar flare-like phenomenon and the presence of a magnetic field. The upper limit reported refers to the photosphere. It will be interesting to measure circular polarization in the emission lines observed by Bolton (1972). Possibly these lines originate from the region responsible for the radio bursts.

The rapidly rotating A_p stars α And ($B9_p$) and ε UMa ($A0_pV$) do not give significant signals (standard deviations respectively 200 and 130 gauss). α And has also been observed photoelectrically by Severny (1970) with no definite effect. Babcock (1958) has found that virtually all A_p stars with sharp enough lines have magnetic fields; therefore it would appear surprising that we have detected no circular polarization. However, we

FIGURE 28

Some null scans determined at the University of Western Ontario. We can see the close agreement between the points in the profile and the instrumental polarization (dashed line) .

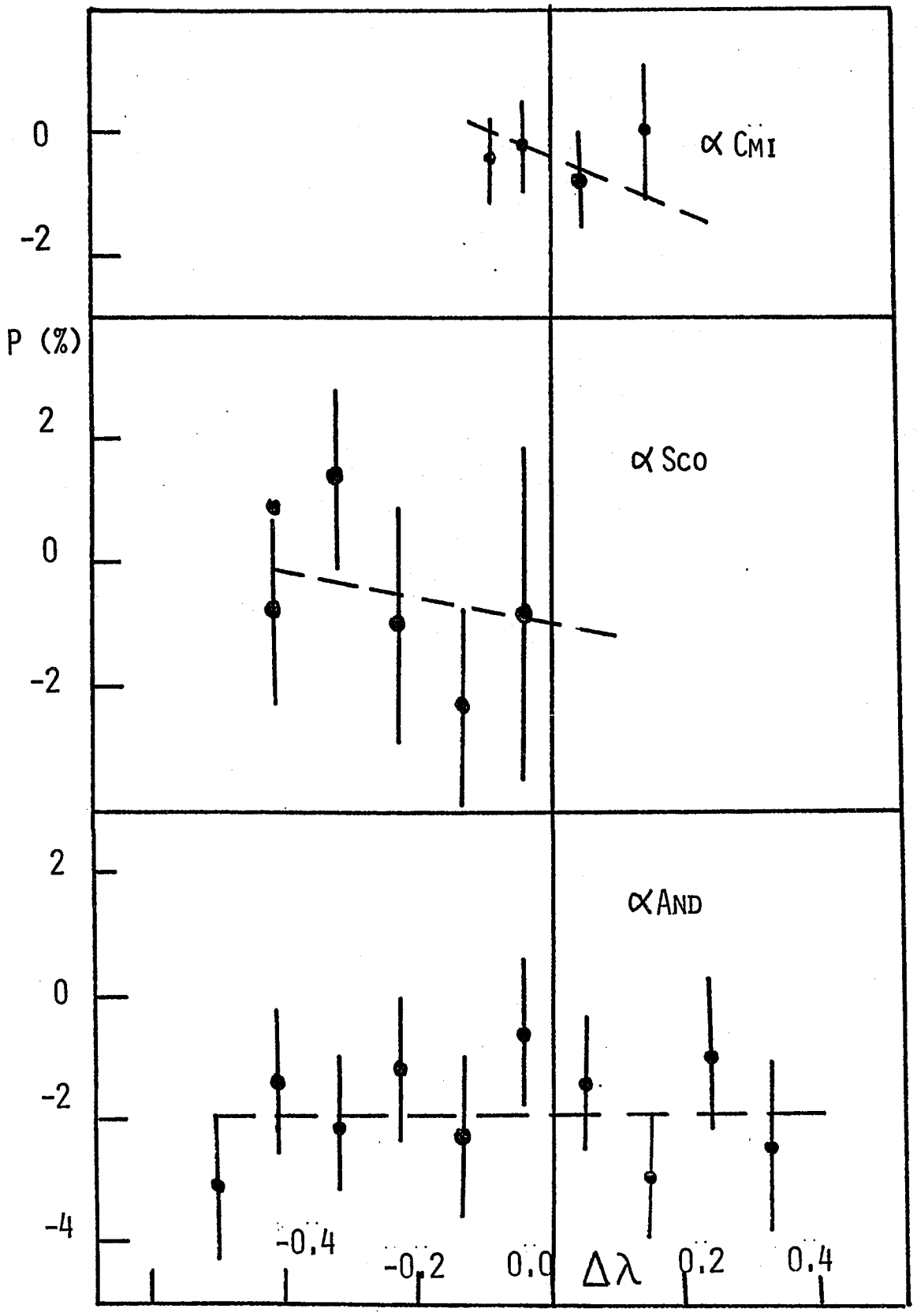
0
-2
∝ CMI
P (%)
2
0
-2
∝ Sco
2
0
-2
-4
∝ AND
-0.4
-0.2
0.0
Δλ
0.2
0.4

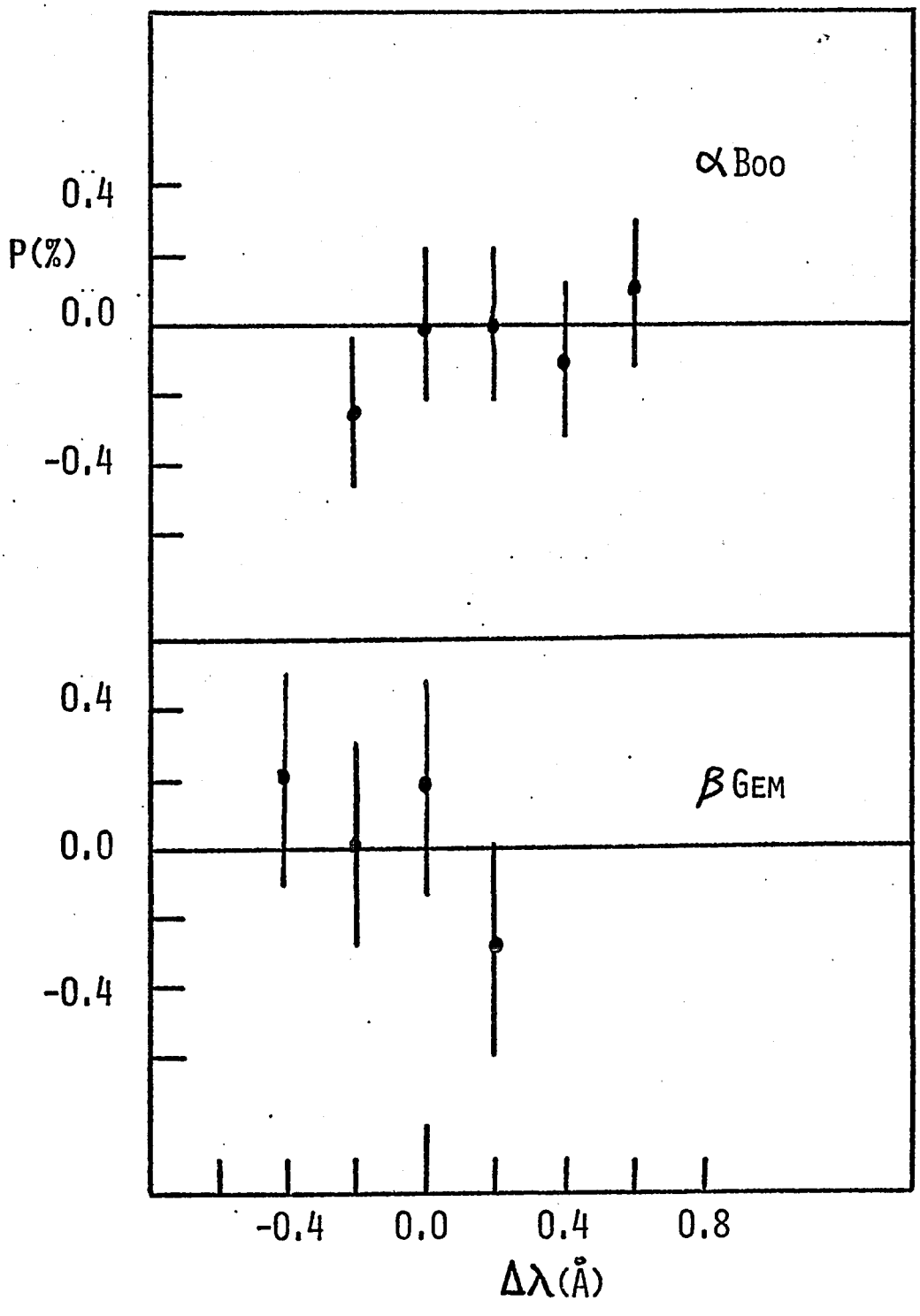

FIGURE 29

Some null results obtained at Mt. Wilson Observatory.

must remember that we are measuring only circular polarization averaged over the visible disk of the star. The field geometry could be of a multipole type and give little circular polarization. However, multipole fields are not present in the slowly rotating A_p stars. Alternatively, a dipolar field could be present and seen equator on. This orientation of the dipole axis has low probability. From a model (see chapter X for details on the computational technique) of a star rotating at 20 Km/sec at the equator, possessing a dipolar field seen perpendicular to the axis of the dipole, with a polar field of 11,000 gauss, we found that the polarization in the line (4254.4 CrI) reaches a miximum of 0.01 %, well below the observational error. The rotation axis and dipole axis coincided in this model.

HD 75337 (σ = 85 gauss) is observed to have an emission component in the core of the Ca II K line. This has been taken to indicate the presence of magnetic field of the order of 10^2 gauss (Skumanich 1972).

β Gem (K0III, σ = 5 gauss) has been observed by Severny (1970). He reports the marginal detection of a field of 100 gauss with a probable error of 50 gauss. With a better line and longer integration times we have reduced the error by an order of magnitude. It is doubtful that β Gem has a longitudinal field of the order of 100 gauss.

Severny (1970) finds a definite effect in β Ori

(B8Ia) and Sirius (A1V). Our upper limit for β Ori (80 gauss) is too high for the reported field of 130 gauss. We will discuss Sirius in the next section.

7) High-resolution observations

A pressure scanned Fabry-Perot interferometer (Vaughan 1967) was used on several nights at Mt. Wilson observatory. The modus operandi is the usual one, with the Fabry-Perot interferometer mounted in front of the movable photomultiplier. In this configuration the Fabry-Perot interferometer is placed behind the polarizing optics and does not affect the polarimetry. The bandpass is 0.038 Å. Table 9 lists the observations.

Figures 30 to 32 show some of the polarization scans obtained. None of the scans gives a significant signal, with the possible exception of the scan of Sirius on J.D. 2441381.7 (figure 30). The dots and the circles indicate two successive scans. We can see that the two scans follow each other very closely. There appears to be an S-shaped profile; however, it is not centred on the CrI 4254.4 line (the strongest in figure 30) but rather seems to be centred on a weaker line to the red. This line is not identified. There is no plausible candidate in the revised multiplet table (Moore 1945). The line is also present in the spectrum of the A0 IV χ Geminorum. There might be a complicated signal on the 4254.4 line; however, it does not stand clearly above noise.

With the limited data available now we can propose

TABLE 9

HIGH-RESOLUTION OBSERVATIONS

STAR	λ	σ(%)	σ(GAUSS)	J.D. 2441+
ι CrB	4233	0.85	30	383.0
Sirius	4254.4	0.31	20	380.7
Sirius	4254.4	SEE TEXT		381.7
Sirius	4254.4	0.10	7	383.7
α^2 Lib	4254.4	0.7	68	382.9

FIGURE 30

High-resolution observation of Sirius taken at Mt. Wilson on J.D. 2441381.7. The dots and circles indicate two consecutive scans. An intensity scan is displayed at the bottom of the figure.

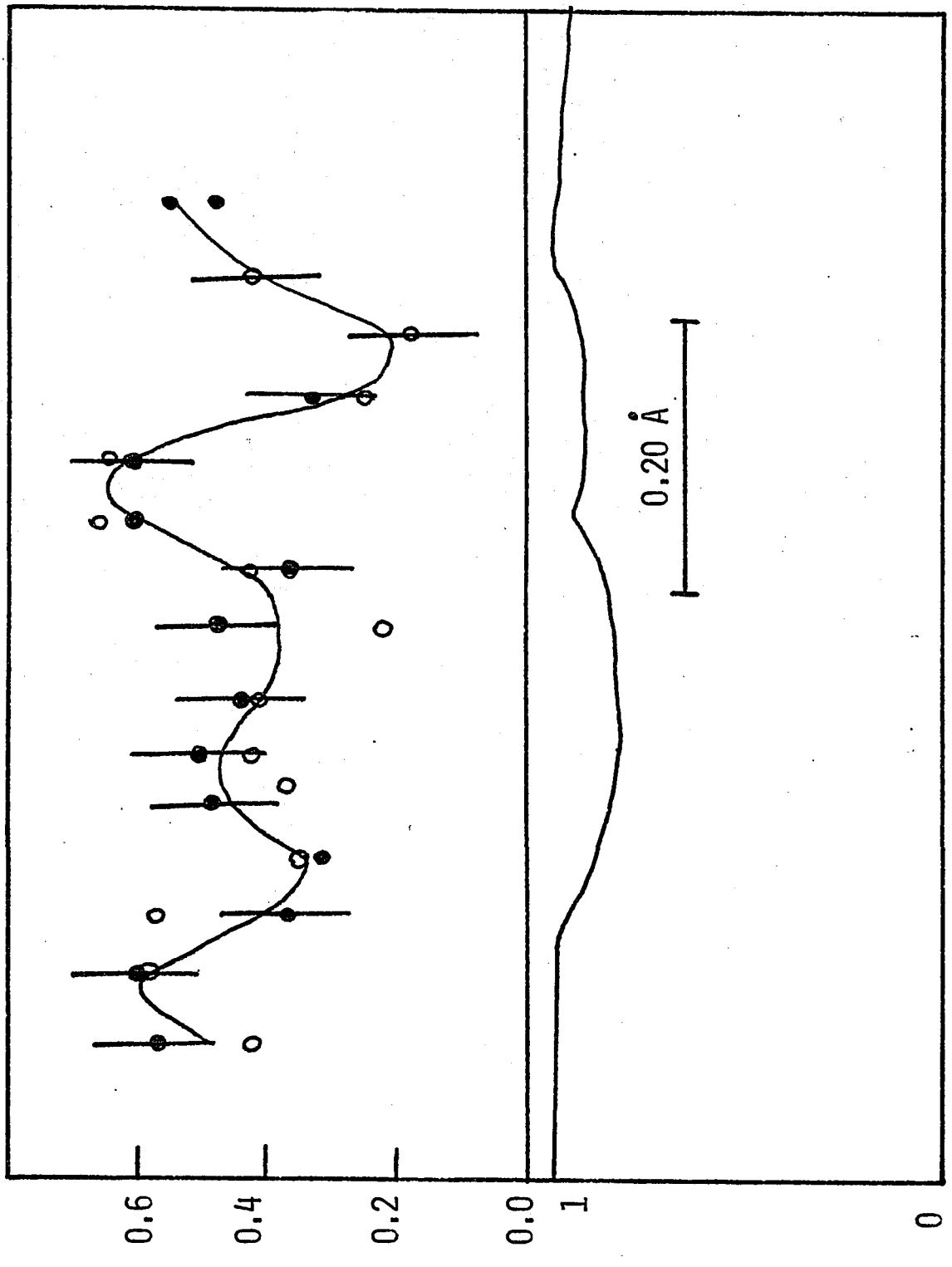
0.6
0.4
0.2
0.0
1
0
0.20 Å

FIGURE 31

High-resolution observation of α^2 Librae.

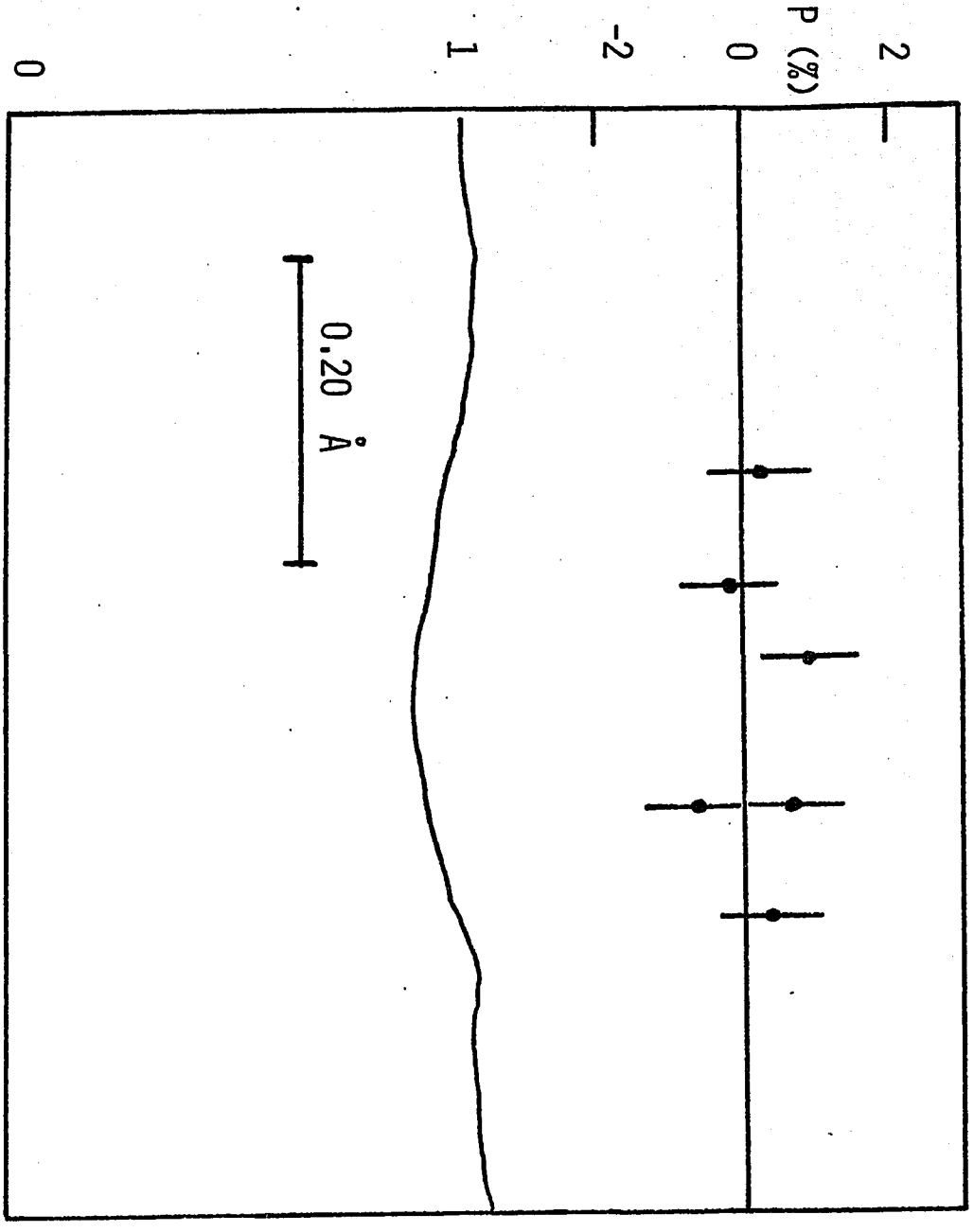
P (%)
2
0
-2
1
0
0.20 Å

FIGURE 32

High-resolution observations of Sirius taken two days after the observation in figure 30. There is no significant signal.

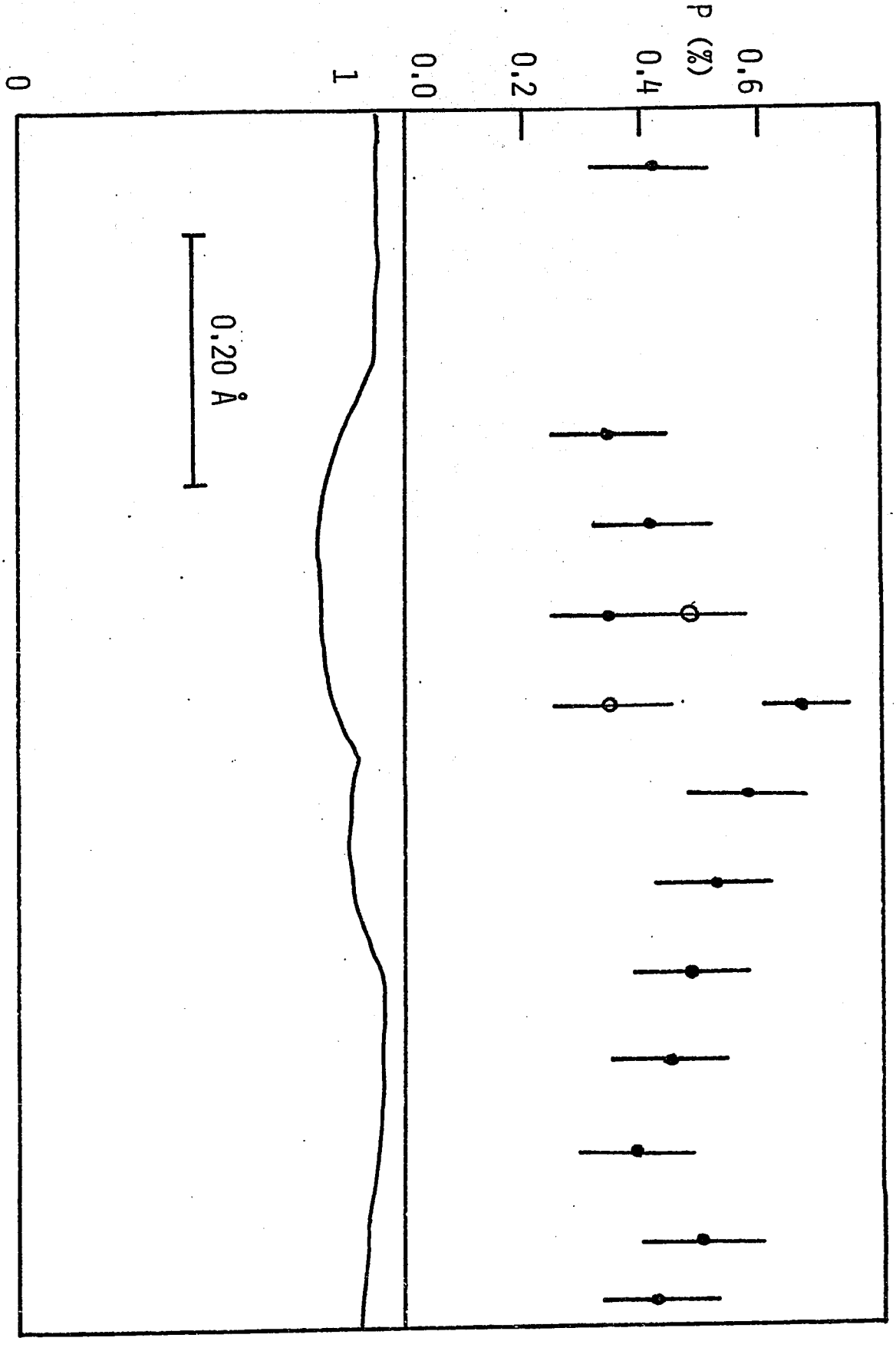
P (%)
0.6
0.4
0.2
0.0
1
0
0.20 Å

two possible interpretations for this observation. The unknown line might have a larger Landé g factor than the 4254.4 CrI line and therefore stand higher above noise. Alternatively, the signal belongs to the 4254.4 line and originates from a red-shifted region. The red-shift is $\sim$ 10 km/sec and there is a hint of a similar signal blue-shifted by 10 km/sec, this last one barely above noise. The rotational velocity of Sirius is essentially zero (notice the sharpness of the lines) and these Doppler shifts cannot be easily explained, unless the spots rotate faster than the star. Note that the regions of the star in which these hypothetical spots are present are necessarily small, compared to the visible disk, as they contribute little to the line profile. Therefore, the field would be stronger than implied by the visible circular polarization, as it is diluted by the unpolarized continuum from the rest of the disk.

8) Conclusions

Of the stars observed, excluding β CrB, only four gave a significant signal. In most observations the random error is still fairly large, although theoretical investigation of the technique shows that considerable improvement is possible.

Our observations raise more questions than they answer. If α Ari and α Aur are definitively confirmed to have magnetic fields we shall have to consider the

origin of those fields. The radius of α Ari should be $\sim$ 21 $R_\odot$ and the radius of α Aur $\sim$17 $R_\odot$. Let us assume that these fields were carried from the main sequence. Let us also, for simplicity, suppose that the stars conserved the geometry of the magnetic field throughout the evolution and let us make the assumption of conservation of magnetic flux from the main sequence. Under those assumptions we can scale the longitudinal field $H_e \propto R^{-2}$, where R is the stellar radius. Both of those stars could originate from a 3 $M_\odot$ star (Iben 1967) with radius 2.5 $R_\odot$ on the main sequence. Thus, having at present longitudinal fields of $\sim$100 gauss we would have $\sim$ 7 kgauss for α Ari and $\sim$ 4.5 kgauss for αAur when the stars were on the main sequence. Both the mass and the longitudinal field for these two stars have reasonable values for an A_p star. Are thus α Ari and α Aur evolved A_p stars?

γ Cygni lies roughly on the evolutionary track of a 9 $M_\odot$ star (Iben 1967). Applying arguments similar to the ones for α Ari and αAur, γ Cyg would have had a longitudinal field $\sim$ 100 kgauss and, assuming a dipole field seen nearly pole on, a surface field of $\sim$ 400 kgauss on the main sequence. Both the mass and the field are too high for an A_p star. The longitudinal field would be one order of magnitude higher than the highest main sequence magnetic fields observed. For a line at 4300 Å with g = 2.0 a field of 400 kgauss would give a separation

of 14 Å between the σ components. Such a magnetic field in an early-type star could hardly escape detection. Unless γ Cyg had an extraordinarily large field on the main sequence, we should thus conclude that there is a mechanism for generation of the magnetic field in the star.

On the other hand, we must consider that the numbers in the preceding discussion are only rough estimates. Besides the assumptions on the behaviour of the magnetic field throughout the evolution of the star, there is an uncertainty in the estimate of the present radii and the radii on the main sequence.

It is not possible to determine a period for γ Cyg from our observations or Severny's. However, from table 5 we notice that the field reverses polarity in $\sim$ 24 hours. If the field is periodically variable, the period is unlikely to be more than three days. This would imply a velocity at the equator much larger than the break-up velocity for a 9 $M_\odot$ star with a 80 $R_\odot$ radius. We are thus not dealing with an oblique rotator.

CHAPTER X

MODELS OF MAGNETIC STARS

1) Introduction

The model that seems to fit best the observations of most of the known magnetic stars is the oblique rotator model (Preston 1971). This model has been discussed by several authors (Babcock 1949, Stibbs 1950, Deutsch 1954, Landstreet 1970, Preston 1971). In this chapter we discuss detailed polarization and line profiles predicted by this model.

The basic assumption of the oblique rotator is that the magnetic field (or other physical parameter such as abundance of a certain element) is distributed about an axis inclined to the rotation axis of the star. The rotation axis itself is inclined at an angle to the line of sight. The magnetic field variations are then produced by the rotation of the star presenting a different field configuration at different phases. In this model the period of rotation of the star is the period of rotation of the magnetic field configuration, hence the name oblique rotator.

Figure 33 shows the geometry of the oblique rotator. The axis s contains the line of sight, the axis of rotation of the star $\vec{\omega}$ is inclined by an angle i to the line of sight. The axis $\vec{m}$ is the axis of symmetry of

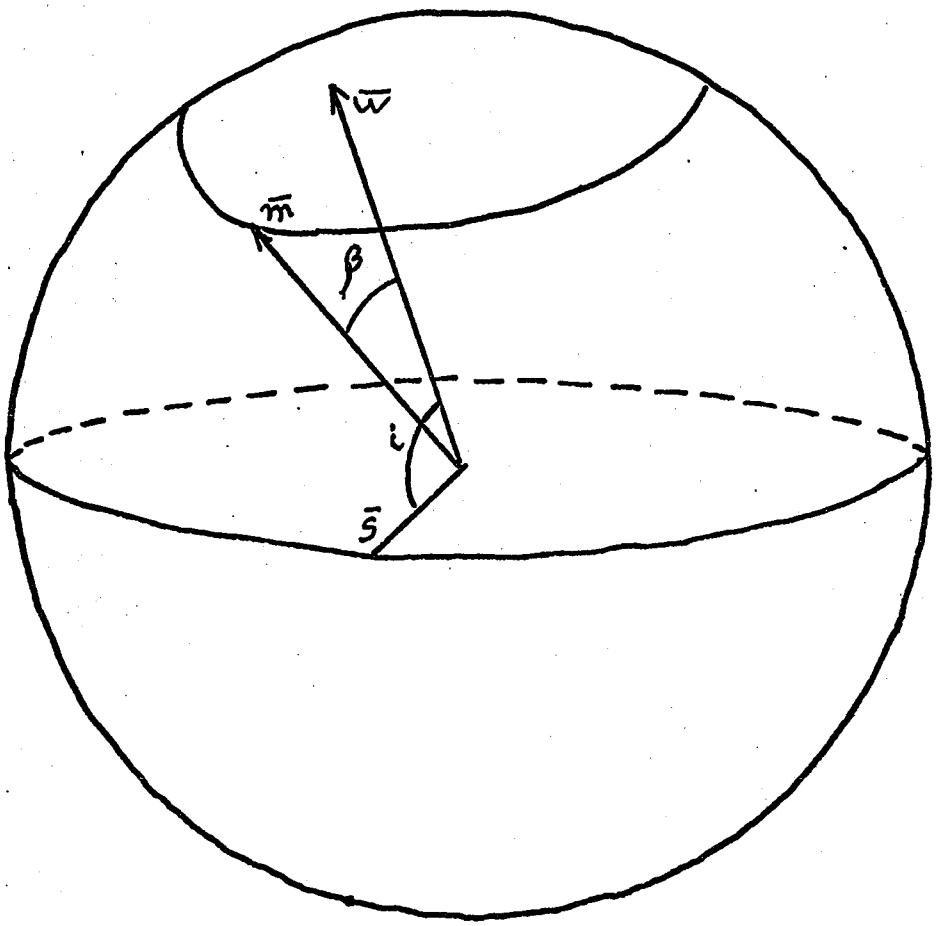

FIGURE 33

The axes and parameters of the oblique rotator are illustrated in this figure. See the text for more details.

the dipole field and is inclined by an angle β about the axis of rotation.

The geometry of the magnetic field we will consider will be of the dipole type. A dipole-like configuration of the magnetic field appears to be generally successful in reproducing the observations of A_p stars (Preston 1971). Some A_p stars appear to have a stronger and a weaker magnetic pole; these may roughly be represented by the displaced dipole model (Landstreet 1970). In this model the dipole is displaced from the centre of the star along its axis of symmetry. In this fashion we obtain an unequal pole strength, but still have a divergence-free geometry of the magnetic field.

2) The computer program

I have written a computer program to compute the wavelength dependence of the Stokes parameters for a spectral line formed in the presence of a magnetic field in a rotating star.

The star is subdivided in slices of roughly equal area. The magnetic field strength, the azimuth (with respect to the rotation axis of the star) of the lines of force and their inclination with respect to the line of sight, are computed for each slice, given the parameters of the magnetic field configuration. For a dipole field, the input parameters are: β the inclination of the dipole axis on the rotation axis; H_p the polar field

strength; a the displacement, in stellar radius units, of the dipole from the centre of the star.

Unno's (1956) analytic solution to the transfer of the Stokes parameters for a line formed in the presence of a magnetic field is used to compute the wavelength dependence of the Stokes parameters for each slice. The rotation of the star is taken into account by Doppler shifting the Stokes parameters using the calculated velocity along the line of sight for each slice. The Stokes parameters are integrated numerically over the visible projected surface of the star.

The program is very versatile, the geometry of the magnetic field is chosen at will, and non-analytic configurations are possible. Even the assumption of an oblique rotator can be lifted by decoupling the dipole frame, or giving different radial velocities to contiguous slices.

The solution to the equations of transfer used here assumes that the line is formed by pure absorption in an atmosphere with a source function linear with depth $B = B_0 + B_1\tau$, and that $\eta_0 = k_e/k_c$ is constant with depth (Milne-Eddington approximation). A depth dependent model could be used; however, the numerical integration over the disc (necessary because of the treatment of rotation) would necessitate a large amount of computing time. Unno's equations would have to be solved for every field strength and inclination of the field lines to the line of sight. It would still be possible to solve the pro-

blem with depth dependent models by making a grid of models and interpolating within tables. The computing time will still be large. Typically, it takes three minutes per model with a DEC PDP 10 using the Milne-Eddington model.

In any event, for a preliminary investigation the Milne-Eddington model approach can give enough insight into the problem. One can leave more sophisticated models to a later date. The existing models for the line profiles from an oblique rotator (Bohm-Vitense 1967, Hockey 1971) are based on much simpler theories and approximations than the present ones.

The input parameters of the program are:

a) effective temperature of the star T

b) microturbulent velocity ξ_m

c) equatorial velocity V_e

d) inclination of the axis of rotation on the line of sight i

e) wavelength of the absorption line λ

f) atomic weight of the element M

g) the ratio $\eta_0 = \kappa_0/\kappa_c$ of the absorption coefficient in the centre of the line to the continuous absorption coefficient

h) the parameter β_0 = B1/B0 for the Milne-Eddington model in which the source function variation with depth is given by $B(\tau) = B0 + B1\tau$

i) the Landé g factor of the line

j) the inclination of the axis of the dipole with respect to the rotation axis of the star, β .

k) H_p, strength of the magnetic field at the pole (for a dipole or quadrupole field)

l) the parameter a that gives the fractional displacement of the dipole from the centre in the Z direction. The ratio of the field strength at Z = +1 to the one at Z = -1 is given by $H_{+1}/H_{-1} = \left[(1+a)/(1-a)\right]^3$

The output of the program gives: the surface field, the longitudinal field and transverse field averaged over the visible surface of the star and weighted by the local liminosity; the Stokes parameters I,Q,U.V as a function of wavelength for the whole star; the line profile seen in left and right circularly polarized light; the displacement between these two lines. The last two pieces of information are useful in trying to understand what is measured by photographic Zeeman analyzers.

3) Circular polarization from an oblique rotator

In the frame-work of the limitations and approximations of the model, we can examine the behavior of the V Stokes parameter when the parameters of the models are changed. It is especially desirable to find a reliable observational parameter to use as a measure of the longitudinal field strength. We will test the accuracy of the reduction procedure used in Chapter IX to translate the observed circular polarization into longitudinal magnetic

fields. We will also examine the reliability of $\Delta\lambda$ as an indicator of the longitudinal field strength. Although we will not examine them here, other measures of the longitudinal field strength that could be considered are: the fit of an S-shaped profile to the polarization signal; or, the determination of the separation between the Zeeman analyzed line profiles from some suitable criterion such as the ones used by photographic observers. For reasons of space and because this investigation is concerned only with the detection of circular polarization, we will not discuss the behavior of the U and Q Stokes parameters.

The main limitations of the models considered are the following:

a) The magnetic field geometry

The field geometry is approximated by a dipole. Although there is evidence that the overall field in known magnetic stars is of the dipole type, it is doubtful whether the field is a perfect dipole over the surface of the star. The actual geometry is probably somewhat spotty. There is also some evidence that for some magnetic stars the oblique rotator model itself is not valid (Steinitz and Pyper 1971).

b) Milne-Eddington approximation

The model for each element of the surface of the star is certainly not strictly correct. The actual source function is not linear with depth and the ratio $\eta_o = \kappa_o/\kappa_c$

is not constant with depth. The results reported in here cannot be interpreted in a rigorously quantitative fashion. It might be interesting to repeat the computations with a Schuster-Schwarzscild approximation to see how model dependent the conclusions are (see Michard 1961).

c) The atomic absorption coefficient is assumed to have a Gaussian dependence with wavelength. This assumption is invalid for strong saturated lines.

d) The results are valid only for lines exhibiting the normal Zeeman effect.

All of the input parameters can, to various extent, influence the amplitude and wavelength dependence of the Stokes parameters integrated over the visible disc of the star. For reasons of space we cannot consider all possible combinations of input data. We will instead set a standard model and standard line and vary sequentially, one at a time, some of the most important parameters. In the following pages we will especially be concerned, in view of the reduction procedure adopted in chapter IX, about the validity of the relation

$$V \propto g\lambda^2 \frac{dI}{d\lambda} H \cos\gamma$$

The standard line has a wavelength of 4300 Å and originates from an ion of atomic weight 52 and a transition with a Landé g factor of 2.0 . The line is slightly saturated, with $\eta_0 = 30.0$. This should reproduce

approximately a typical line we measured. The model atmosphere has β_o = 2.0 giving a line depth of ~60% at saturation. The temperature of the atmosphere and the microturbulent velocity give a Doppler width = 0.045 Å .

The standard star has a dipole geometry (a = 0.0). The strength of the magnetic field at the poles is 1000.0 gauss. The rotation axis is perpendicular to the line of sight and the equatorial velocity is taken to be negligable (Ve = 0.0). The axis of the dipole is inclined at 90° to the rotation axis, with the dipole seen pole on. In this configuration, the longitudinal field is He = 336 gauss and the surface field Hs = 806 gauss. Figure 34 shows the line profile and V parameter resulting from the standard line and model. The line profiles seen through a Zeeman analyzer are symmetric. The approximations of chapter VI are still valid for the longitudinal field case.

a) Varying the strength of the polar field H_p

Table 10 gives the polar field strength H_p, the effective longitudinal field H_e and surface field H_s averaged over the visible disk of the star, the circular polarization V (V = 1.0 corresponds to 100% circular polarization). H_c is the longitudinal field derived from V following the reduction procedure of chapter IX.

$\Delta\lambda$ is the separation in Å between the lines seen in left and right circularly polarized light.

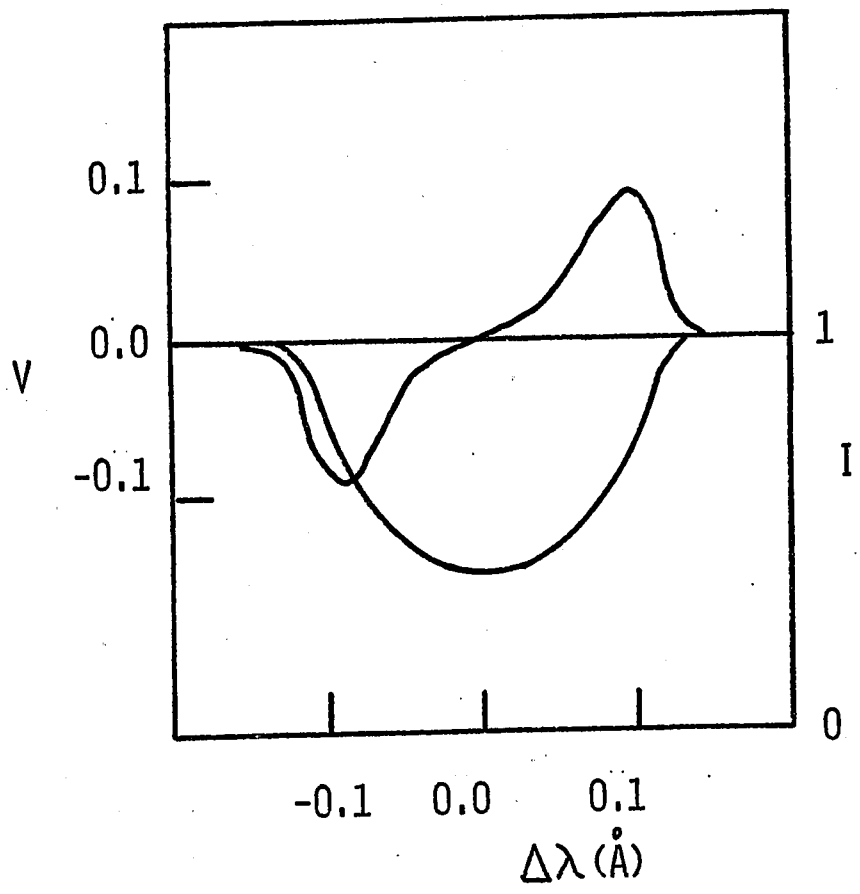

FIGURE 34

Line profile I(λ) and circular polarization V(λ) for the standard model and standard line.

TABLE 10

PARAMETERS OBTAINED VARYING H_p

H_p	H_e	H_s	V	H_c	$\Delta\lambda$	H_Δ
100	34	81	.011	34	.0014	40
200	67	161	.022	68	.0028	80
300	101	242	.033	102	.0041	119
400	134	323	.044	136	.0055	160
500	168	403	.054	170	.0068	198
600	202	484	.064	198	.0082	240
700	235	564	.074	228	.0095	273
800	269	645	.082	252	.0108	315
900	302	726	.091	280	.0120	350
1000	336	806	.098	320	.0133	385
2000	670	1610	.148	720	.025	730
3000	1000	2420	.171	890	.036	1050
4000	1340	3230	.184	1330	.046	1330
5000	1680	4030	.192	1920	.057	1650
6000	2020	4840	.197	2520	.068	1970
7000	2350	5640	.200	4000	.081	2340
8000	2690	6450	.201	4400	.095	2720
9000	3020	7260	.202	5950		

The parameter $\Delta\lambda$ is defined by

$$\Delta\lambda = \frac{\int r_1(\lambda)\,\lambda\,d\lambda}{\int r_1(\lambda)\,d\lambda} - \frac{\int r_2(\lambda)\,\lambda\,d\lambda}{\int r_2(\lambda)\,d\lambda} \qquad (32)$$

where $r_1(\lambda)$ and $r_2(\lambda)$ represent the line profiles seen in the two opposite signs of circular polarization. H_Δ is obtained from $\Delta\lambda$ using the formula (Babcock 1962)

$$H_\Delta = 52.7 \left(\frac{4500}{\lambda}\right)^2 \frac{\Delta\lambda}{g} \times 10^3 \qquad (33)$$

In figure 35 we have plotted the highest value of V in the line as a function of H_e and in figure 36, H_c as a function of H_e, the dashed line corresponds to the locus where $H_e = H_c$. The slope of the line profile, $\frac{dI}{d\lambda}$, used for the reduction has been determined with a ruler using line profiles displayed graphically by the computer. In this fashion, we reproduce closely the actual reduction procedure, including the difficulty in determining the slope when the line profile is deformed by a strong magnetic field or by rotation.

We can see that V increases linearly with H_e only for weak longitudinal fields ($H_e \sim 300$ gauss, $H_p \sim 1000$ gauss). Correcting for the slope of the line improves H_c, however, for longitudinal fields greater than 2000 gauss, we overestimate grossly H_e. This can be explained because the basic assumption in the reduction formula is that the slope of the line is the same in the two polarization signs and the line seen in total light. Figure 37 shows the line profiles seen in total light and

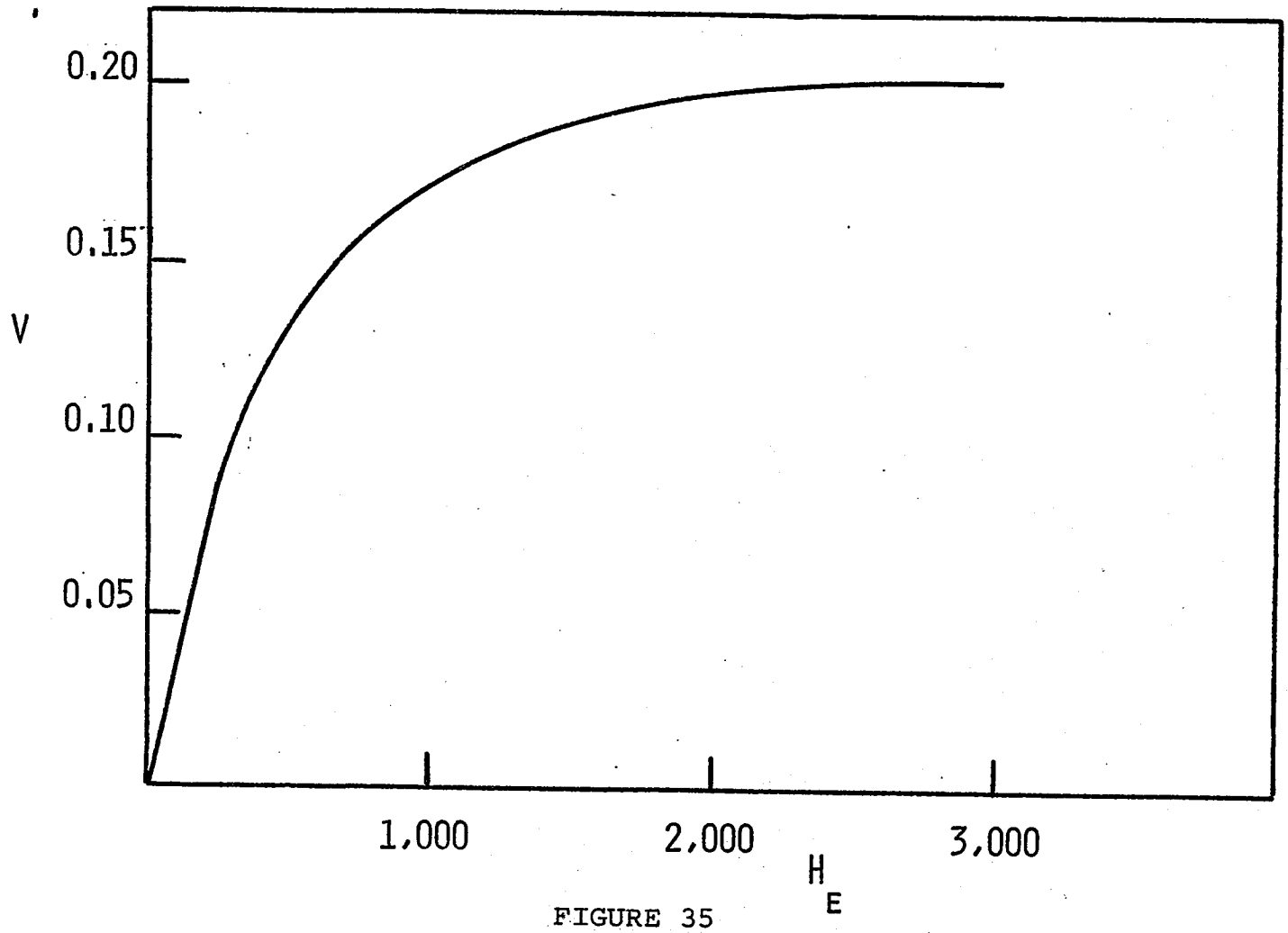

FIGURE 35

The highest value for the circular polarization across the line is plotted against H_e.

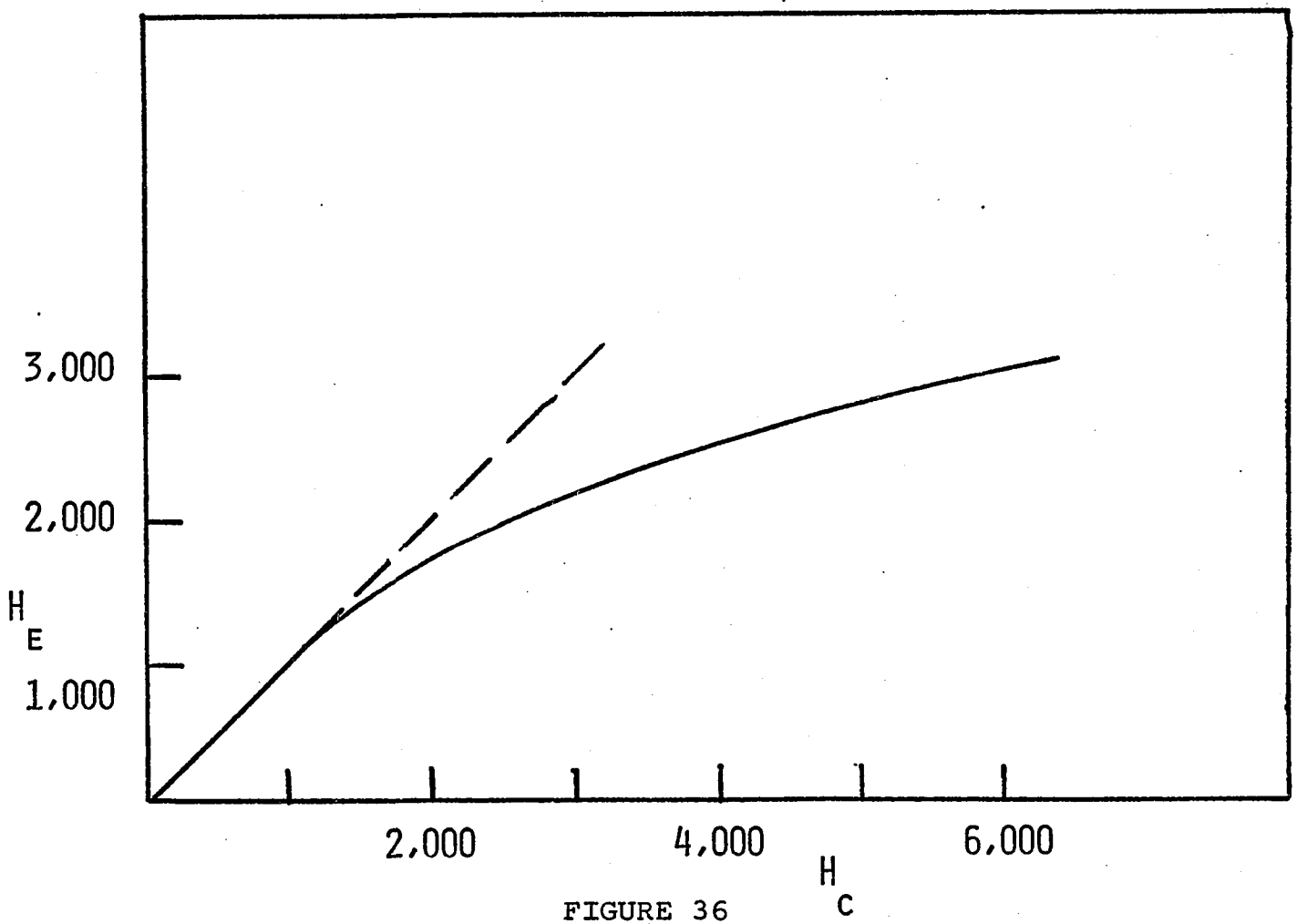

FIGURE 36

H_c is plotted as a function of the effective longitudinal field H_e. The dashed line indicates the locus $H_c = H_e$.

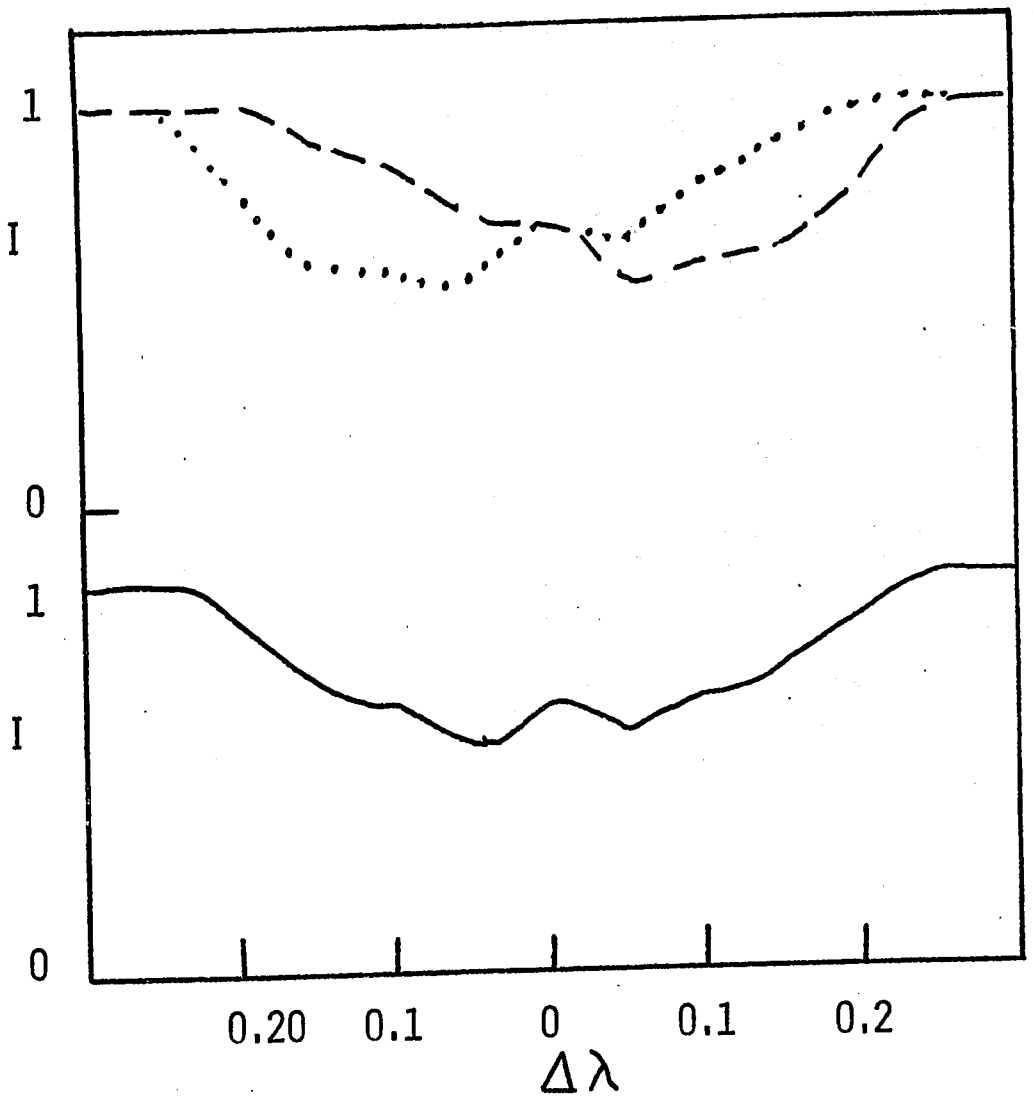

FIGURE 37

Line profiles for the standard model with H_p = 8,000 gauss (H_e = 2700 gauss). The full line is the line profile seen in total light. The dashed and dotted lines are the line profiles seen through the Zeeman analyzer.

Zeeman analyzed (respectively, full line, dashed and dotted lines), for a longitudinal field of 2700 gauss (H_p = 8000 gauss). We can see that the line profiles seen in polarized light are strongly asymmetrical.

We must notice that $\Delta\lambda$ is a much better measure of the longitudinal field, for strong fields. For example, for the model H_p = 8000 gauss, a separation of 0.095 Å (using equation 31) gives a longitudinal field of 2720 gauss, in excellent agreement with H_e = 2690 .

b) Changing the inclination of the dipole

Table 11 shows the characteristics of a strong field model (H_p = 6000 gauss) when α , the angle between the dipole axis and the line of sight changes. We see that the computed longitudinal field H_c gives us an overestimate when α is small, therefore H_e large. When the angle α is large and therefore H_e small, we tend to underestimate the longitudinal field. Again we have that $\Delta\lambda$ gives a better estimate of H_e .

c) Changing the strength of the line

Table 12 lists the characteristics of the models with increasing line strengths η_o . The agreement between H_c and H_e is satisfactory. There is perhaps a tendency to underestimate somewhat the field for weak lines. $\Delta\lambda$ seems, instead, to give too large a field for weak lines; however, the error is small.

TABLE 11

PARAMETERS OBTAINED VARYING THE INCLINATION

α	H_e	H_s	V	H_c	$\Delta\lambda$	H_Δ
0°	2015	4840	.197	2560	.068	1970
18°	1920	4740	.188	2500	.065	1900
36°	1630	4470	.160	1780	.056	1620
54°	1190	4150	.118	1170	.042	1220
72°	620	3890	.063	650	.022	640
76°	500	3860	.050	420	.018	520
79°	380	3830	.038	300	0.014	410
83°	250	3810	.025	214	.0090	260
87°	130	3800	.013	110	.0045	130

TABLE 12

PARAMETERS OBTAINED VARYING THE INTENSITY OF THE LINE

η_o	v	H_c	$\Delta\lambda$	H_Δ
2	.053	310	.0137	398
4	.067	310	.0136	394
8	.079	336	.0135	392
16	.090	336	.0134	388
32	.099	336	.0133	386
64	.106	340	.0132	382

d) Influence of rotation

Rotation is the parameter influencing most the wavelength dependence of the Stokes parameters because of the Doppler effect. In an oblique rotator the only phases at which the wavelength dependence of the V Stokes parameter is still S-shaped is close to phases 0.0 and 0.5 when the dipole axis is close to the line of sight. The models in table 13 are computed for phase 0.0 .

We can see from table 13 that we overestimate by as much as a factor of two the longitudinal field. Even an equatorial velocity as small as 5 Km/sec gives a large error in H_e. The somewhat erratic behavior of H_c as a function of V_e , gives also an idea of the difficulty of determining the slope of the line for a line broadened by rotation. Notice that $\Delta\lambda$ is not affected at all by rotation and gives an accurate measure of the longitudinal field.

e) Conclusion

The reduction procedure seems to be reasonably good for weak fields. However, there are substantial systematic errors for large fields. This is no limitation for the reduction procedure. We can still measure strong longitudinal fields if we use lines with small Landé g factor, thus increasing the value of H_e at which saturation sets in.

A serious case where the reduction procedure seems

TABLE 13

INFLUENCE OF ROTATION

V_e	V	H_c	$A\lambda$	H_A
0	.099		.0133	386
5	.066	490	.0133	386
10	.041	450	.0133	386
15	.027	690	.0133	386
20	.017	570	.0133	386
50	.0029	620	.0133	386

to fail is when rotation is important. Therefore, the problem is especially bad for main-sequence stars earlier than F5. Not only does it give systematic errors when the dipole is seen pole on, but the problem is hopeless during cross-over. We will discuss the problem of rotation in more detail in the next section when making models for some particular A_p stars. We will see that H_Δ gives a reasonable estimate of H_e.

4) Models for some known magnetic stars

a) β Coronae Borealis

The magnetic star β CrB is the second brightest magnetic star in the sky and it has been extensively studied using the photographic technique. The longitudinal field is reasonably strong and the strength of the spectral lines is not seen to vary during the magnetic field cycle. This star is thus an ideal candidate for any attempt to determine the geometry of the magnetic field.

Wolff and Wolff (1970) using data from Preston and Sturch (1967) and Preston (1969_c) and through the analysis of high dispersion spectrograms of β CrB, attempted to determine the geometry of the magnetic field. They concluded that the variations of the longitudinal and surface fields can be represented by an oblique rotator model with the parameters H_p = 11,000 gauss, a = 0.1, i = 20° , β = 87° and V_e = 6 Km/sec.

We have additional data in the form of our own photoelectric observations and those of Severny (1970) with which to work. From models of β CrB we can have some idea of what to expect in the search for new magnetic stars. For these reasons, it appears worthwhile to construct a model for β CrB.

The line we will choose is the CrI 4254.4 line (g = 1.8), since most of our observations have been made using this line. Severny (1970) makes use of the same line. The microturbulent velocity is taken to be 1.0 Km/sec, $\eta_o = 100$, $\beta o = 2.0$.

The parameters given by Wolff and Wolff (1970) seem to give too high a circular polarization when compared to the photoelectric observations we have, especially the high-resolution ones (chapter IX). The polarization predicted from their model gives peaks of circular polarization of 15% for the phases at which we have the high-resolution observations. The discrepancy with figures 22 and 23 is probably too high to be accounted for by approximations of the Milne-Eddington model. One can decrease the polarization by introducing a higher microturbulent parameter. However, this might be in conflict with the sharpness of the magnetic null line FeI λ = 4065.4 seen in β CrB (Preston 1967).

We must be careful when comparing quantitatively our observations to the models. First, we do not have enough photoelectric observations, especially high-resolution

ones, spread throughout the magnetic cycle. Secondly, the models have the basic limitations and assumptions discussed in the previous section. Thirdly, as we will see, the model of β CrB predicts a component of linear polarization as strong as the circular one and some cross-talk is certainly present. We have not taken special precautions to avoid cross-talk during the observations.

We have chosen to use a model of β CrB with H_p = 11,000 gauss, β = 90° , i = 10° and a = 0.10 . The circular polarization given by this model is in better agreement with our observations and Severny's. Moreover, Preston (1967) finds that the magnetic null line FeI 4065.4 has a half-width $\sim$ 3 Km/sec in β CrB. After removing the thermal velocity of 1.5 Km/sec (Te = 8,000 degrees) he finds a residual velocity of $\sim$ 2.0 Km/sec. Considering a period of 18.5 days and the main-sequence radius of an A9 star he obtains an equatorial velocity V_e = 6.0 Km/sec . The inclination i = 20° is obtained assuming a microturbulent velocity of 0.0 Km/sec. So small a value, as Preston points out, is rather unlikely. A smaller inclination and non zero microturbulent velocity are probably more realistic. With the parameters i = 10° and β = 90° we obtain peak longitudinal fields of - 390 gauss and 545 gauss. These values are low when compared to the extrema given by Wolff and Wolff (1970) (+1000 and -900 gauss). However, it is plausible that systematic errors of interpretation of the photographic data might

account for a factor of two. The main factor is probably the difficulty of finding a suitable criterion to determine the effective wavelength of lines with a complicated wavelength dependence. We should note that Severny finds for β CrB a maximum positive field of the order of 500 gauss which would confirm the previous discussion.

Table 14 gives the surface field H_s, the effective longitudinal field H_e, the separation between the Zeeman analyzed line profiles $\Delta\lambda$ and, H_Δ the longitudinal field computed from the separation $\Delta\lambda$, for various phases. Figure 38 gives H_e (full line) and H_Δ (dashed line) as a function of phase. Figure 39 shows the wavelength dependence of the V Stokes parameter at phases 0.5, 0.6, 0.7, 0.8, 0.9, 1.0 . The figures at phases 0.1, 0.2, 0.3, 0.4, are mirror images of the figures at phases 0.9, 0.8, 0.7, 0.6, respectively, with the signs of polarization inverted.

For illustration, figure 40 shows the Q and U Stokes parameters predicted at phases 0.5, 0.6, 0.7, 0.9, 1.0 . Phase 0.0 is taken to be when the axis of the dipole is oriented in the plane containing the line of sight. This corresponds approximately to phase 0.8 with the ephemeris used by Wolff and Wolff (1970) .

We will not discuss the linear polarization in detail. Let us only notice that the model predicts a linear polarization comparable to the circular one and that the sign

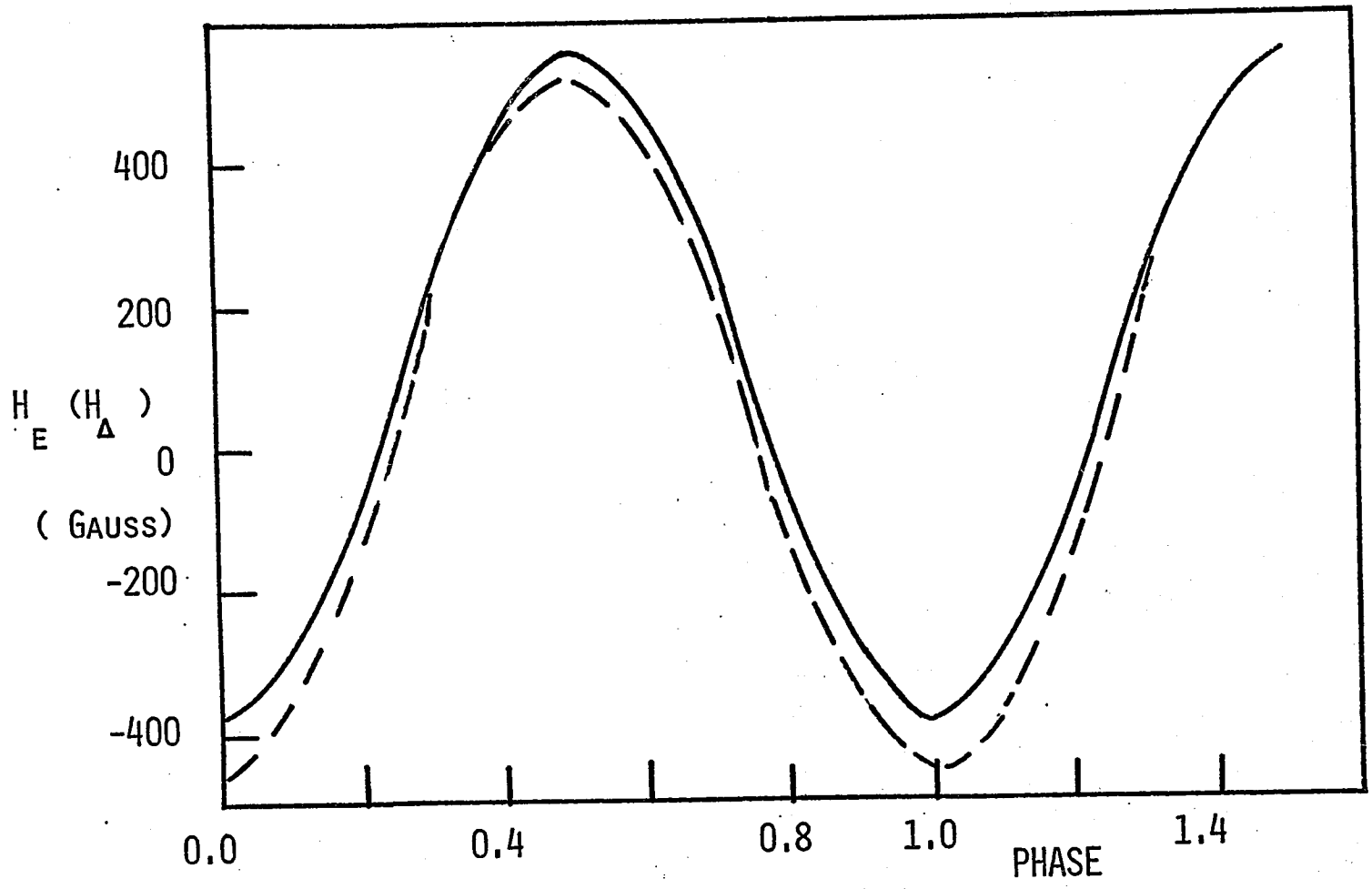

FIGURE 38

The effective longitudinal field (full line) and the longitudinal field computed from the separation of the Zeeman analyzed line profiles (dashed line) are plotted as function of phase for β CrB.

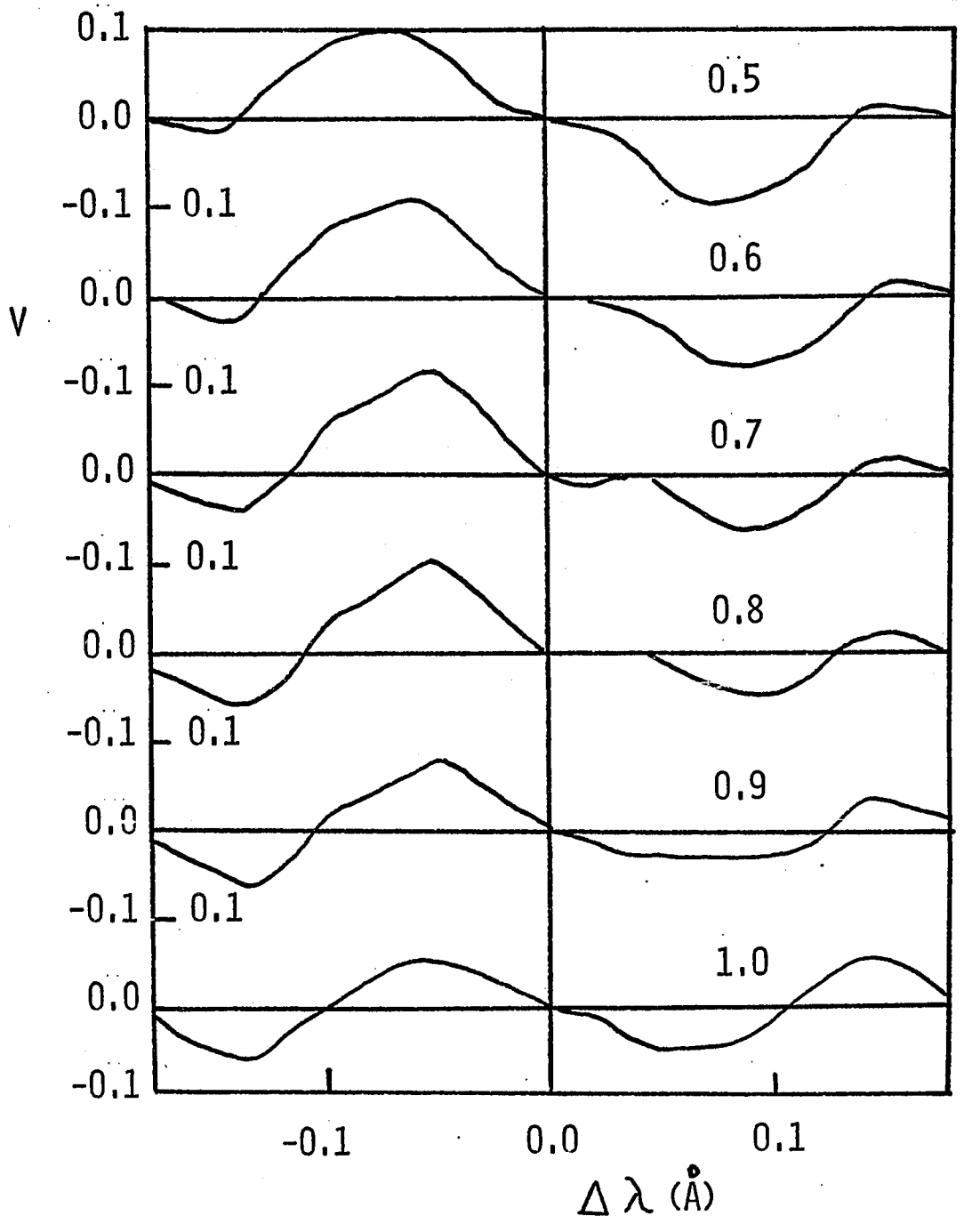

FIGURE 39

Wavelength dependence of the V Stokes parameter for the magnetic star β CrB is shown for phases 0.5, 0.6, 0.7, 0.8, 0.9 and 1.0 .

TABLE 14

CHARACTERISTICS OF THE MODEL

FOR β CrB FOR VARIOUS PHASES

PHASE	H_s	H_e	$\Delta\lambda$	$H\Delta$
0.5	4934	+545	.0160	525
0.6	4955	+460	.0132	430
0.7	5026	+230	.0059	190
0.8	5145	- 60	-.0035	-115
0.9	5267	-299	-.0113	-365
1.0	5320	-391	-.0143	-470
0.1	5267	-300	-.0113	-365
0.2	5145	- 61	-.0035	-115
0.3	5026	+230	.0057	190

FIGURE 40

The Q (full line) and U (dashed line) Stokes parameters predicted at phases 0.5, 0.6, 0.7, 0.9, 1.0, are plotted as a function of wavelength. At phases 0.5 and 1.0, U is not plotted as it is never larger than 0.015 .

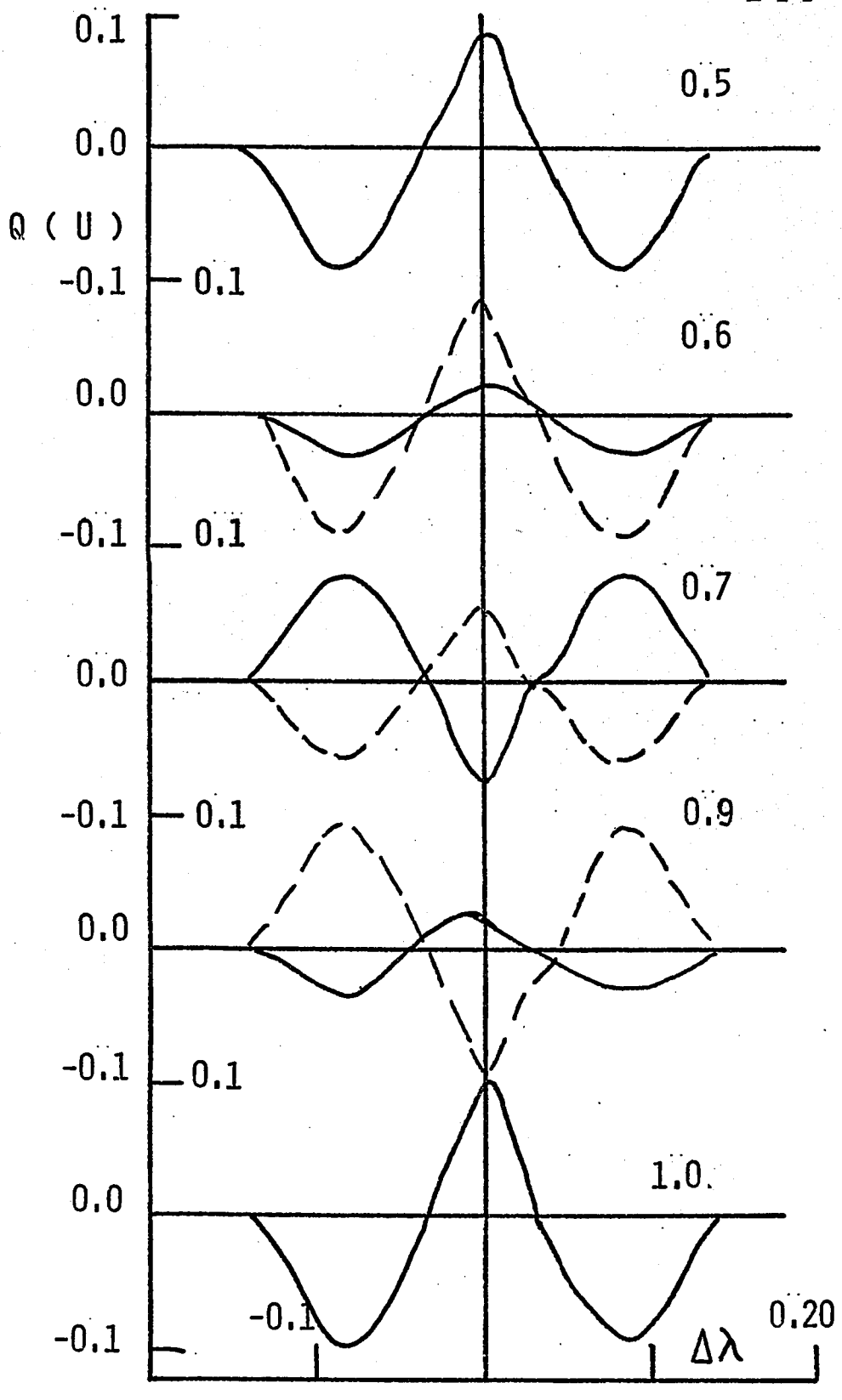
0.1
0.0
Q (U)
-0.1
0.1
0.5
0.6
0.7
0.9
1.0.
-0.1
0.20
Δλ

of polarization changes often over a small wavelength interval. To measure it one will need fairly high-resolution ~ 0.05 Å .

From figure 38 we can see that H_A reproduces surprisingly well the H_e curve. The error is typically $\sim 10\%$, getting worse for high inclinations of the dipole to the line of sight. Our reduction procedure would be hopeless during a great part of the cycle. Figure 39 clearly shows that the circular polarization, because of the cross-over effect, does not decrease linearly with decreasing H_e . Both H_e and H_A reproduce poorly the photographically determined H_e curve (Wolff and Wolff 1970). The positive field portion of the magnetic curve is broader than the negative one.

Is this a spurious effect, due to errors in the reductions? Consider what is measured by the photographic observer. Ideally he attempts to measure the effective wavelengths and separation between two lines having the same shape. The V signal from such a situation is S-shaped. When the two lines have complicated and different shapes (V is no longer S-shaped) the photographic observer is in trouble. He will, because of the complicated wavelength dependence, assume cross-over and therefore a small separation and field, or, using different parts of the line (such as the core or some point in the wing) to obtain the wavelength separation, he will see different separations and therefore different longitud-

inal fields (for example, see phases 0.9 and 1.0 in figure 41). Let us now examine figure 39. We can see that from phases 0.5 to 0.7 (and therefore 0.3 to 0.5) we have, to a good approximation, an S-shaped curve. Thus, our hypothetical photographic observer will easily measure the separation and from it assign a longitudinal magnetic field (not necessarily the correct one). From phases 0.8 to 1.0 he is in trouble. The wavelength dependence of V is complicated and so is the wavelength dependence of the Zeeman analyzed line profiles. Remember that V is given by $V = r_1(\lambda) - r_2(\lambda)$. One is tempted to speculate that the broader shoulder in the positive portion of the magnetic curve merely reflects the fact (figure 39) that the S-shape is present over a large portion of the cycle near maximum positive polarity (phases 0.3 to 0.7) and is not present near maximum negative polarity. In the same light, one might wonder whether the large scatter near maximum south polarity (Preston 1967, figure 6) is not due to the greater difficulty in measuring the separation between the components at these phases. In this respect, does the 10.5 year period for the south polarity merely reflect the fact that different criteria to measure the separation have been adopted by different people reducing the photographic data? Microphotometer tracings of Zeeman analyzed spectra of β CrB should answer those speculations. As an illustration, in figure 41 we can see the line profiles in left and

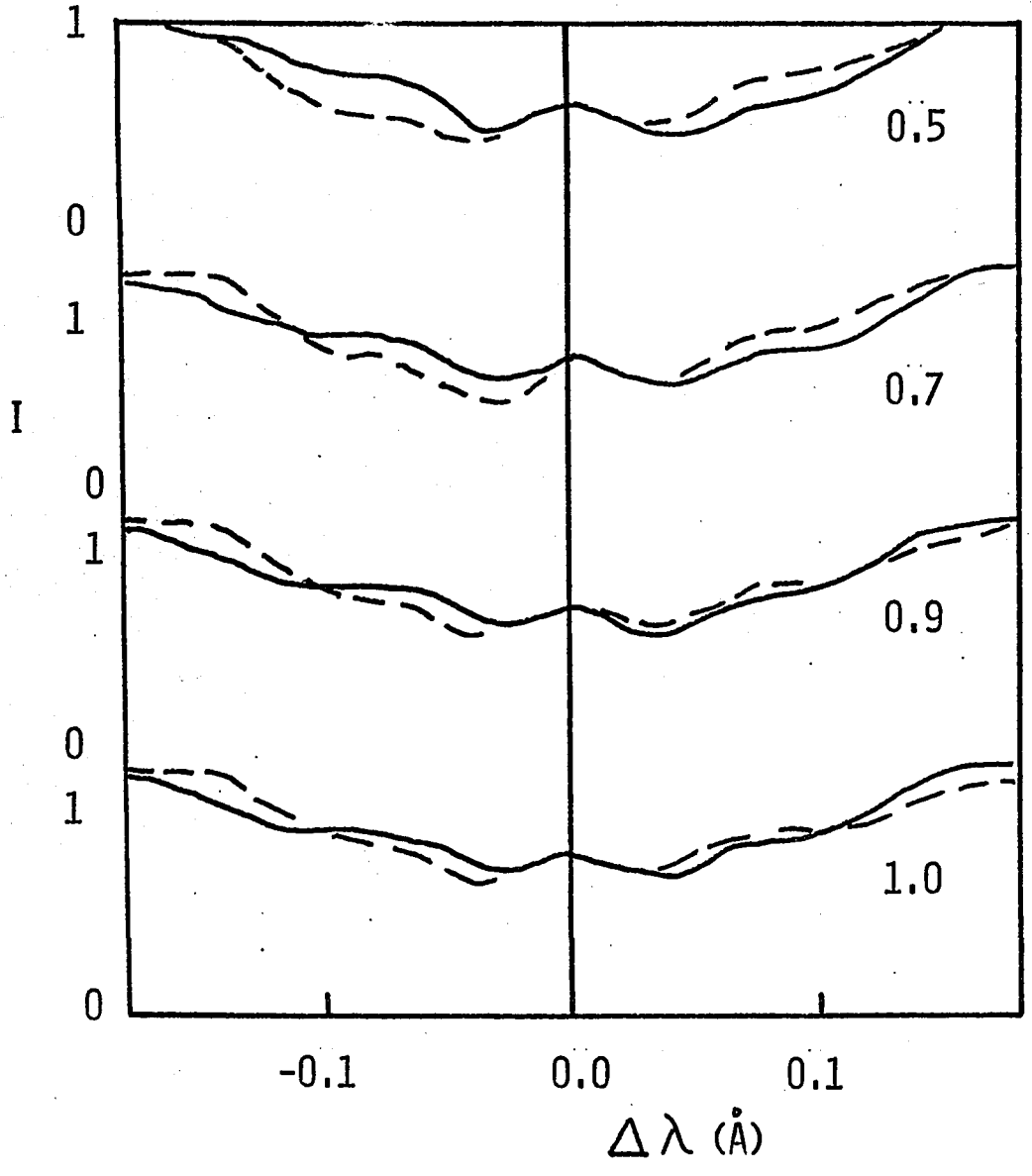

FIGURE 41

Theoretical Zeeman analyzed line profiles for β CrB, seen in right circularly polarized light (full line) and left circularly polarized light (dashed line).

right circularly polarized light at phases 0.5, 0.7, 0.9, and 1.0 , generated by our model of β CrB.

Notice that at phase 1.0 we do not have an S-shaped profile, but rather a double S . This might explain why Severny (1970) finds zero field or cross-over instead of maximum South polarity. With a large bandpass (0.20 Å), the signal at phase 1.0 will depend on the position of the bandpass inside the line, possible giving the signals observed by Severny.

Let us also compare the high-resolution observation we have to our model. The observation at J.D. 2441382.0 is obtained at approximately phase 0.7 to 0.8 in the theoretical phase notation. In figures 42 and 43 we have the observed and theoretical circular polarization (in percents) and line profiles. We can see that the line profile is reproduced rather poorly; this is not surprising considering the crude theory of line formation we have used. The theoretical line profile is too narrow and too shallow. Some broadening would be introduced by the instrumental profile (half-width 0.038 Å). The main reason is probably that the 4254.4 CrI line in βCrB is very strong, with well developed damping wings. The assumption of a gaussian wavelength dependence for the absorption coefficient is clearly wrong. The error in the depth of the line comes from the crudeness of the LTE Milne-Eddington model for such a strong line. Notice that the observed line profile is asymmetrical, possibly

FIGURE 42

Experimental circular polarization and line profile obtained for β CrB on J.D. 2441382.0 . The observation is the same as in figure 23.

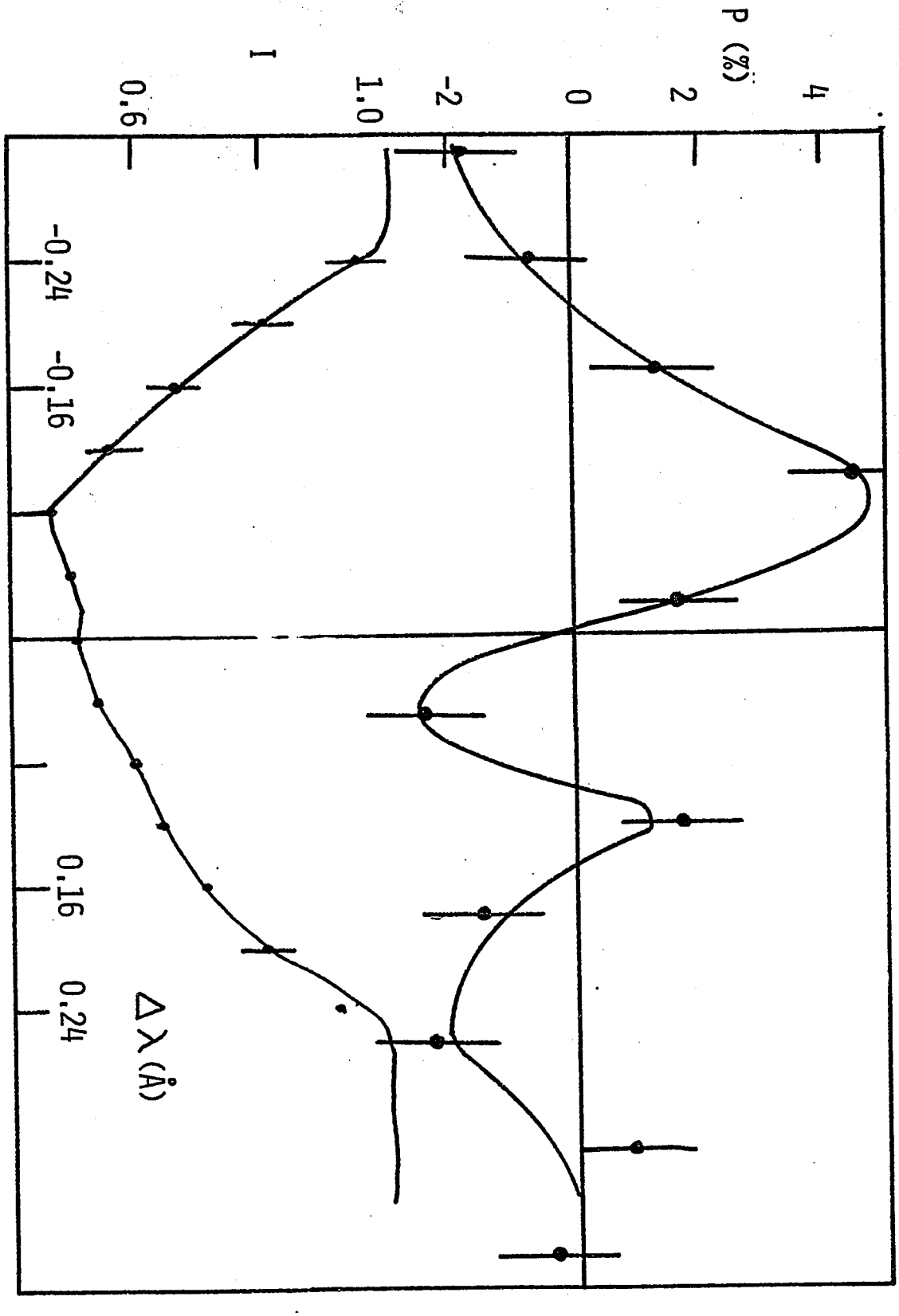
P (%)
4
2
0
-2
I
1.0
0.6
-0,24
-0,16
0,16
0,24
Δλ (Å)

FIGURE 43

Circular polarization and line profile predicted using our adopted model for β CrB at phase 0.7 . This should correspond approximately to the phase at which the observation of J.D. 2441382.0 was taken.

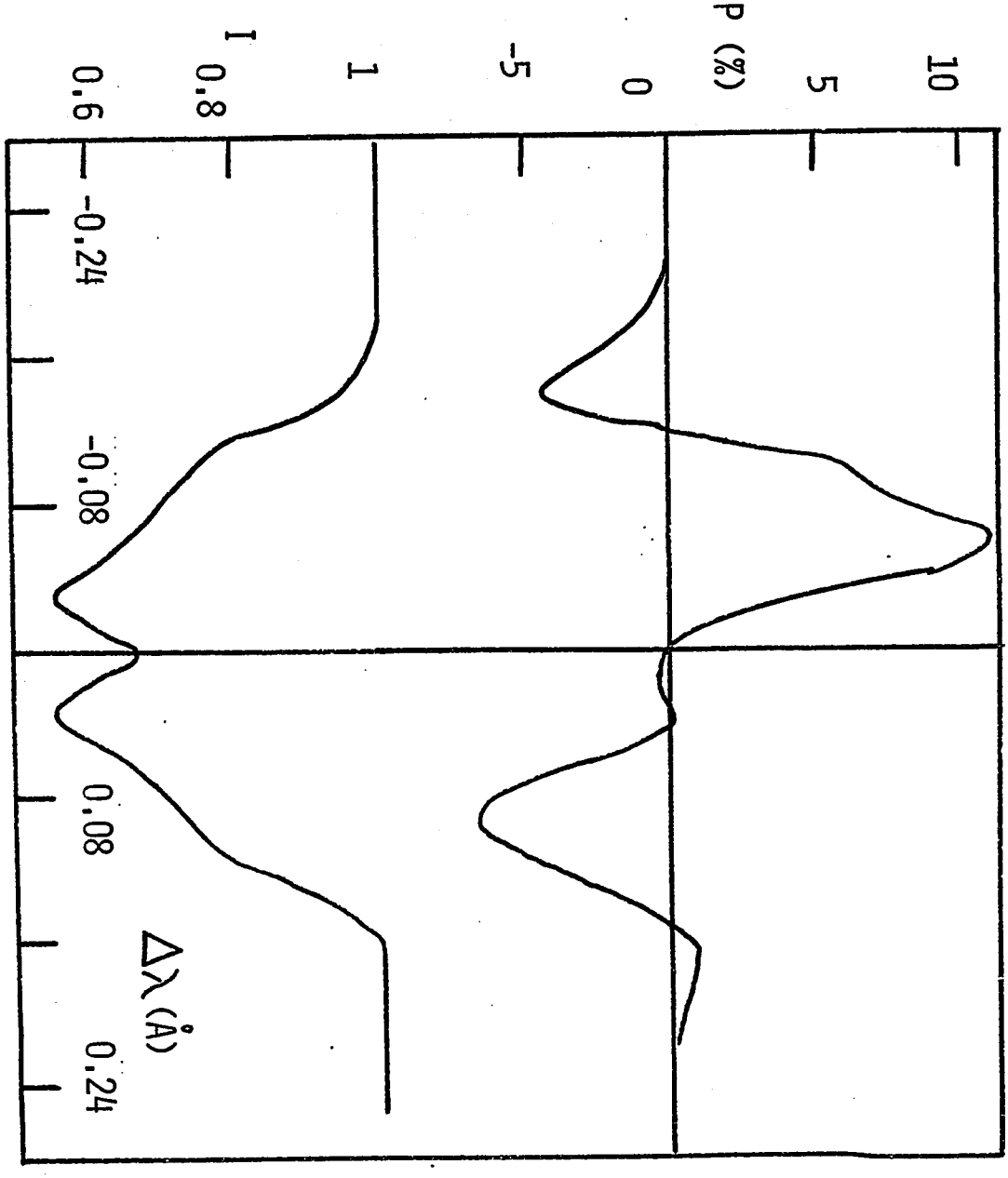
P (%)
10
5
0
-5
I
1
0.8
0.6
-0.24
-0.08
0.08
0.24
Δλ (Å)

indicating a slightly unequal distribution of CrI over the surface of the star.

Comparing the wavelength dependence of the circular polarization, we can see a qualitatively good agreement, within the experimental error, when allowance is made for the narrower theoretical line width. The fact, that the line profile for each element on the surface of the star is poorly reproduced by the Milne-Eddington model does not affect greatly the qualitative discussion of the circular polarization. Consider that the V Stokes parameter essentially comes from the subtraction of two line profiles, its wavelength dependence is always S-shaped and less drastically model dependent than the line profile itself.

The 4254.4 line in β CrB is a poor line to use in comparison between models and observations. A weaker line would be better represented by the LTE Milne-Eddington approximation and the assumption of a gaussian wavelength dependence for the absorption coefficient. These approximations save much computing time.

The observed circular polarization is lower than the theoretical one. Besides errors in the model, this can be explained by the effect of the instrumental profile, lower resolution and lower slope of the wings of the observed line profile.

I have changed most of the parameters of the model, trying to see how much information one can obtain from

measurements of the circular polarization alone and in particular from figure 42. The results are too extensive to be discussed here. It appears that high-resolution observations of the circular polarization alone, extended over the whole cycle, can give much information on the geometry of the field. For illustration, in figures 44 to 46 we see the V parameter that is predicted by models with respectively a = 0.0, a = 0.2 and $\beta = 80°$, at phases 0.5, 0.8, and 1.0. All other parameters are kept the same, in each model, to the ones adopted for β CrB.

From figure 42 alone, we cannot infer too much about the exact parameters of the field in β CrB. Most of the changes predicted at phases 0.7 or 0.8, changing parameters of the models, are too small to be observable within the observational accuracy. What we can say, is that figure 42 is consistent with an oblique rotator model with displaced dipole geometry. Notice how different the V signal, obtained with a = 0.0, is from figure 42.

What is clearly desirable to determine completely the geometry of the magnetic field is the observation of all of the Stokes parameters with a resolution ~ 0.03 Å, extended over the whole cycle. One should choose a weak spectral line in an uncrowded region of the spectrum. Our preceding discussion assumes that the 4254.4 CrI is not blended with a line giving a significant contribution to the polarization signal.

From all of the models computed for β CrB it appears

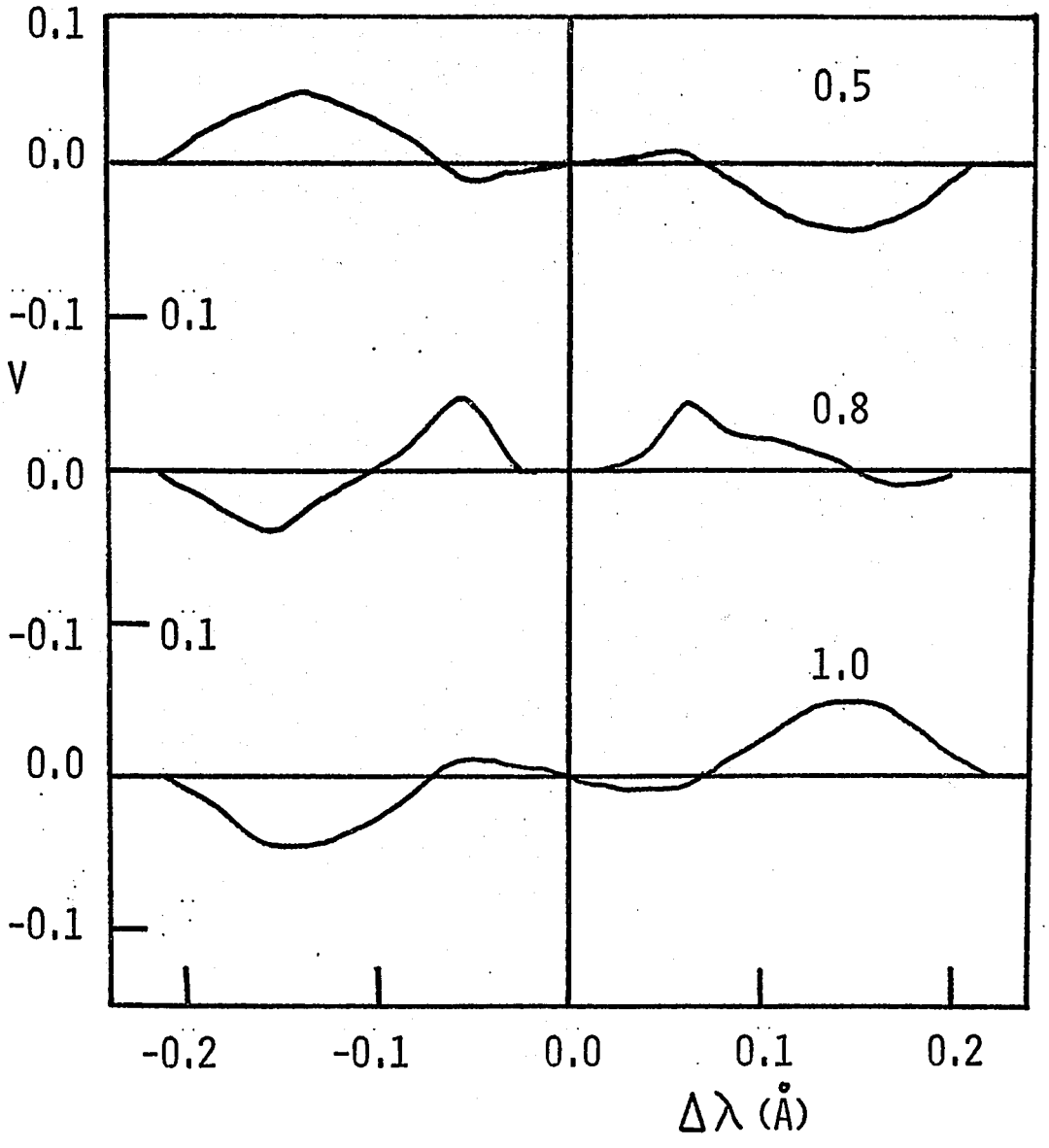

FIGURE 44

Circular polarization predicted by a model of β CrB with a = 0.0 .

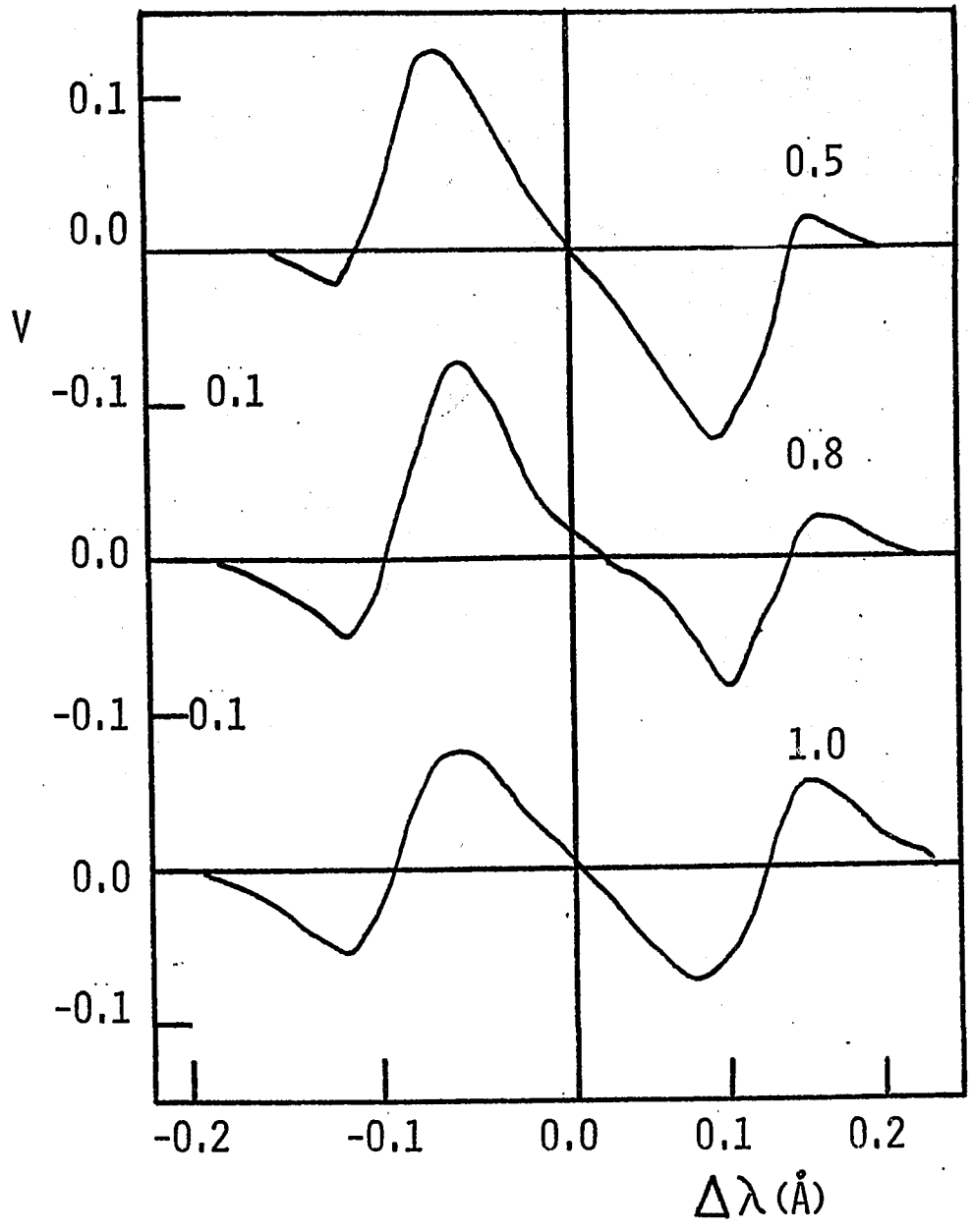

FIGURE 45

Circular polarization predicted by a model of β CrB with a = 0.2 .

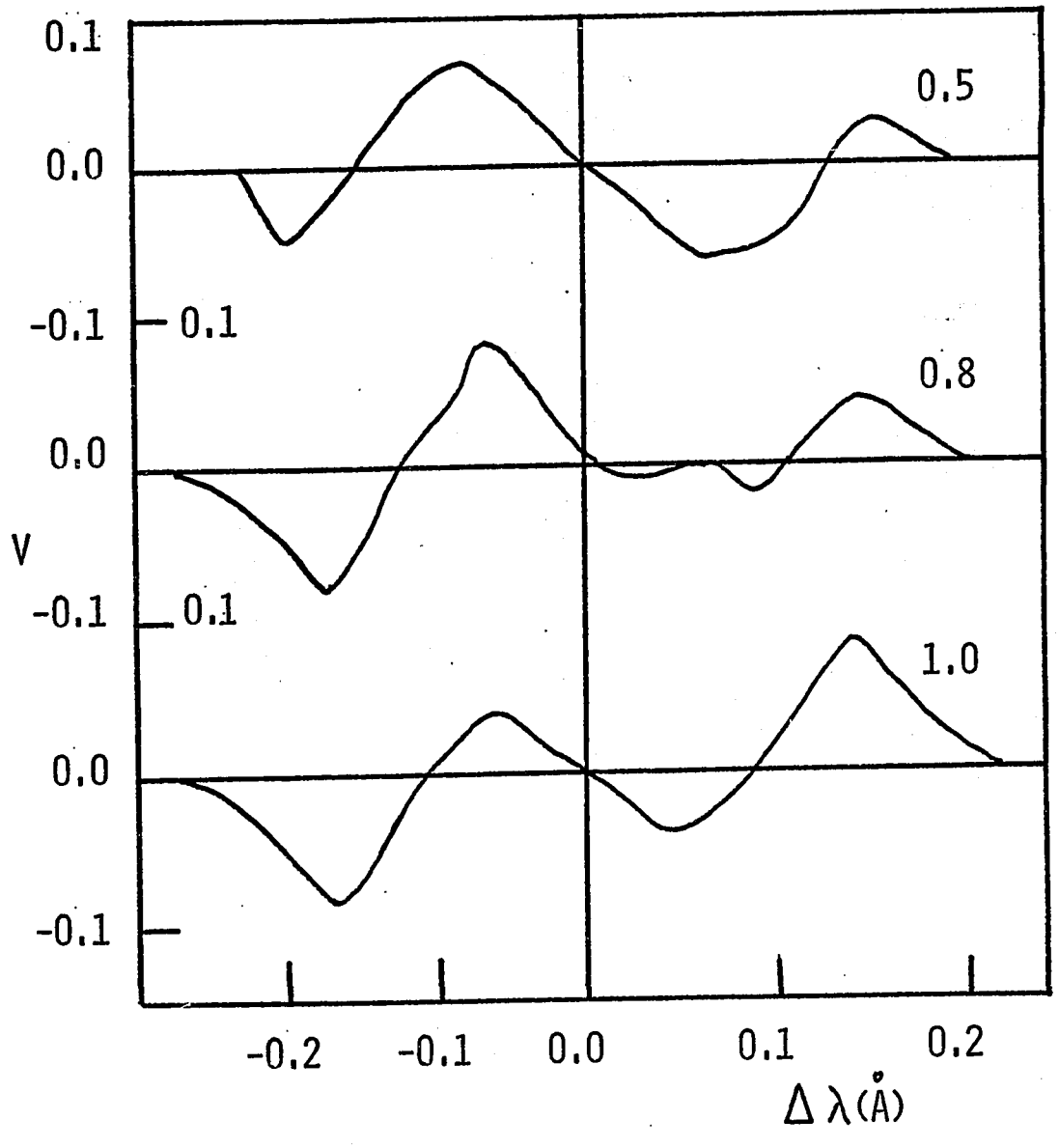

FIGURE 46

Circular polarization predicted by a model of β CrB with β = 80° .

that H_A reproduces H_e to within 10 to 20% accuracy. For high inclinations of the dipole on the line of sight ($H_e \sim 50$ gauss) the error is much larger ($\sim$100 %).

b) 53 Camelopardalis

Huchra (1972) has determined a model for 53 Cam. The parameters he gives for the model are H_p = 28,400 gauss, a = 0.145, $\beta = 80°$, i = 50° . The period of the magnetic variations (8.03 days) gives, under the assumption of an oblique rotator, $V_e \sim 14$ Km/sec. We will compute the Stokes parameters for the FeI line λ = 4260 (g = 1.6) . The parameters of the Milne-Eddington model are ξ_m = 1.0 Km/sec, β_o = 1.0, η_o = 30 . Table 15 gives H_e , H_A , and H_s for this model at phases 0.0, 0.1, 0.2, 0.3, 0.4, 0.5 . Figure 47 shows the V parameter at the same phases. Figure 48 shows the H_e and H_A curves. Phase 0.0 is taken to be the one at which the strongest pole of the dipole points towards the observer.

The same remarks regarding the H_e and H_A curves made for β CrB can be repeated for 53 Cam . The positive polarity curve broad shoulder is not reproduced by the model, possibly due to systematic errors in the reduction.

The model predicts a linear polarization comparable to the circular polarization.

c) Conclusions

Notwithstanding the approximations and imperfections of these two models, we can have an idea of the signals

TABLE 15

MODEL FOR 53 Cam

PHASE	H_s	H_e	$\Delta\lambda$	H_Δ
0.0	17260	-4960	-0.1640	-5350
0.1	15860	-4066	-0.1319	-4300
0.2	13008	-1780	-0.0525	-1700
0.3	10972	+ 872	+0.0324	+1080
0.4	10390	+2820	+0.0893	+2900
0.5	10390	+3500	+0.108	+3540

FIGURE 47

V parameter predicted for a model of 53 Cam.

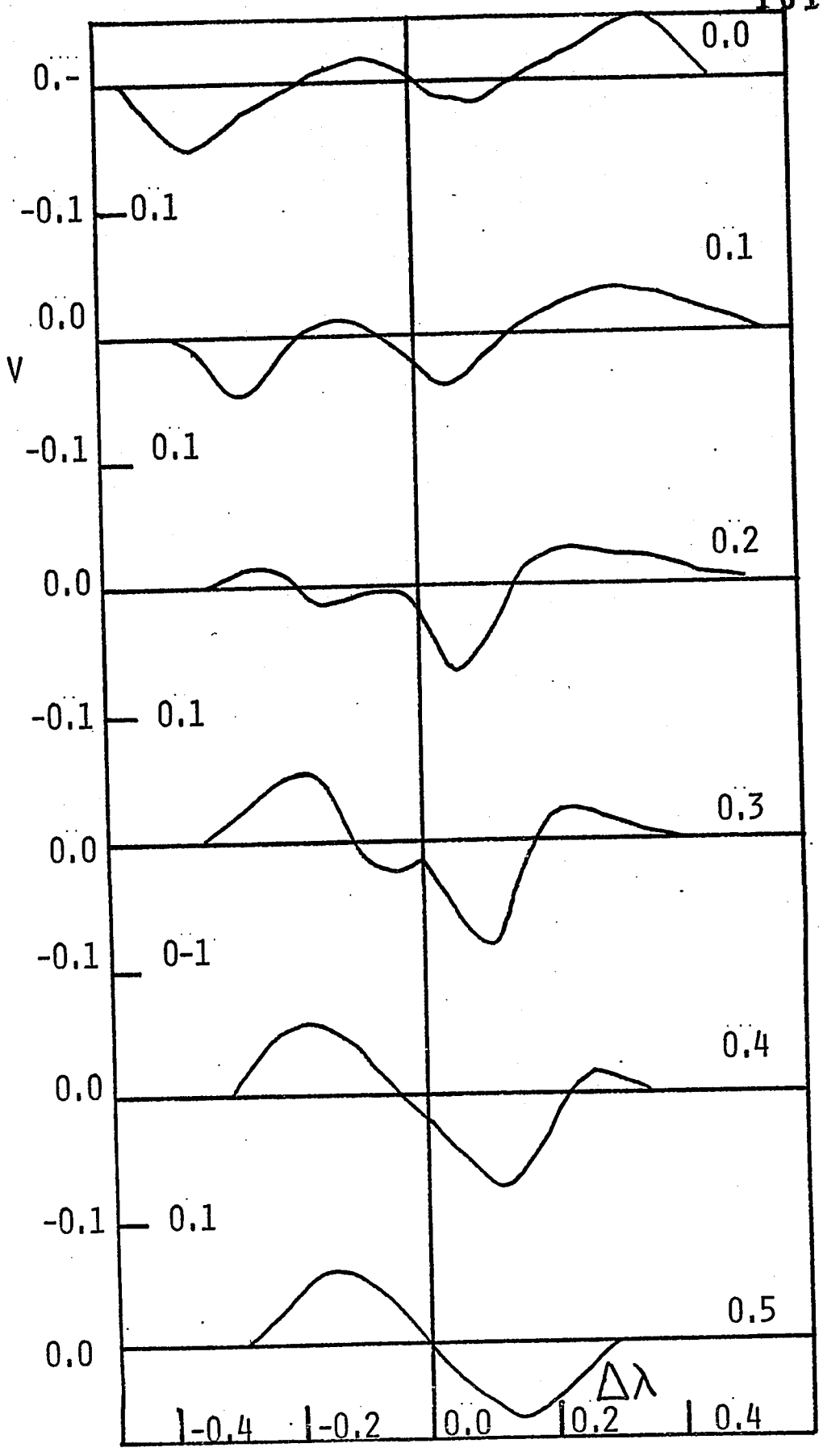
0.0
0.-
-0.1
0.1
0.1
0.0
V
-0.1
0.1
0.2
0.0
-0.1
0.1
0.3
0.0
-0.1
0-1
0.4
0.0
-0.1
0.1
0.5
0.0
Δλ
-0.4
-0.2
0.0
0.2
0.4

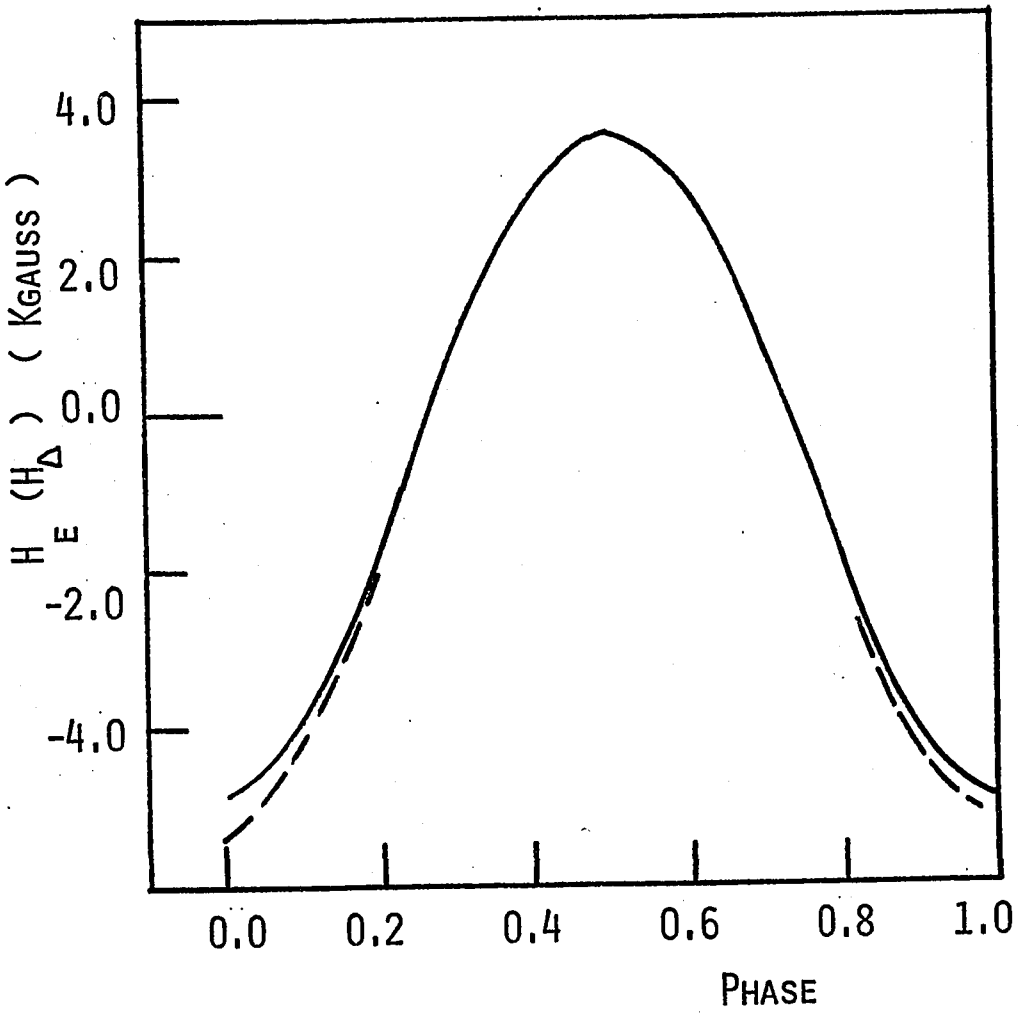

FIGURE 48

H_e and H_Δ (full and dashed lines) plotted as a function of phase for the A_p star 53 Cam.

that we might encounter in photoelectric polarization observations of magnetic stars. The Fabry-Perot interferometer, permitting a high resolution with a large entrance slit, is a useful instrument in observing the complicated wavelength dependence of the circular polarization during cross-over. It is thus an ideal tool in attempts to determine the geometry of the magnetic field.

The most difficult and unsolved problem facing us is how to assign an effective longitudinal magnetic field to the observed circular polarization. The reduction procedure used by us and by Severny is rather poor during cross-over. H_Δ appears to be a more reliable measure of the effective longitudinal field. However, one needs to know $r_1(\lambda)$ and $r_2(\lambda)$; therefore, high-resolution is needed. Low resolution observations obtained with a bandpass $\sim$ 0.20 Å are thus useful only for survey work, or for work on broad lines (when the broadening is not caused by rotation). H_Δ suffers from systematic errors. However, it could be used for a first order model to be refined with detailed comparisons of the wavelength dependence of the Stokes parameters.

CHAPTER XI

SUGGESTIONS FOR FUTURE WORK

1) Instrumentation

The most pressing need is to improve the present instrumentation which has to be considered only as a first transitory step. The present instrumentation has the advantage, for a preliminary program, that it is cheap and easy to set up, if a high-dispersion (~ 2 Å/mm) line profile scanner is available.

Several improvements are possible. As mentioned earlier, using a piece of calcite as a polarizing beam splitter and two optically superimposed photomultipliers we can improve the photon count by a factor of two. The use of a multichannel detector such as a TV camera or image dissector should also improve greatly the efficiency.

Work at the coudé focus introduces spurious instrumental polarization and phase shifts which are both inconvenient and a source of additional error. It would be highly desirable to work at the cassegrain focus. This can be achieved by making use of an echelle spectrograph similar to the one described by Schroeder and Anderson (1971). An echelle spectrograph dedicated to the measurement of stellar magnetic fields would present several advantages over the work we are presently doing at the

coudé focus as follows:

a) There are no oblique reflections off metallic mirrors. Thus one avoids the nuisance of instrumental polarization and phase shifts.

b) Higher efficiency would be obtained because an echelle spectrograph allows a large entrance slit and one avoids several metallic reflections.

c) The instrument can be attached to any type of telescope and one is not limited to the use of the handful of telescopes with high-dispersion photoelectric line-profile scanners. The major disadvantage of an echelle spectrograph is the very strong wavelength dependence of the efficiency. This is not an important handicap as we can work with only one line. A TV camera or image dissector could be used with the spectrograph. The TV camera could record the two-dimensional spectrum obtained with the cross-dispersion. We could then measure polarization in several lines.

2) Observations

The field is wide open as little photoelectric work has been done. Some interesting topics are listed below.

a) The technique is not limited to sharp-lined stars and one could search for fields in rapidly rotating stars.

b) Some of the brightest T-Tauri-like stars should be within reach. Magnetic fields have been postulated to be present in these young stars.

c) Little is known about the evolutionary status of magnetic stars. One should search for weak fields in late-type stars.

d) One should measure all of the Stokes parameters in the brightest A_p stars to obtain detailed information on the geometry of the magnetic field.

e) Measurements should be made of magnetic fields in stars showing emission in the core of the Ca II K line (Skumanich 1972).

f) Babcock (1958) has reported the marginal detection of magnetic fields in several stars. These should be measured with a higher signal to noise ratio.

g) Photoelectric measurements can give a time resolution higher than the photographic ones. One should search for rapid variations in the magnetic field (e.g. Steinitz and Pyper 1970). A_p stars showing rapid light variations are prime suspects.

3) Theoretical work

The models used in chapter X should be refined. One should check to what extent the conclusions reached are model dependent. The basic theory and techniques to compute depth dependent models are available (Moe 1968).

When high-resolution observations of the Stokes parameters for some magnetic stars are available, one should attempt an analysis similar to the one used in chapter X for β CrB.

The plate files of the Hale and Lick Observatories have Zeeman analyzed plates of many known magnetic stars. The information contained in the line profiles could be used and compared to numerical models.

CHAPTER XII

CONCLUSION

This investigation is to be considered only an exploratory step in the photoelectric measurement of stellar magnetic fields. Much work has to be done before a clearer picture of "weak magnetism" in stars emerges. Only a few of the stars observed revealed the possible presence of a magnetic field. This is to be expected. Although every star may have a net magnetic field it is generally probably weak (e.g. the sun), well below the upper limits obtained in this work.

The work presently carried at the coudé focus should be done at the cassegrain focus. Probably it is the only way very accurate measurements of the Stokes parameters and the detection of very small polarization can be carried out. Considering the importance of the measurements of magnetic fields for the study of stars, it is justified to expend considerable effort to build accurate and efficient equipment specifically for this purpose.

In concluding, it is worthwhile to examine briefly the latent capabilities of the technique. Consider the observation of H.D. 75332 in table 8. The standard deviation of 1.2 % polarization was obtained with a twenty minute integration time for this $m_v = 6.1$ star using

the 100-inch telescope. Let us consider possible improvements in the photon count.

Improvement	Gain
beam splitter	2
image slicer or echelle	3
multichannel detector	at least 5
two hours integration time	6
200-inch telescope	at least 2

We have a total gain of 400 in the photon count. This can be translated into the possibility of measuring circular polarization of about 1% in a 12th to 13th magnitude star, obtaining an error from 100 to 20 gauss, depending on the line used. Alternatively, a longitudinal field of the order of 1 gauss could be measured in a sixth magnitude star. Little comment has to be added to these impressive figures.

APPENDIX I

Let us send a beam of circularly polarized light into the telescope. The first two reflections off the primary and the secondary will not introduce modifications.

Consider mirror three, circularly polarized light from the secondary hits it, resolves it in two components, parallel (P) and perpendicular (S) to the plane of incidence. A phase shift Δ is introduced between the components which are reflected with different reflection coefficients r_s and r_p. The outgoing beam can be described with the two components

$$r\,a_{p3}(t) = r_p \sin(\omega t)$$
$$r\,a_{s3}(t) = r_s \sin(\omega t \pm \tfrac{\pi}{2} - \Delta)$$

The amplitude of the electric vectors of the incoming beam has been set to unity.

The plane of incidence of the light reflected by mirror three is the plane containing the incident ray from the secondary parallel to the axis of the telescope and the reflected beam down the declination axis. The plane of incidence of light reflected by mirror four is the plane containing the incident light parallel to the declination axis and the reflected beam down the polar axis.

These two planes coincide when the telescope points

at the North Celestial Pole (NCP). As the telescope moves in H.A. the relative orientation of these two planes does not change. The orientation will change as the telescope is moved in declination.

We will adopt the usual convention of considering positive an anticlockwise rotation when looking towards the incoming beam.

The component $r a_{p3}$ of the electric vector will be decomposed along the optical axis of mirror four

$$r a_{p3} \rightarrow S_4 \rightarrow r a_{p3} \cos\delta$$
$$r a_{p3} \rightarrow P_4 \rightarrow -r a_{p3} \sin\delta$$

where δ is the declination of the telescope.

Similarly for $r a_{s3}$

$$r a_{s3} \rightarrow S_4 \rightarrow r a_{s3} \sin\delta$$
$$r a_{s3} \rightarrow P_4 \rightarrow r a_{s3} \cos\delta$$

Composing the waves on the fast axis of mirror four we get

$$a_{p4}(t) = a_{p4} \sin(\omega t - \theta_{p4})$$

where the amplitude a and phase θ_{p4} are given by the usual formulae for addition of waves.

Similarly we have

$$a_{s4}(t) = a_{s4} \sin(\omega t - \theta_{s4})$$

The oblique reflection will again introduce a phase shift and different reflectances for the s and p directions.

The light off mirror four can be described with the two components

$$r a_{p4}(t) = a_{p4} r_p \sin(\omega t - \theta_{p4})$$
$$r a_{s4}(t) = a_{s4} r_s \sin(\omega t - \theta_{s4} - \Delta)$$

The beam has at this stage the characteristics of a beam at the exit of the coudé path for a four mirror system.

In a five mirror system an additional reflection occurs.

The plane of incidence on mirror five contains the polar axis and the path to the coudé room. The orientation of this plane never changes. What changes with hour angle is the orientation of the plane of incidence of mirror four. The planes of mirrors four and five coincide for HA = 0 hours.

Again, composing waves, we obtain

$$r a_{p4} \rightarrow P_5 \rightarrow r a_{p4} \cos\gamma$$
$$r a_{p4} \rightarrow S_5 \rightarrow r a_{p4} \sin\gamma$$

where γ is the HA in degrees

$$r a_{s4} \rightarrow P_5 \rightarrow -r a_{s4} \sin\gamma$$
$$r a_{s4} \rightarrow S_5 \rightarrow r a_{s4} \cos\gamma$$

Again, after reflection off mirror five we can describe the light as

$$r a_{p5}(t) = a_{p5} r_p \sin(\omega t - \theta_{p5})$$
$$r a_{s5}(t) = a_{s5} r_s \sin(\omega t - \theta_{s5} - \Delta)$$

We have thus the amplitudes and phase difference between the s and p component at the entrance of the coudé spectrograph for a five mirror system and for light originally 100% circularly polarized. Note that to describe similarly the problem for linearly polarized light, one has to introduce a phase shift of 180° and unequal amplitudes for the incoming light.

APPENDIX II

Mueller matrices for aluminized mirrors

Each mirror can be represented as the product of an homogeneous non-scattering, non-depolarizing, non-birefringent polarizer $[P]$ with principal transmission coefficients $k_s = r_s^2$ and $k_p = r_p^2$, and an ideal homogeneous linear retarder $[M]$ with retardance Δ.

From Shurcliff (1962) we have that the polarizer with the transmission axis "horizontal" can be written as

$$[P_o] = \frac{1}{2}\begin{bmatrix} k_s + k_p & -k_s + k_p & 0 & 0 \\ -k_s + k_p & k_s + k_p & 0 & 0 \\ 0 & 0 & 2\sqrt{k_s k_p} & 0 \\ 0 & 0 & 0 & 2\sqrt{k_s k_p} \end{bmatrix}$$

The Mueller matrix at some general angle θ can be obtained by making use of the rotator matrix $[T(2\theta)]$

$$[P_\theta] = [T(-2\theta)]\,[P_o]\,[T(2\theta)]$$

$$[T(2\theta)] = \begin{bmatrix} 1 & 0 & 0 & 0 \\ 0 & c_2 & s_2 & 0 \\ 0 & -s_2 & c_2 & 0 \\ 0 & 0 & 0 & 1 \end{bmatrix}$$

$$c_2 = \cos 2\theta \qquad s_2 = \sin 2\theta$$

we obtain that

$$[P_\theta] = \frac{1}{2}\begin{bmatrix} k_s+k_p & c_2(k_s-k_p) & s_2(k_s-k_p) & 0 \\ c_2(k_s-k_p) & c_2^2(k_s+k_p)+2s_2^2\sqrt{k_s k_p} & c_2 s_2(k_s+k_p)-2s_2 c_2\sqrt{k_s k_p} & 0 \\ s_2(k_s-k_p) & s_2 c_2(k_s+k_p)-2s_2 c_2\sqrt{k_s k_p} & s_2^2(k_s+k_p)+2c_2^2\sqrt{k_s k_p} & 0 \\ 0 & 0 & 0 & 2\sqrt{k_s k_p} \end{bmatrix}$$

θ is measured from the transmission axis of the polarizer; for a metallic mirror this corresponds to the s direction.

Shurcliff gives the Mueller matrix for an ideal homogeneous retarder with retardance Δ and azimuth ρ measured from the fast axis

$$[M(\rho)] = \begin{bmatrix} 1 & 0 & 0 & 0 \\ 0 & D^2+G^2-E^2 & 2DE & -2EG \\ 0 & 2DE & -D^2+G^2+E^2 & 2DG \\ 0 & 2EG & -2DG & 2G^2-1 \end{bmatrix}$$

$$D = Q \sin \tfrac{1}{2}\Delta \qquad E = U \sin \tfrac{1}{2}\Delta \qquad G = \cos \tfrac{1}{2}\Delta$$

where Q and U are the second and third Stokes parameters of the normalized fast eigenvector of the retarder. Q is given by $\cos 2\rho$ and U by $\sin 2\rho$. Given the retardance Δ the angles θ and ρ and the reflection coefficients k_s, k_p the Mueller matrix for a mirror can be written as the product $[P(\theta)] \times [M(\rho)]$. Note that ρ is measured from the p direction while θ is measured from the s direction. Therefore, for an individual mirror $\theta = \rho + 90°$

BIBLIOGRAPHY

Angel,J.R.P.,and Landstreet,J.D.,1970,Ap.J.Lett.,160,L147

Babcock,H.W. 1949a,Ap.J.,110,126

_____ 1949b,The Observatory,69,191

_____ 1953,Ap.J.,118,387

_____ 1955,Carnegie Inst.Washington,Yearbook N 54,p.27

_____ 1958,Ap.J. Suppl.,3,141

_____ 1960,in Stellar Atmospheres,ed. Jesse L. Greenstein (The University of Chicago Press)

_____ 1962, in Astronomical Techniques,ed. William A. Hiltner (The University of Chicago Press)

Baur,T. 1971,Personal Research Memo,High-Altitude Observatory,University of Colorado

Beckers,J.M. 1969,Air Force Cambridge Laboratories Report,AFCRL-69,0115

Billings,B.H. 1949a,J.O.S.A.,39,797

_____ 1949b,J.O.S.A.,39,802

_____ 1952,J.O.S.A.,42,12

Bohm-Vitense,E. 1967,Z.Ap.,67,1

Bolton,C.T. 1972,J.R.A.S.C.,66 (in press)

Bray,R.J. and Loughhead,R.E.,1964,Sunspots,(John Wiley and Sons Inc.)

Deutsch,A.J. 1954,Trans.I.A.U.,8,801

Drude,P. 1959,The Theory of Optics,(Dover Publications Inc.)

Gollnow,H. 1965,I,A.U. Symposium No.22,Editor R.Lust,(North-Holland Publishing Co.)

Gray,D.F. and Wehlau,W.H.,1972,preprint

Hale,G.F. 1933,Annual Report of the Director, Mt.Wilson Observatory,Carnegie Inst. Yearbook

Harvey,J. and Livingston,W.,1969,Solar Phys.,10,283

Hass,G. and Waylonis,J.E.,1961,J.O.S.A.,51,719

Hjellming,R.M.,Wade,C.M.,and Webster,E.,1972,Nature Phys. Sciences,236,43

Hockey,M. 1971,M.N.R.A.S.,152,97

Huchra,J. 1972,Ap.J.,174,435

Hughes,V.A.,and Woodsworth,A.,1972,Nature Phys.Sciences, 236,42

Iben,I. 1967,Annual Review of Astronomy and Astrophysics,Vol.5,571

Jenkins,F.A.,and White,H.A.,1957,Principles of Optics, (McGraw-Hill Book Company, Inc.)

Kiepenheuer,K.O. 1953,Ap.J.,117,447

Kiess,C.C.,and Meggers,W.F.,1929,Bureau of Standards J. of Research,1,64

Landstreet,J.D. 1970,Ap.J.,159,1001

Livingston,W.C. 1968,Ap.J.,153,929

Michard,R. 1961,C.R. Acad.Sci.,253,2857

Nikulin,N.S.,Kuvshinov,V.M.,and Severny.A.B.,1971,Ap.J.Lett., 170,L53

Moe,O.K. 1968,Solar Phys.,4,267

Moore,C.E. 1945,Princeton Contr.,N 20

O'Bryan,H.M. 1936,J.O.S.A.,26,122

Preston,G.W. 1967,in the Magnetic and Related Stars, ed. R.C. Cameron (Mono Book Corporation)

_____ 1969a,Ap.J.,157,247

_____ 1969b,Ap.J.,158,243

_____ 1969c,Ap.J.,158,1081

_____ 1971,Pub.A.S.P.,83,571

Preston,G.W.,and Pyper,D.M.,1965,Ap.J.,142,983

Preston,G.W.,and Sturch,C.,1967,in the Magnetic and Related Stars,ed. R.C. Cameron (Mono Book Corporation)

Severny,A.B. 1970,Ap.J. Lett.,159,L73

Schroeder,D.J.,and Andersen,C.M.,1971,Pub.A.S.P.,83,438

Schulz,L.G.,and Tangherlini,F.R.,1954,J.O.S.A.,44,362

Schulz,L.G. 1954,J.O.S.A.,44,357

Shurcliff,W.A. 1962,in Polarized Light (Harvard University Press)

Skumanich,A. 1972,Ap.J.,171,565

Steinitz,R.,and Pyper,D.M.,1971,Astrophys.and Space Sci., 11,322

Stepanov,V.E. 1958,Izv.Krym.Astrofiz.Obs.,18,136

Stibbs,D.W. 1950,M.N.R.A.S.,110,395

Unno,W. 1956,P.A.S.J.,8,108

Vaughan,A.H.,Jr. 1967,Annual Review of Astronomy and Astrophysics,Vol.5

Wehlau,W.H. 1970,J.R.A.S.C.,64,1

Wilson,O.C. 1968,Ap.J.,153,221

Wolff,S.C.,and Wolff,R.C.,1970,Ap.J.,160,1049

END OF REEL

RC-30